The
Massachusetts Bay Hydrodynamic Model: 2006-2007 Simulation

Massachusetts Water Resources Authority
Environmental Quality Department
Report 2009-10

The Massachusetts Bay hydrodynamic model: 2006-2007 simulation

Submitted to

Massachusetts Water Resources Authority
Environmental Quality Department
100 First Avenue
Charleston Navy Yard
Boston, MA 02129
(617) 242-6000

Prepared by
Changsheng Chen[1], Robert C. Beardsley[2], Qichun Xu[1], Michael J. Mickelson[3], Rucheng Tian[1], Pengfei Xue[1], Geoffrey W. Cowles[1], Brian J. Rothschild[1]

[1]Department of Fisheries Oceanography
School for Marine Science and Technology
University of Massachusetts-Dartmouth
New Bedford, MA 02744

[2]Department of Physical Oceanography
Woods Hole Oceanographic Institution
Woods Hole, Ma. 02543

[3]Massachusetts Water Resources Authority
100 First Avenue
Boston, Massachusetts 02129

July 2009

Citation:

Chen C, Beardsley RC, Xu Q, Mickelson MJ, Tian R, Xue P, Cowles GW, Rothschild BJ. 2009. **The Massachusetts Bay hydrodynamic model: 2006-2007 simulation.** Boston: Massachusetts Water Resources Authority. Report 2009-10. 77 p.

A few acronyms and definitions

ECOM-si	Estuarine and Coastal Ocean Model, semi-implicit. A structured grid hydrodynamic model.
FVCOM	Finite-Volume Coastal Ocean Model. An unstructured grid hydrodynamic model.
GoM/GB FVCOM	FVCOM applied to the Gulf of Maine/Georges Bank.
RCA	Row Column Advanced Ecological Systems Operating Program. A water quality model, which must be coupled to a hydrodynamic model.
BEM	Massachusetts Bay Eutrophication Model. RCA applied to Massachusetts Bay, and typically coupled to ECOM-si.
MM5	Pennsylvania State University/NCAR Mesoscale Model 5
WRF	Weather Research and Forecast Model (a newer version of MM5)
Sigma coordinates	Depths following the bathymetry
Cyclone	Wind circulation associated with a low-pressure system - counterclockwise in the northern hemisphere.
RMS error	Root mean square error

EXECUTIVE SUMMARY

Massachusetts Water Resource Authority (MWRA) contracted University of Massachusetts at Dartmouth (UMassD) to model the water currents, temperature, salinity (hydrodynamics) and water quality in Massachusetts Bay for years 2006 and 2007, using procedures similar to those used for 2005 and previous years. This report covers results of the hydrodynamic model.

Not surprisingly, model results for 2006-2007 have an accuracy similar to previous years. Model-simulated variables generally tended to resemble observed data, but there were noticeable mismatches due to the uncertainty of model forcing and boundary conditions.

The modelers next focused on ways to improve the existing model. The existing model assumes for simplicity that at any one time wind blows with the same strength and direction over the bay. They found that model results were improved by incorporating the fact that wind is not uniform over the bay. This is most noticeable with passage of storms and fronts.

Model performance was also better with use of second a model having a slightly different layout of grid cells. That model performed better largely because it has more recent refinements such as finer grid cells.

UMassD recommends that future hydrodynamic modeling for MWRA use this second model as well as incorporate the spatial wind field. Further improvements in the modeling should be possible in conjunction with a greater focus on particular events and important system processes.

Table of Contents

1 Introduction 8

2 Procedures for running ECOM-si 10

2.1 The hydrodynamic model ECOM-si 10

2.2 The computational domain, resolution and time step 10

2.3 Forcing data 10

2.4 Initial conditions 14

3 The 2006 and 2007 ECOM-si results 15

3.1 Experiment A: Single buoy wind without nudging 15

3.2 Experiment B: Single buoy wind with nudging 22

3.3 Experiment C: MM5 wind with nudging 23

3.4 Spatial distribution of observed versus Experiment-A-computed temperature and salinity 29

3.5 Noteworthy cooling events: buoy observations versus Experiment-A-computed temperature 30

4 FVCOM and ECOM-si comparison 31

4.1 The hydrodynamic model FVCOM 31

4.2 The computational domain, resolution and time step 32

4.3 Forcing data 32

4.4 Model – data comparisons for two models (Experiments D and E) 33

5 Summary and conclusions 36

6 Recommendations 38

7 References 39

List of Tables

Table 1-1 Model experiments. 9

Table 2-1 Data used for external forcing of ECOM-si. 11

Table 3-1 RMS errors in temperature and salinity at GoMOOS Buoy A for three experiments. 16

Table 3-2 RMS errors in currents at GoMOOS Buoy A for three experiments, ... 17

Table 3-3 RMS errors of temperature and salinity at MWRA monitoring sites for three experiments. 20

Table 3-4 Comparison between models of the RMS errors listed in Table 3.3 21

Table 3-5 Statistics of storms affecting Massachusetts Bay. 24

Table 4-1 Data used for external forcing of FVCOM and ECOM-si for 2005 Experiments D and E. 33

Table 4-2 RMS errors in temperature and salinity at USGS Buoy LT-A for two experiments. 34

	List of Figures		
Figure	Description	Spatial location	Date
Fig 1.1	Bathymetry and buoy locations.	Model domain	
Fig 2.1	ECOM-si curvilinear grid, and hydrographic monitoring sites selected for the model validation.		
Fig 2.2	Shortwave radiation, air pressure, humidity, air temperature and wind velocity	NOAA Buoy 44013	2006
Fig 2.3			2007
Fig 2.4	Daily discharges	Rivers and the MWRA outfall	2006-2007
Fig 2.5	Monthly averaged surface elevations.	Open boundary	2006-2007
Fig 2.6	Monthly averaged temperature and salinity.		2006-2007
Fig 2.7	Times series of water temperature and salinity.	GoMOOS Buoy B	2006-2007
Fig 2.8	Time series of currents.		2006-2007
Fig 3.1	Comparison of modeled and observed temperature and salinity.	GoMOOS Buoy A	2006-2007
Fig 3.2	Comparison of modeled and observed currents.		2006-2007
Fig 3.3	Comparison of modeled and observed temperature and salinity.	monitoring sites F26, F27, F29, N04, N07 and F17	2006
Fig 3.4		monitoring sites F31, N01, N10 F07, F01 and F02	2006
Fig 3.5		monitoring sites F26, F27, F29, N04, N07 and F17	2007
Fig 3.6		monitoring sites F31, N01, N10 F07, F01 and F02	2007
Fig 3.7	Monthly-averaged wind velocity field.	Region	2006-2007
Fig 3.8	Paths of storms or center of the cold air fronts over and around the Gulf of Maine.		2006-2007
Fig 3.9	Surface wind velocity and air pressure		Apr 4 2006 and Jun 8 2006

Fig 3.10			Jul 13 2006 and Aug 20 2006
Fig 3.11			Apr 5 2007 and May 19 2007
Fig 3.12			Jun 4 2007 and Oct 12 2007
Fig 3.13	Difference in currents modeled using spatial wind minus that using uniform wind.	Model domain	April 4 2006
Fig 3.14			June 8 2006.
Fig 3.15			July 13 2006.
Fig 3.16			August 20 2006
Fig 3.17	Difference in modeled surface temperature using spatial wind minus that using uniform wind.		Apr 4, Jun 8, Jul 13 and Aug 20 2006
Fig 3.18	Difference in modeled surface salinity using spatial wind minus that using uniform wind.		
Fig 3.19	Difference in currents modeled using spatial wind minus that using uniform wind.		April 5 2007
Fig 3.20			May 19 2007
Fig 3.21			June 4 2007
Fig 3.22			October 12 2007
Fig 3.23	Difference in modeled surface temperature using spatial wind minus that using uniform wind.		Apr 5, May 9, Jun 4 and Oct 12 2007
Fig 3.24	Difference in modeled surface salinity model using spatial wind minus that using uniform wind.		
Fig 3.25	Comparison of observed and modeled surface temperature and salinity.	Monitoring sites and model domain	Day 12.4, February 2006
Fig 3.26			Day 12.4, April 2006
Fig 3.27			Day 19.6, June 2006
Fig 3.28			Day 22.7, August 2006
Fig 3.29			Day 21.2, April 2007
Fig 3.30			Day 19.1 June 2007
Fig 3.31			Day 21.2, August 2007
Fig 3.32	Comparison of observed and ECOM-si-detected cooling events.	NOAA Buoy 44013	2006-2007

Fig 4.1	Unstructured grid of the first generation Gulf of Maine FVCOM.	Model domain	
Fig 4.2	Comparison of observed, ECOM-si-modeled, and FVCOM-modeled temperature and salinity.	USGS Buoy LT-A	2005
Fig 4.3		Monitoring sites and model domain	May 2005
Fig 4.4	Comparison of distributions of observed, ECOM-si-and FV COM-computed trajectories of a drifter.	Massachusetts Bay	Subsurface (4 m) drifter#56202. June 28 to July 10 2005.
Fig 4.5			Near-surface (1-m) drifter#57201. July 18 to July 24 2005.
Fig 4.6			Near-surface (1-m) drifter#57202. July 18 to July 23 2005.

1 Introduction

Massachusetts Bay is a typical inner bay connected to harbors, estuaries, numerous islands, sounds, a narrow canal, wetlands and tidal creeks along the coast and bounded by the steep bottom topography of Stellwagen Bank in the western Gulf of Maine (**Figure 1.1**). A substantial amount of modeling has been done on the bay, particularly to understand the effects of the Massachusetts Water Resources Authority (MWRA) outfall, which is also shown in the figure. MWRA relocated its discharge of secondary treated effluent from Deer Island in Boston Harbor to the new outfall in Massachusetts Bay on September 6, 2000. Modeling helped with decisions about where to best site the MWRA outfall in Massachusetts Bay, and on an ongoing basis has been helping to address remaining concerns about the outfall.

We continued the modeling effort for years 2006-2007. The current model is a coupled hydrodynamic/water-quality model, and for convenience we describe the hydrodynamic model results in this report, and the water quality model results in a companion report (Tian et al., 2009). The hydrodynamic model computes the movement of water, changes in water surface elevation, water column temperature and salinity, and changes in vertical density structure in response to wind stress, freshwater inflows, solar radiation, and also the tidal forcing, mean elevation, and fluxes at the open boundary.

For 2006-2007, we followed the procedure used for 2005 (Jiang and Zhou, 2008). We did that for continuity with previous model runs and to directly meet the requirement for modeling stated in MWRA's discharge permit.

Compared our modeling work with previous work, we found that all these studies were mainly focused on model validation and found relatively little difference in overall model performance from year to year.

In addition, with the intention of finding ways to improve the modeling effort, we conducted sensitivity tests to explore the importance and merit of three factors:

- "Nudging" to assimilate buoy data near the boundary.
- Using a detailed wind field.
- Using a different hydrodynamic model.

Much of this report focuses on those sensitivity tests rather than on the issue of model validation, which has been well-covered by previous year's reports. Furthermore, those previous reports have shown similar levels of reliability and accuracy of the model from year to year so we did not want to belabor that finding here.

The 2005 model run of Jiang and Zhou (2008) used the model ECOM-si (Estuarine and Coastal Ocean Model, semi-implict) nudging under a uniform rather than spatially detailed wind field. We followed their procedure but also did sensitivity tests with no nudging, detailed spatial winds, and the model FVCOM (Finite-Volume Coastal Ocean Model). The design of the sensitivity tests, or "experiments", is listed in Table 1-1

Table 1-1 Model experiments.

Experiment	model	year	wind	nudging	Section
A	ECOM-si	2006 & 2007	single buoy wind	with**out** nudging	3.1
B	ECOM-si	2006 & 2007	single buoy wind	with nudging	3.2
C	ECOM-si	2006 & 2007	MM5 wind	with nudging	3.3
D	ECOM-si	2005	MM5 wind	with nudging	4
E	FVCOM	2005	MM5 wind	with nudging	4

A. ECOM-si run for 2006-2007 using the procedures described in Section 2 but omitting nudging (Section 2.3.5).

B. As with experiment A but including nudging. This corresponds to the procedure used by Jiang and Zhou (2008) for 2005. We nudged the currents; water temperature and salinity on GoMOOS buoy B onto the open boundary conditions to evaluate the role of the upstream open boundary flux on stratification and currents inside the Bay.

C. As with experiment B but using spatially variable wind. Rather than assuming a spatially uniform wind field identical to that at NOAA Buoy 44013, we used the spatially variable MM5 wind field to examine quantitatively the influence of spatial variation of wind forcing during storm passages on the temporal variation and spatial distribution of currents and water properties in Massachusetts Bay.

D. As with experiment C but for year 2005. We did this as a control for experiment E.

E. FVCOM ran otherwise similar to experiment D.

2 Procedures for running ECOM-si

2.1 The hydrodynamic model ECOM-si

ECOM-si ("Estuarine and Coastal Ocean Model, semi-implicit") is the modified semi-implicit version of the three-dimensional, free-surface, primitive equation structured-grid, finite-difference Princeton Ocean Model (POM) (Blumberg, 1994).

The model parameterizes vertical turbulence mixing with the Mellor and Yamada (1982) level 2.5 (MY-2.5) turbulent closure scheme, and horizontal mixing with the Smagorinsky (1963) turbulence closure scheme.

ECOM-si was first configured for Massachusetts Bay by Signell et al (1996) and calibrated to realistically simulate the currents and water stratification in the Bay by HydroQual and Signell (2001).

We were familiar with ECOM-si well before starting this project, and have used it to study the tidal mixing frontal dynamics and frontal ecosystem processes over Georges Bank (GB) and the Gulf of Maine (Chen and Beardsley 1995, Chen et al. 1995, Franks and Chen 1996, Chen et al. 2001, Franks and Chen 2001, and Ji et al. 2006). We have found that this model is robust and can resolve the key tidal and wind-induced physical processes in this region.

2.2 The computational domain, resolution and time step

ECOM-si uses curvilinear coordinates in the horizontal. The grid used in this model remains the same as the original setup by Signell et al. (1996). **Figure 2.1** shows the model domain, covering the entire Bay region, with an open boundary running across the shelf from Cape Cod, MA, turning northwestward through the interior of the western Gulf of Maine (GoM) and then across the shelf to the coast off Portsmouth, NH. This horizontal extent of the domain is divided into 68×68 orthogonal curvilinear grid lines. The horizontal resolution varies from 10 km near the open boundary to 0.7 km inside Boston Harbor.

ECOM-si uses sigma-coordinates in the vertical. The vertical extent of the model domain is divided vertically into 12 sigma-levels (layers that vary with water column depth). The sigma-depth is defined as 0 at the surface to 1 at the bottom; the upper three sigma-levels are located at 0.01, 0.04 and 0.1 and the rest are evenly divided from 0.1 to 1. The model uses smoothed bottom topography, which varies from 140 m in the deep region to 3 m at the coast.

The time step used for the time integration is 207 seconds, so 216 time steps covers an M_2 tidal cycle. Numerical stability criteria suggest this time step is appropriate.

2.3 Forcing data

The model is driven by meteorological forcing, river discharges and the outfall, tides with specified monthly averaged water properties (temperature and salinity) at the open boundary. In addition, the boundary properties may be "nudged" to agree with data from a nearby buoy. The data sources of the forcing are listed in Table 2-1.

Table 2-1 Data used for external forcing of ECOM-si.

Experiment	Parameters	Temporal averaging of forcing data	Source
A-E	Solar radiation	Hourly	Primary: WHOI pyranometer[1]. Secondary: MM5 4/25-5/4/2006 and 4/1-7/13/2007
A-E	Air pressure Air temperature Winds	Hourly	Primary: NOAA Buoy 44013[2] Secondary: Logan Airport
C-E	Spatially variable winds	Hourly	MM5
A-E	Humidity	Hourly	Logan Airport
A-E	River discharges	Daily	USGS
A-E	Outfall effluent flow	Daily	MWRA
A-E	Tidal forcing	12 minutes	Tidal prediction submodel
A-E	Boundary elevation, temperature, salinity	Monthly	Output from GoM/GB FVCOM
B-E	Nudging: GoMOOS Buoy B temperature, salinity, currents	Hourly	University of Maine (Petigrew, 2009)

Note: Experiment A omits the nudging step.
Experiments A and B do not use MM5 winds.

2.3.1 Meteorological forcing

ECOM-si was driven by external meteorological forcing at the surface, including winds and net heat flux. Net heat flux is the sum of shortwave (0.3-3 um) radiation, net long-wave (3.5-50 um) radiation, sensible heat flux and latent heat flux. It is indirectly calculated from solar radiation (shortwave as measured with a pyranometer), air pressure, air temperature, wind, and humidity (**Figures 2.2 and 2.3**). For periods with no NOAA buoy observations, the meteorological measurements at Logan Airport were used to fill gaps. For periods with no WHOI solar radiation data, the shortwave radiation output from MM5 and WRF were used to fill gaps.

Subsurface heating is forced by short-wave irradiance penetrating into the water column. That is calculated assuming light entering the water decays exponentially with depth, with the light attenuation coefficient used in previous years (HydroQual and Signell, 2001; Jiang and Zhou, 2008).

[1] Courtesy Dr. Richard Payne http://cis.whoi.edu/science/PO/climate/index.cfml
[2] http://www.ndbc.noaa.gov/station_page.php?station=44013

Single Buoy Wind. Previous model runs for MWRA assumed for convenience that the wind field over the model domain was spatially uniform, and matched that measured at a single meteorological buoy (NOAA Buoy 44013, shown in bottom panels of **Figures 2.2 and 2.3**). This ignores the true spatial variability of the wind field, so after running the model with this "single buoy wind" in Experiments A and B we repeated the run using the spatially variable wind described below for Experiments C-E.

MM5 Wind. This wind was produced by running the regional MM5 model (for 2005-2006) and its successor WRF model (for 2007) with assimilation of all available buoy winds (including the wind data measured at buoy 44013 in the Mass Bay. This spatially variable wind field was used to drive ECOM-si in the "MM5 wind" experiments C-E.

MM5 is a fifth-generation regional mesoscale weather model developed originally by NCAR/Penn State (Dudhia et al. 2003) and modified by Chen et al. (2005) to improve the estimation of sensible and latent heat fluxes. MM5 features non-hydrostatic dynamics, terrain-following sigma-coordinate, variable domain and spatial resolution, multiple grid nesting and 4-dimensional data assimilation, and uses NCEP weather reanalysis model fields as initial and boundary conditions with two-way nesting capability. MM5 is configured with a “regional” domain (covering the Scotian Shelf/GoM/GB/New England Shelf) and a “local” domain (New England Shelf/Massachusetts Bay) with horizontal grid spacing of 9 km and 3 km respectively, and 31 sigma levels in the vertical with finer resolution in the planetary boundary layer. WRF is the Weather Research Forecast model as replacement of MM5. The configuration of WRF in this region is the same as MM5. The forcing fields in both 2006 and 2007 are based on the 9-km model grid.

2.3.2 Freshwater discharges

The model included the freshwater discharges from four rivers: the Merrimack River, the Charles River, the Neponset River and the Mystic River. It was also driven by the sewage effluent discharged by the MWRA outfall. The rivers and the outfall were treated as point sources, each entering the model at a single grid cell. The greatest flow is from the Merrimack River. The Charles, the Neponset, and the MWRA outfall each discharge about 2% of that from the Merrimack River, although closer to the region of interest to MWRA. Discharge from the Mystic River is negligible.

River discharges differed appreciably between years (**Figure 2.4**). Merrimack River flow peaked in May 2006, but a month earlier in 2007, with slightly lower flow. The Charles and Neponset Rivers showed two runoff peaks in May and June 2006, but only one peak in April 2007. The MWRA outfall showed a similar pattern. The winter and fall discharge was greater in 2006 than 2007. Such a fall and winter peak was also seen in 2005 (Jiang and Zhou, 2008). Overall, 2006 was relatively fresher than 2007.

2.3.3 Tidal forcing

The tidal forcing is specified on the open boundary. It consists of the amplitudes and phases of five major tidal constituents (M_2, N_2, S_2, K_1 and O_1) at points along the boundary.

Specification of those tidal constituents has been laborious because ECOM-si does not track true clock time (model time starts at zero in each simulation), so that the tidal constituents must be time-adjusted for each year's run. That was the method for previous runs for MWRA, but we

found it more convenient to modify ECOM-si so it now includes the Foreman (1978) tidal forecast module. We routinely use that module in other models such as GoM/GB FVCOM because it allows us to start running a model at any arbitrary time with the correct tidal phases automatically set on the open boundary.

2.3.4 Monthly mean sea level and temperature and salinity conditions on the open boundary

ECOM-si uses monthly means for these parameters rather than a finer temporal resolution (i.e. at any point on the boundary, the value experiences an abrupt step change at the end of each month). Although we have hourly estimates, we decided to average the hourly estimates by month to give a forcing consistent with previous ECOM-si runs. We recommend that future runs use hourly estimates; we know the elevation is a particularly important forcing variable as it strongly affects velocity.

Sea level. We calculated monthly mean sea level at points along the open boundary by averaging hourly subtidal surface elevation that we obtained as simulation results output from a larger scale model (GoM/GB FVCOM GOM1 for 2006 and NECOFS FVCOM GOM3 for 2007). We chose this approach for seal level, temperature, and salinity rather than the "objective mapping method" of Jiang and Zhou (2008), because there were not sufficient observational data available for mapping. In comparison tests, we found that our approach was more convenient, less subjective, and gave more plausible circulation and hydrography results in Massachusetts Bay.

Year 2006 differed from 2007 in terms of monthly sea level on the open boundary (**Figure 2.5**). For example, the monthly mean sea level gradient in January implies that 2007 had a stronger outflow along Cape Cod and inflow from the northern coast of Massachusetts Bay. In February, the gradients near the middle of the boundary had different direction between years. In May through August, the patterns had similar shape but were quantitatively different.

Temperature and salinity. We calculated monthly mean water temperature and salinity at points along the open boundary (**Figure 2.6**) for each sigma layer by averaging the assimilated model output from the same larger scale models as for sea level. The GOM model for 2006 assimilated salinity, but since the 2007 hydrographic data were not available at the time when this modeling service was conducted, the GoM model for 2007 (used for this service) did not assimilate salinity. Hence the striking change in salinity between Dec 2006 and Jan 2007 in the figure might be caused by the inaccurate simulation of the salinity in 2007. The GoM model for 2007 updated with assimilation of salinity after this project completed. The result of salinity simulation in the interior is similar to the ECOM-si experiment with nudging (experiment C), we did not feel it was necessary to go back and correct this oversight for 2007 in this report. In comparing RCA and UG-RCA (unstructured grid version) for 2006-2008, the correction will be reported.

Years 2006 and 2007 showed subtle differences in temperature. For example, in January the water was much colder off Cape Cod and more strongly stratified in the interior along the boundary in 2006. Also, a subsurface warm region was found off the coast of New Hampshire in March 2006 but not in 2007. Two years are similar during the summer season, although the mixed layer thicknesses differed.

2.3.5 Assimilating the GoMOOS Buoy B measurements by nudging

Jiang and Zhou (2008) used a nudging algorithm in the 2005 model run. We followed that approach for 2006-2007 but also ran the model again without nudging as a sensitivity test (experiment A).

Hydrographic and current data used in the nudging assimilation for the 2006-2007 simulations were taken from the measurements at GoMOOS Buoy B. The water temperature and salinity were measured at water depths of 1, 20 and 50 m and the currents were at water depths of 2, 22 and 50 m (**Figures. 2.7 and 2.8**; velocity is rotated to be parallel to the nearby coast of Maine).

2.4 Initial conditions

The initial conditions for water temperature and salinity at 00:00 AM of January 1 2006 were specified using the assimilated model output on December 31 2005 from the 2005 ECOM-si run conducted by Jiang and Zhou (2008).

3 The 2006 and 2007 ECOM-si results

In experiments A-C listed in Table 1-1, we ran the model with or without nudging, and with or without a spatially detailed wind field. We compared the results of the model experiments to observations at locations consistent with previous MWRA modeling reports: temperature and salinity and velocity at GoMOOS Buoy A (**Figure 1.1**), and temperature and salinity at twelve stations from the MWRA monitoring network (Libby et al., 2009) listed below and mapped in **Figure 2.1**. The comparisons at these stations were made at about 2 m below the surface and at the following bottom depths:

Station	Average depth of bottom sample (m)	Attribute
F26	50	
F27	102	Offshore region close to the open boundary
F29	62	
N04	47	
N07	47	Interior of the Bay near 50m isobath
F17	73	
F31	13	
N01	29	Northwestern coastal area or shallower than 30m near Boston Harbor
N10	22	
F07	52	
F01	24	Middle and southern area of the bay
F02	30	

The water temperature and salinity are measured on the GoMOOS Buoy A at water depths of 1 and 50 m. We linearly interpolated the ECOM-si model-computed temperature and salinity to match those depths for the comparison before comparing with observed data. Currents are measured at water depths of 2 m and 50 m. We hourly-averaged the data and applied a 40-hour low-pass filter WHOI64 (Pawlowicz et al., 2002).

3.1 Experiment A: Single buoy wind without nudging

3.1.1 Exper A: Temperature and salinity at GoMOOS Buoy A

ECOM-si provided reasonable simulation results of the seasonal variation of water temperature and salinity at measurement depths of 1 and 50 m for both 2006 and 2007 (**Figure 3.1**, with RMS errors summarized in Table 3.1).

However, the model apparently underestimated warming and freshening at the surface during the spring and early summer, which caused the modeled water temperature to be much lower than observed in May through July in 2006 and in late April through April to October in 2007. At the 50-m depth, the model-predicted temperature was in reasonable agreement with the observation in 2006 but it was a few degrees higher after late April in 2007.

Table 3-1 RMS errors in temperature and salinity at GoMOOS Buoy A for three experiments.

		2006				2007					
		temperature		salinity		temperature		salinity			
		1m	50m	1m	50m	1m	50m	1m	50m		
A	Single buoy wind w/o nudging	2.10	1.06	1.05	0.15	4.03	1.94	1.00	0.96		
B	Single buoy wind w/ nudging	1.81	1.35	0.89	0.28	1.06	1.52	0.69	0.34		
C	MM5 wind w/ nudging	1.12	1.28	0.64	0.18	1.09	1.48	0.70	0.32	mean	p
	(A-B)/(A+B)/2)	0.15	-0.24	0.16	-0.60	1.17	0.24	0.37	0.95	0.27	0.22
	(B-C)/(B+C)/2)	0.47	0.05	0.33	0.43	-0.03	0.03	-0.01	0.06	0.17	0.06

Explanation of Table 3.1: The RMS errors are shown in the figures and listed again here. The units of RMS error are the same as the underlying variable, in this case degrees C or PSU.

Row A denotes results for this Section 3.1. Rows B and C relates to Sections 3.2 and 3.3, respectively. The next two rows compare the RMS error values for 2 models using Eq. 3.1. We color-coded those two rows as follows:

$x \geq +0.6$	RMS error improved by more than 60%
$+0.6 > x \geq +0.3$	RMS error improved by 30 to 60%
$-0.6 < x \leq -0.3$	RMS error worsened by 30 to 60%
$x \leq -0.6$	RMS error worsened by more than 60%

For example, the -0.60 for salinity at 50 m in 2006 means that experiment B was 60% worse than experiment A. The +1.17 for temperature at 1m in 2007 means that experiment B was 117% better than experiment A. The mean of the comparisons between experiments A and B is 0.27, which is not significantly different from zero in a 2-tailed one-sided t-test (p=0.22, N=8).

2006 surface Modeled salinity matched observed values during the winter season until late March, but the model failed to reproduce the substantial drop of salinity in May during which the peak runoff was measured in the upstream Merrimack River. This offset carried forward so that modeled salinity remained 1-2 PSU higher than observed during summer. The observed salinity showed a substantial drop in late November coincident with Merrimack River flow. This observed feature however, was not resolved in ECOM-si, even though the model did show a decreasing trend during that period. In this year, the temperature and salinity root-mean-square (RMS) errors were 2.10 ^{o}C and 1.05 PSU, respectively.

2006 bottom Model-predicted salinity was in excellent agreement with the observation during the entire year. Temperature and salinity RMS errors were small - only 1.06 ^{o}C and 0.15 PSU.

2007 surface Observed salinity slightly increased in late January through early February and then remained steady in mid-February through March. It then dropped rapidly from ~32 PSU to ~26 PSU in late April, rose back to ~30 PSU in May and then gradually increased over summer and fall. The drop of the salinity was correlated to a rapid increase of freshwater discharge at the Merrimack River. The ECOM-si-computed salinity captured the big drop in late April, but failed to

reproduce the gradual increasing trend in winter seasons and during summer through fall. Temperature and salinity RMS errors were 4.03 ^{o}C and 1.00 PSU, respectively.

2007 bottom — Modeled salinity matched with the observation in January but then remained lower through the entire year. The overall temperature and salinity RMS errors were 1.94 ^{o}C and 0.96 PSU, respectively, which were larger than those found in 2006.

3.1.2 Exper A: Subtidal currents at GoMOOS Buoy A

In both 2006 and 2007, the measurements showed that the most substantial variation of water currents occurred in late spring through early summer, during which the maximum subtidal currents at the buoy site reached ~60 cm/s near the surface (**Figure 3.2**; Table 3.2). This seasonal feature was captured by ECOM-si, but the model-predicted short-term variability of phases and magnitude of water currents significantly differed from the observations.

In 2006, the RMS current errors were 12.29 cm/s at 2 m and 6.17 cm/s at 50 m for *U* (east-west component) and 11.94 cm/s at 2 m and 5.20 cm/s at 50 m for *V* (north-south component). These errors were about 20% and 25-30% of the observed maximum velocities near the surface and bottom, respectively.

In 2007, the subtidal currents varied around 10-20 cm/s in most of the year, but they reached 40-60 cm/s in spring and early summer. The RMS current errors were 11.51 cm/s at 2 m and 5.20 cm/s at 50 m for *U* and 9.81 cm/s at 2 m and 5.27 cm/s at 50 m for *V*. These errors are the same order of uncertainty as reported in 2006.

Table 3-2 RMS errors in currents at GoMOOS Buoy A for three experiments,

		2006				2007					
		U (cm/s)		V (cm/s)		U (cm/s)		V (cm/s)			
		2m	50m	2m	50m	2m	50m	2m	50m		
A	Single buoy wind w/o nudging	12.29	6.17	11.94	5.02	11.51	5.20	9.81	5.27		
B	Single buoy wind w/ nudging	12.87	6.87	11.07	4.76	12.93	5.34	9.90	4.99		
C	MM5 wind w/ nudging	11.61	4.21	10.92	4.35	12.31	5.55	9.31	4.08	mean	p
	(A-B)/(A+B)/2)	-0.05	-0.11	0.08	0.05	-0.12	-0.03	-0.01	0.05	-0.02	0.58
	(B-C)/(B+C)/2)	0.10	0.48	0.01	0.09	0.05	-0.04	0.06	0.20	0.12	0.07

Explanation of Table 3.2: same as Table 3.1

3.1.3 Exper A: Temperature and salinity at MWRA monitoring stations

The results are shown in **Figures 3.3 to 3.6** and the RMS errors are summarized in Table 3.3. The orange shading in the table highlights the poorest fit. Averaged across parameters, the poorest fit was at station N10 in 2006, and F17 in 2007. Year 2007 had far more poor fits than 2006.

3.1.3.1 Sites F26, F27 and F29

(**Figures 3.3 and 3.5**). Near the surface, for both 2006 and 2007, ECOM-si provided reasonable simulations of water temperature in fall and winter seasons, but substantially underestimated the

surface warming during the summer. The model resolved the seasonal pattern of salinity for both years, but substantially under-predicted the salinity drop in spring of 2006, which is consistent with the simulation of the continuous data at GoMOOS Buoy A.

Near the bottom, the modeled seasonal patterns of water temperature and salinity were in good agreement with observations. In 2006, the modeled water temperature showed a reasonable agreement with observations at all three stations for much of the year except in the northeastern coastal region (F26 and F27) during winter and spring seasons. In this year, the modeled salinity matched well with the observations. In 2007, the modeled water temperature was in reasonable agreement with observations in winter and spring seasons, but substantially over-predicted a warming tendency near the bottom in summer through fall. In this year, the model substantially under-predicted the salinity off the coast.

3.1.3.2 Sites N04, N07 and F17

(**Figures 3.3 and 3.5**). Near the surface, the comparison results were very similar to the off-coastal stations F26, F27 and F29. The model captured well the seasonal pattern of water temperature and salinity, but substantially underestimated surface warming in July in 2006 and during May through September in 2007. The model captured a rapid drop of the salinity during spring of 2007 but failed to resolve such a drop in spring of 2006.

Near the bottom, the modeled water temperature and salinity were in good agreement with the observations in 2006, but they over-predicted warming in spring through fall and under-predicted salinity in much of 2007. These disparities were the same as those reported at off-coastal stations.

3.1.3.3 Sites F31, N01 and N10

(**Figures 3.4 and 3.6**). F31 is located in the Boston Harbor area where the water temperature was vertically well mixed through 2006 and 2007. At this station, the model-predicted surface and bottom water temperatures matched well with the observations for both years. In 2007, the observations showed a relatively substantial vertical stratification in summer resulting from the surface-bottom salinity difference at that station, but this stratification was not resolved in the model. As a result, salinities in late winter and fall were under-estimated by the model.

N01 and N10 are located around the 30-m isobath off Boston Harbor area where the water was stratified during the summer through fall for both years. The modeled surface water temperature and salinity agreed reasonably with observations at these two stations in 2006 and 2007, while the modeled bottom temperature showed a remarkable temporal variation during summer through fall of 2006. This feature, however, was not observed in the field. In 2007, the model overestimated vertical mixing at these two stations in summer through fall. As a result, the modeled bottom water temperature was much higher than observations during that period.

3.1.3.4 Sites F07, F01 and F02

(**Figure 3.4 and 3.6**). F07 is located around the 50-m isobath in the middle region of the Bay between Race Point, Cape Cod and Cape Ann, at the northern Massachusetts Bay boundary. The observations showed that the water at that point was vertically well mixed in January through May 2006 and then became strongly stratified in July through October 2006. Similar seasonal variability was also observed in 2007. At this station, the modeled surface seasonal variation pattern of water temperature agreed well with the observations for both 2006 and 2007, but in

2007 the model substantially under-predicted surface warming in summer and bottom salinity during the entire year.

F01 and F02 are located around the 30-m isobath in the southwestern and southeastern coastal regions of the Bay, respectively. The water at this station was vertically well mixed in winter, but strongly stratified in summer through fall in both 2006 and 2007. The model provided a reasonable simulation of surface water temperature and bottom salinity in 2006 as well as surface salinity in 2007, but in 2007 it substantially over-estimated bottom warming during summer through fall and under-estimated bottom salinity during the entire year. It is clear that ECOM-si seemed to overestimate the vertical mixing in the southern coastal region of the Bay during summer and fall seasons in 2007. As with N01 and N10, the model predicted a relatively strong temporal variation of the bottom water temperature during summer and fall seasons in 2006, but that feature was not observed in the survey data.

3.1.3.5 Summary

In summary, ECOM-si did a good job during the winter season but not during the seasonal transition periods. ECOM-si was able to capture a rapid surface salinity drop in spring of 2007 but not the gradual decrease rate of the surface salinity in spring through summer of 2006. Also, ECOM-si failed to capture an increase in surface water temperature for both 2006 and 2007. The key information obtained from the model-data comparison in this region is that the model did not capture the low frequency seasonal warming near the surface during the seasonal transition period in 2006 and 2007, over-predicted the warming tendency and under-predicted salinity near the bottom in 2007. It is clear that improvement of the open boundary condition is critical to ensure the success of the simulation in the interior of the Bay.

Table 3-3 RMS errors of temperature and salinity at MWRA monitoring sites for three experiments.

		A: Single buoy wind w/o nudging				B: Single buoy wind w/ nudging				C: MM5 wind w/ nudging			
		temperature		salinity		temperature		salinity		temperature		salinity	
year	Station	surface	bottom	surface	bottom	surface	bottom	surface	bottom	surface	bottom	surface	bottom
2006	F26	2.28	1.14	1.23	0.22	1.62	0.99	0.76	0.20	1.18	1.01	0.45	0.12
2006	F27	2.53	1.74	0.88	0.45	2.00	1.54	0.72	0.56	1.63	1.56	0.51	0.56
2006	F29	2.16	1.41	0.71	0.28	2.18	1.34	0.78	0.34	1.32	0.36	0.51	0.16
2006	N04	2.00	0.80	0.51	0.20	1.89	1.33	0.50	0.23	1.03	1.56	0.43	0.17
2006	N07	1.84	1.02	0.61	0.28	1.72	1.31	0.57	0.24	1.04	1.19	0.54	0.19
2006	F17	2.40	1.33	0.47	0.18	2.18	1.32	0.49	0.13	1.37	1.67	0.58	0.27
2006	F31	1.16	1.30	0.20	0.34	1.47	0.86	0.48	0.38	1.09	1.78	0.63	0.85
2006	N01	2.05	1.33	0.66	0.31	1.85	1.82	0.64	0.37	0.90	1.74	0.57	0.38
2006	N10	1.82	2.20	1.06	0.41	1.83	2.36	0.95	0.49	1.33	2.36	0.84	0.57
2006	F07	1.87	0.86	0.57	0.21	1.60	1.13	0.52	0.22	1.04	1.37	0.41	0.16
2006	F01	1.95	1.78	0.45	0.18	1.62	1.67	0.44	0.34	1.89	1.59	0.41	0.36
2006	F02	2.19	1.88	0.54	0.26	2.02	1.58	0.53	0.27	1.56	1.28	0.41	0.25
2007	F26	2.61	2.27	1.12	0.98	1.01	1.90	0.49	0.31	0.79	1.76	0.81	0.26
2007	F27	3.25	2.08	1.69	0.91	0.79	1.51	1.05	0.38	0.68	1.48	1.05	0.36
2007	F29	2.99	2.80	0.67	1.03	0.82	0.93	0.43	0.46	0.93	1.10	0.26	0.45
2007	N04	3.43	3.00	0.86	1.03	0.99	1.74	0.60	0.43	0.75	1.73	0.50	0.40
2007	N07	3.01	3.04	0.83	0.85	1.08	1.64	0.50	0.36	0.79	1.69	0.38	0.34
2007	F17	3.92	3.11	2.20	0.98	1.34	1.20	2.72	0.37	1.36	1.40	2.64	0.36
2007	F31	1.22	0.79	0.67	0.69	1.44	0.86	0.99	0.58	1.03	1.02	0.47	0.54
2007	N01	2.32	3.02	0.78	0.85	1.17	1.85	0.59	0.43	0.83	1.80	0.46	0.40
2007	N10	1.31	2.82	0.69	0.78	1.39	2.25	0.51	0.52	0.90	2.47	0.36	0.45
2007	F07	3.47	3.05	0.75	1.00	1.14	1.32	0.54	0.42	1.03	1.31	0.42	0.32
2007	F01	2.31	2.81	0.71	0.73	0.81	1.43	0.50	0.42	1.29	1.38	0.30	0.35
2007	F02	2.35	3.40	0.55	0.72	0.98	0.93	0.44	0.34	1.39	1.70	0.31	0.38
2006	avg	2.02	1.40	0.66	0.28	1.83	1.44	0.62	0.31	1.28	1.46	0.52	0.34
2007	avg	2.68	2.68	0.96	0.88	1.08	1.46	0.78	0.42	0.98	1.57	0.66	0.38
	avg	2.35	2.04	0.81	0.58	1.46	1.45	0.70	0.37	1.13	1.51	0.59	0.36

	Models A & B & C			
avg	1.65	1.67	0.70	0.43
90 pctile	2.52	2.81	1.05	0.85
80 pctile	2.18	2.20	0.83	0.57

Explanation of Table 3.3: We color-coded the worst 80th and 90th percentile RMS errors, calculating percentiles for a parameter and depth without regard to model.

percentile of the RMS error > 0.9 RMS error is 90th percentile or higher.

0.9 > percentile of the RMS error > 0.8 RMS error is 80th to 90th percentile.

For example, the upper left value of 2.28 for F26 surface temperature in 2006 is between 2.18 and 2.52, which are the 80th and 90th percentiles of surface temperature.

Table 3-4 Comparison between models of the RMS errors listed in Table 3.3

		Model A vs B				Model B vs C			
		temperature		salinity		temperature		salinity	
year	Station	surface	bottom	surface	bottom	surface	bottom	surface	bottom
2006	F26	0.34	0.14	0.47	0.10	0.31	-0.02	0.51	0.50
2006	F27	0.23	0.12	0.20	-0.22	0.20	-0.01	0.34	0.00
2006	F29	-0.01	0.05	-0.09	-0.19	0.49	1.15	0.42	0.72
2006	N04	0.06	-0.50	0.02	-0.14	0.59	-0.16	0.15	0.30
2006	N07	0.07	-0.25	0.07	0.15	0.49	0.10	0.05	0.23
2006	F17	0.10	0.01	-0.04	0.32	0.46	-0.23	-0.17	-0.70
2006	F31	-0.24	0.41	-0.82	-0.11	0.30	-0.70	-0.27	-0.76
2006	N01	0.10	-0.31	0.03	-0.18	0.69	0.04	0.12	-0.03
2006	N10	-0.01	-0.07	0.11	-0.18	0.32	0.00	0.12	-0.15
2006	F07	0.16	-0.27	0.09	-0.05	0.42	-0.19	0.24	0.32
2006	F01	0.18	0.06	0.02	-0.62	-0.15	0.05	0.07	-0.06
2006	F02	0.08	0.17	0.02	-0.04	0.26	0.21	0.26	0.08
2007	F26	0.88	0.18	0.78	1.04	0.24	0.08	-0.49	0.18
2007	F27	1.22	0.32	0.47	0.82	0.15	0.02	0.00	0.05
2007	F29	1.14	1.00	0.44	0.77	-0.13	-0.17	0.49	0.02
2007	N04	1.10	0.53	0.36	0.82	0.28	0.01	0.18	0.07
2007	N07	0.94	0.60	0.50	0.81	0.31	-0.03	0.27	0.06
2007	F17	0.98	0.89	-0.21	0.90	-0.01	-0.15	0.03	0.03
2007	F31	-0.17	-0.08	-0.39	0.17	0.33	-0.17	0.71	0.07
2007	N01	0.66	0.48	0.28	0.66	0.34	0.03	0.25	0.07
2007	N10	-0.06	0.22	0.30	0.40	0.43	-0.09	0.34	0.14
2007	F07	1.01	0.79	0.33	0.82	0.10	0.01	0.25	0.27
2007	F01	0.96	0.65	0.35	0.54	-0.46	0.04	0.50	0.18
2007	F02	0.82	1.14	0.22	0.72	-0.35	-0.59	0.35	-0.11
2006	avg	0.10	-0.03	0.07	-0.13	0.35	-0.01	0.16	-0.07
2007	avg	0.85	0.59	0.21	0.71	0.10	-0.07	0.16	0.09
	avg	0.47	0.34	0.15	0.45	0.25	-0.04	0.16	0.02

Model A vs B		Model B vs C	
avg	p	avg	p
-0.03	0.96	0.03	0.34
0.50	0.02	0.06	0.26
0.31	0.02	0.04	0.25

Explanation of Table 3.4: The upper left value of 0.34 of F26 surface temperature in 2006 is (2.28-1.62) / ((2.28+1.62)/2) which is Eq. 3.1 applied to models A and B. We color-coded the cells with the same color scheme as Table 3-1, repeated here for convenience:

x > + 0.6	RMS error improved by more than 60%
+ 0.3 > x > + 0.6	RMS error improved by 30 to 60%
– 0.3 < x < – 0.6	RMS error worsened by 30 to 60%
x < – 0.6	RMS error worsened by more than 60%

The mean of all the comparisons between models A and B is 0.31, which is significantly different from zero in a 2-tailed one-sided t-test (p=0.02, N=8).

3.2 Experiment B: Single buoy wind with nudging

Experiment B is like Experiment A, but with nudging. We nudged ECOM-si's boundary assumptions with measurements of water temperature, salinity and currents at GoMOOS Buoy B with the intention of improving the water and mass transport from the northern coastal open boundary.

To compare the RMS errors between two experiments (for example the model runs with and without nudging assimilation), we define the change of RMS error in percent between these two experiments as

$$\Delta\mathrm{RMS} = \frac{\mathrm{RMS}(\text{experiment 1}) - \mathrm{RMS}(\text{experiment 2})}{(\mathrm{RMS}(\text{experiment 1}) + \mathrm{RMS}(\text{experiment 2}))/2} \times 100\% \qquad (3.1)$$

This ratio is used for all variables included in the model-data comparison. It can range in value from -200% to +200%.

3.2.1 Exper B: Temperature, salinity, and currents at GoMOOS Buoy A

2006 (**Figures 3.1**; Table 3.1,). Nudging only slightly improved RMS error for surface temperature and salinity by 15% and 16%, respectively. RMS error for bottom temperature and salinity worsened by 24% and a remarkable 60%,

(**Figure 3.2**; Table 3.2). Negligible effect on RMS error for currents.

2007 (**Figure 3.1**; Table 3.1). Nudging improved RMS error for surface temperature and salinity by 117% and 24%. Bottom temperature and salinity also improves, by 24% and 95%. Such improvements suggest that waters in the northwestern region of the Bay were strongly affected by conditions at the northwestern open boundary.

(**Figure 3.2**; Table 3.2). Negligible effect on RMS error for currents.

Overall, at the GoMOOS A Buoy the nudging assimilation improved the RMS error of temperature and salinity together by 27%, and worsened that of currents by 2%. Neither change was significantly different from zero in a one-sample t-test.

3.2.2 Exper B: Temperature and salinity at MWRA monitoring stations

Table 3.3 lists the RMS errors and Table 3.4 shows how those errors changed after including nudging in the model. In 2006, the RMS error of temperature and salinity changed little with nudging, with only a few stations showing changes for better or worse. In 2007 there were substantial improvements at all stations except F31. In both years, averaging the change across parameters and depths, F26 was the station most improved by nudging, and F31 was the station most worsened. Overall, nudging significantly improved the RMS error by 31% (p=0.02).

Figures 3.3 to 3.4 show the results for 2006, and **Figures 3.5 to 3.6** show the results for 2007.

3.3 Experiment C: MM5 wind with nudging

Experiment C is like experiment B but with a spatially variable wind field (both are nudged, and both use hourly wind data). Before we compare the results of the experiments we begin with a description of the spatial variability of wind on a monthly-average basis and then during a snapshot of several storms.

3.3.1 Notable winds patterns in 2006 and 2007

3.3.1.1 Monthly averaged wind velocity and RMS variation ellipses

Figure 3.7 shows the fields of monthly averaged wind velocity vector and its RMS variation ellipses. These were calculated using the hourly output wind data from MM5 (for 2006) and WRF (2007).

Note: in the figure the ellipse is positioned at the tail of the wind vector so that this sketch example represents substantial east-west variability with a mean residual northwesterly wind. By definition, northwesterly wind moves in a southeastward direction.

The main conclusion is that there is little or no spatial variability in wind on a monthly-average time scale. Although the months and years differ substantially, the ellipses and residuals look similar within a month (spatially uniform), apart from the pattern of lighter winds closer to and on land.

It is also worth noting that the mean wind was noticeably greater than wind variability in Feb 2007 (i.e. the residual vector protrudes from the ellipse). Apart from Feb-Mar 2006 and Jan-Mar 2007 the mean generally tended to be smaller than the variability

3.3.1.2 Storms and short-term spatial wind variations

Although spatial variability is masked by monthly-averaging, it may be apparent at any particular time. We therefore next looked at snapshots of the wind field during storms, because their stronger winds would have greater effect on water circulation.

There were a total of 28 and 30 storms or cold front passages in 2006 and 2007 that affected the northeastern coastal region (**Figure 3.8**). Most of these storms came from southwest and west directions and passed over the Gulf of Maine region or nearby the region over a time scale of a few days. Based on the storm definition (with wind stress of > 0.2 Pa and duration of > 12 hours) used by Butman et al. (2008), 25 events in 2006 and 20 events in 2007 reached the storm level (Table 3.5).

Table 3-5 Statistics of storms affecting Massachusetts Bay.

date	hour	Duration (h)	Iwinds (Pa*h)	A-stress (Pa)	MaxStress (Pa)	Vawsm (Pa)	Direction (degree)
01/03/06	11	28	8	0.3	0.42	0.29	34
01/15/06	06	53	20	0.39	0.77	0.38	307
01/18/06	06	14	5	0.4	0.72	0.39	133
01/18/06	22	16	4	0.28	0.45	0.26	240
01/31/06	12	16	5	0.34	0.5	0.33	20
02/06/06	04	13	3	0.28	0.37	0.28	233
02/12/06	05	30	13	0.46	0.89	0.38	9
02/17/06	14	18	7	0.44	0.75	0.37	264
02/18/06	14	21	6	0.33	0.5	0.32	301
02/24/06	12	18	6	0.38	0.65	0.37	307
02/26/06	19	35	10	0.31	0.43	0.3	297
02/28/06	17	14	4	0.29	0.4	0.28	277
03/03/06	10	29	8	0.31	0.44	0.31	306
03/14/06	23	33	10	0.31	0.57	0.3	278
03/20/06	21	15	3	0.25	0.33	0.25	305
05/02/06	00	21	6	0.3	0.4	0.3	30
05/09/06	12	24	7	0.3	0.44	0.28	19
05/14/06	08	15	4	0.32	0.41	0.3	82
10/21/06	00	15	6	0.45	0.72	0.45	279
10/28/06	09	14	7	0.5	0.75	0.49	124
10/29/06	02	40	14	0.35	0.6	0.34	245
11/23/06	02	35	12	0.37	0.75	0.36	26
12/01/06	23	14	4	0.34	0.7	0.26	233
12/02/06	15	15	4	0.3	0.41	0.3	283
12/08/06	05	25	8	0.36	0.5	0.35	301
01/10/07	17	16	4	0.26	0.29	0.25	293
01/19/07	18	49	18	0.38	0.81	0.37	298
01/26/07	03	25	7	0.29	0.43	0.29	313
02/05/07	00	39	16	0.41	0.89	0.41	277
02/08/07	06	32	9	0.3	0.5	0.29	268
02/15/07	01	60	26	0.44	0.85	0.43	274
02/19/07	00	26	10	0.41	0.65	0.41	304
02/23/07	19	24	8	0.34	0.64	0.34	318
03/05/07	21	36	15	0.42	0.67	0.42	296
03/16/07	07	26	10	0.39	0.58	0.39	40
03/18/07	07	17	4	0.25	0.34	0.24	274
04/08/07	20	19	5	0.27	0.36	0.27	273
04/15/07	20	19	11	0.6	1.1	0.6	94
04/17/07	07	35	14	0.42	0.69	0.41	16
05/18/07	10	21	5	0.27	0.33	0.26	13
11/03/07	08	27	14	0.53	1.13	0.43	356
11/16/07	11	30	9	0.32	0.53	0.32	288
12/01/07	01	26	8	0.34	0.73	0.29	298
12/03/07	21	29	10	0.37	0.56	0.37	290
12/17/07	02	33	12	0.37	0.7	0.35	283

We selected four examples each year to demonstrate the spatial variation of the wind field. Some of these examples were not included in Table 3.5 because they did not actually reach the storm level as defined by Butman et al. (2008). A brief description of the wind field for these examples is given below.

Figure 3.9a: April 4, 2006 11:00 EST. A surface low-pressure system swept over Massachusetts Bay. The low-pressure center was located over the land north of the Bay (low pressure = blue shading; warm temperature; counterclockwise rotation). The wind velocity was opposite in the northern and southern regions of the Bay. In the southern region, it featured a convergence zone of northwesterly and southwesterly winds, while in the northern region it was dominated by southeasterly wind.

Figure 3.9b: June 8, 2006 17:00 EST. A cold air front passed Massachusetts Bay, pushing a low-pressure center east to the western Gulf of Maine region. The northern region of the Bay featured northerly wind while the southern region was dominated by northwesterly wind, even though the wind speed was similar over the entire Bay.

Figure 3.10a: July 13, 2006 8:00 EST. An air front passed the northern part of the Gulf of Maine. The northern region of Massachusetts Bay was dominated by the northerly wind with increasing speed southward, while the southern region featured westerly or southwesterly wind. The two distinct wind vectors in northern and southern regions caused a strong convergence zone in the middle area of the Bay.

Figure 3.10b: August 20, 2006 14:00 EST. A low pressure was found over the northwestern region of the Gulf of Maine. The northern region of Massachusetts Bay featured a weak westerly wind, while in the southern region was dominated by relatively strong southwesterly and southerly winds. A wind convergence zone was located in the northern area of the Bay.

Figure 3.11a: April 5, 2007 5:00 EST. A storm moved northeastward to pass Nantucket Sound. A low-pressure center was located in Nantucket Sound, which produced a strong cyclonic (counter clockwise) wind velocity in Massachusetts Bay. The southern region of the Bay featured strongly southeasterly or easterly wind, while the northern region was dominated by strongly northeasterly wind.

Figure 3.11b: May 19, 2007 11:00 EST. A cold air front was passing Massachusetts Bay. A weak low-pressure center was in the interior of the Gulf of Maine. The northern region of Massachusetts Bay was dominated by northerly wind, while the southern region featured northwesterly wind, although the wind speeds were similar in northern and southern regions.

Figure 3.12a: June 4, 2007 17:00 EST. An air front appeared over the land area, which produced the cyclonic wind field in Massachusetts Bay. The southern region of the Bay was dominated by southerly winds, while the northern region featured southeasterly winds.

Figure 3.12b: October 12, 2007 2:00 EST. An air front was located over the land west of Massachusetts Bay, which produced the cyclonic wind field in the Bay. The southern region of the Bay was dominated by the southwesterly and southerly winds, while the northern region featured southeasterly winds. The wind speed was much larger in the northern region than in the southern region.

It is clear from these examples that the wind can vary substantially in space over Massachusetts Bay during storm and air front events. The variation depends on the location and intensity of the storm and cold air fronts. This spatial wind variation has not been included in previous

ECOM-si modeling experiments in Massachusetts Bay because due to unavailability of such the wind field data.

3.3.2 Exper C: Temperature, salinity, and currents at GoMOOS Buoy A

In 2006, using the spatially non-uniform winds to drive ECOM-si substantially improved the modeled temperature and salinity at the GoMOOS Buoy A (**Figure 3.1** and Table 3.1). The RMS errors reduced by 47% and 5% in the surface and bottom temperatures and 33% and 43% in the surface and bottom salinities. In this experiment, the model provided a better simulation of the warming tendency at the near surface in late spring through summer and the freshening tendency near the surface in spring and early summer. This suggests that the spatial variability of the wind should be taken into account.

In 2007, however, there was negligible change in RMS error of temperature and salinity at this buoy site after adding the spatially non-uniform winds (**Figure 3.1**;Table 3.1).

Overall the RMS error improved by 17% (p=0.06)

Table 3.2 shows that the spatial wind field improved the eastward velocity at 50m by 48% in 2006, but otherwise negligible change.

Overall, the improvement was 12% (P=0.07).

3.3.3 Exper C: Temperature and salinity at MWRA monitoring stations

Table 3.4 shows that overall, the spatial wind field did not change the RMS errors (+4%, p=0.25).

The stations most improved in 2006 and 2007 were F29 and F31, respectively. The stations most degraded in 2006 and 2007 were F31 and F02, respectively.

Figures 3.3-3.4 show the results for 2006, and **Figures 3.5-3.6** show the results for 2007.

3.3.4 Exper C: Spatial distributions of currents, temperature and salinity

Those comparisons were based on temporal data. A better comparison may be based on spatial data. Here we describe the spatial patterns resulting from the four cases selected in section 3.3.1.2 that relate to storm or cold air frontal passages. We present the difference of modeled surface currents, temperatures and salinities from Experiments C and B (spatial wind case minus the single-buoy wind case; both were nudged). The difference represents features that were seen in the model when using non-uniform spatial wind, but not resolved when using uniform single-buoy wind.

3.3.4.1 Currents - 2006

Figure 3.13. April 4, 2006. The current difference from these two cases showed that there was a relatively strong inflow from off-coastal region to Massachusetts Bay, which was not resolved in the modeling case with the single buoy wind. The magnitude of the current difference was ~10 cm/s or larger.

Figure 3.14. June 8, 2006. The current difference suggested that there were relatively strong northeastward currents along the northern coast of Massachusetts Bay, remarkable offshore currents along the western Massachusetts Bay coast and outflow around Cape Cod. These currents were ~5-20 cm/s and again, were not resolved in the case with the single buoy wind.

Figure 3.15. July 13, 2006. The current difference showed that a coastal inflow of ~10-20 cm/s entered into Massachusetts Bay along the northwestern coast and continuously moved westward and then southward along the coast. A cyclonic current pattern appears in the southern region of Massachusetts Bay. This current was underestimated with the single buoy wind.

Figure 3.16. August 20, 2006. The spatially non-uniform wind field also predicted stronger southward along-coast currents on the western Massachusetts Bay coast as well as the stronger inflow and outflow around the northern coast and Cape Cod.

3.3.4.2 Temperature - 2006

Those differences in surface currents caused differences surface temperature (again, Experiment C minus Experiment B):

Figure 3.17, April 4, 2006. Compared to the single-buoy wind case, the spatial wind case predicted warmer surface water in the middle region and colder water in some coastal regions. It also produced much colder water along the northern coastal area north of Massachusetts Bay, likely due to stronger mixing in that area.

Figure 3.17, June 8, 2006. The surface water temperature in the entire Bay region was about 1.0 ^{o}C or higher with spatial wind than single buoy wind. On that day, downwelling-favorable wind prevailed over the Bay, which produced relatively strong southwestward current against the western coast. The offshore-coastal currents displayed in the current difference in the two cases with single and spatially non-uniform winds suggests that the single buoy wind overestimated the flow towards the coast in this case. This overestimated horizontal currents caused the surface water to be colder than that observed in the spatially non-uniform wind case.

Figure 3.17, July 13, 2006. The surface water temperature was warmer with spatial winds in most of the Bay except in the southwestern coastal region. The stronger northeastward wind predicted by MM5 produced stronger mixing in the southern region of the Bay and formed a colder water zone in that area. This event was not resolved in the single buoy wind case.

Figure 3.17, August 20, 2006. The southern region was dominated by an off-coast upwelling-favorable wind and northern region featured an offshore eastward wind. This spatially variation wind produced the colder region along the coastal region. This colder zone was underestimated in the single buoy wind case.

3.3.4.3 Salinity - 2006

The response of the salinity field to spatial variation in the wind field is similar to that of the temperature field:

Figure 3.18b. June 8, 2006. On this day, for example, the strong southwestward wind brought more upstream fresher water into the northern coastal area and more energetic mixing in the near-coastal regions. As a result, the salinity along the coast north of Cape Ann was much lower with spatial winds.

Figure 3.18d. August 20, 2006. The modeled salinity in the coastal area was lower with spatial winds, probably due horizontal advection from offshore.

3.3.4.4 Currents - 2007

Figure 3.19. April 5, 2007. The storm-generated wind has opposing directions in the northern and southern regions of Massachusetts Bay. As a result, the modeled surface currents in the spatially non-uniform wind case differed substantially from the currents in the single buoy wind case. The northwestward wind in the southern region produced a relatively strong off-Cape Cod flow. This flow was not resolved in the single buoy wind case.

Figure 3.20. May 19, 2007. The wind increased its speed from the northern region to the southern region, which intensified the southward currents near the surface and outflow around Cape Cod.

Figure 3.21-22. June 4, 2007 and October 12, 2007. The wind field was cyclonic over the Bay. That enhanced the southward current in the interior of the Bay and thus outflow around Cape Cod.

3.3.4.5 Temperature - 2007

Figure 3.23a. April 5, 2007. The surface water was colder in the northern region and warmer in the southern region (Figure 3.64a). A relatively colder zone also appeared east of Cape Cod due to storm-induced stronger mixing.

Figure 3.23b. May 19, 2007. The wind pushed the surface convergence toward the southern coast of the Bay. The enhanced wind speed in the southern region also caused stronger vertical mixing to form the colder water zone on the southern coast.

Figure 3.23c. June 4, 2007. All regions of Massachusetts Bay were colder with spatial winds except near the central area where the center of the cyclonic wind field was located. The colder water was mainly due to enhanced local vertical mixing.

Figure 3.23d. October 12, 2007. The entire Bay surface was colder in the spatial non-uniform wind case, with the largest temperature difference in the southwestern coastal region. That was also consistent with the spatial cyclonic wind distribution observed on that day.

3.3.4.6 Salinity - 2007

Figure 3.24. Storm-enhanced vertical mixing was also evident in the spatial distribution of the salinity. During these four storm cases, the surface salinity in most of the Massachusetts Bay region was higher in the spatially non-uniform wind case than in the single buoy wind case.

These examples demonstrate that the spatial variation of the wind field can have a substantial influence on the temporal and spatial variation of currents, water temperature and water salinity as well as vertical mixing and horizontal advection. This argues in favor of including this spatial wind variation in future model simulations.

3.4 Spatial distribution of observed versus Experiment-A-computed temperature and salinity

In previous Section we compared the observations with the ECOM-si model results of Experiment A. That was a comparison of time series at fixed locations. Now we compare them spatially at fixed times, again with model results from Experiment A.

To give a fairer comparison we smoothed the model time series (with an M_2 tidally averaging filter) centered on a time close to the middle time of each hydrographic survey. In 2006, four examples were selected: survey periods of February 10-13, April 11-14, June 19-21 and August 21-24. In 2007, three examples were chosen: survey periods of April 21-22, June 18-20 and August 20-22. The comparisons were made for surface measurements. The modeled temperature and salinity were from the first sigma layer, where the temperature and salinity were calculated at the mid-point of that layer. The thickness of the first sigma layer was 0.01. This means that the temperature and salinity was calculated at 0.7 m below the surface at the 140-m isobath. Therefore, the model output in this layer should be very close to the surface.

Figure 3.25. February 10-13, 2006. Data and model agree that there is a colder and fresher area in the Boston Harbor area and southwestern coastal region, and warm and saline water in the middle and off-coastal regions. The model results, however, are about 1 ^{o}C colder than observations near shore.

Figure 3.26. April 11-14, 2006. The observations show warm and less saline water in Boston Harbor and cold and saline water in the middle and off-coastal regions. This pattern was also resolved by ECOM-si, though the temperature and salinity values were different.

Figure 3.27. June 19-21, 2006. Data and model show fresher waters in Boston Harbor and around Cape Ann. However, the model overestimated the freshening in Boston Harbor and underestimated the low-salinity water intrusion around the northern coastal region. Modeled temperature was a few degrees lower than the observations.

Figure 3.28. August 21-24, 2006. Data and model show the same salinity pattern, but modeled temperature differed substantially from the observations. The model is too warm in Boston Harbor and nearby.

Figure 3.29. April 21-22, 2007. The model showed a big low-salinity water intrusion from the Merrimack River into Massachusetts Bay. Less so for the data. The model is too cold in its low-salinity water intrusion, and too fresh in Boston Harbor.

Figure 3.30. June 18-20, 2007. The modeled salinity was much lower than observed in Boston Harbor and higher in the rest of the Bay. Modeled temperature was much too cold.

Figure 3.31. August 20-22, 2007. The model and observations were very different. The model is too cold and too fresh.

In summary, ECOM-si was able to capture the general spatial distribution patterns of temperature and salinity in much of the year. However, the modeled values were substantially different from the observations, a conclusion which is consistent with the results of our earlier comparison of the time series of field data and model runs for Experiment A (no nudging; single buoy wind). (We did not have time to conduct this kind of spatial comparison for data versus Experiments B and C.)

3.5 Noteworthy cooling events: buoy observations versus Experiment-A-computed temperature

Dr. Rocky Geyer (WHOI) compared surface water temperature data from NOAA Buoy 44013 to meteorological data to infer the cause of noteworthy cooling events (33-hour low passed temperature drop > 1.2 ^{o}C/day) that occurred at the buoy (section 4.1 of Libby et al. 2009). Geyer concluded that upwelling was responsible for most of the cooling events, but that wind-induced mixing and effect of cold air were also important.

We plotted Geyer's noteworthy cooling vents as blue dots in **Figure 3.32** overlaying the buoy data, and also plotted the ECOM-si model results from Experiment A. The model results are disappointing. It failed to capture most of the rapid temperature drops seen in the buoy measurements. Although the model results often moved in the right direction, they did not move far enough. A further examination should be made to find the cause of this failure. The problem may lie with the external forcing used to drive the model, particular regarding the methods used to calculate sensible and latent heat fluxes.

4 FVCOM and ECOM-si comparison

In this Section we compare results from ECOM-si to those from a version of FVCOM applied to Massachusetts Bay. We ran the comparison for year 2005, and denote these tests as Experiments D and E in Table 1-1.

4.1 The hydrodynamic model FVCOM

FVCOM is an unstructured-grid, finite volume, 3-D, free surface primitive equation coastal ocean model developed originally by Chen et al. (2003). FVCOM has similarities with and differences from ECOM-si, which we described in Section 2.1.

4.1.1 Similarity to ECOM-si

The governing equations used in FVCOM are the same as in ECOM-si. Both are composed of external and internal modes that are computed separately using two split time steps.

Like ECOM-si, FVCOM uses the modified MY-2.5 and Smagorinsky turbulent closure schemes for vertical and horizontal mixing, respectively.

4.1.2 Difference from ECOM-si

The major difference from ECOM-si and POM is that FVCOM is solved numerically by the flux calculation in an integral form of the governing equations over non-overlapping, unstructured triangular grids. Flux calculation ensures the conservation of mass and momentum over individual control volumes and thus the entire computational domain. The finite-volume numerical approach combines the advantage of finite-element methods for geometric flexibility and finite-difference methods for simple discrete code structure and computational efficiency.

FVCOM's triangular grids fit irregular coastlines more readily than ECOM-si's rectangular grid.

4.1.3 More updates and improvements in FVCOM than in ECOM-si

The General Ocean Turbulence Model (GOTM) developed by Burchard's research group in Germany (Burchard, 2002) was implemented to FVCOM to provide optional vertical turbulence closure schemes. Unlike ECOM-si, FVCOM features a generalized terrain-following hybrid coordinate in the vertical (Pieterzak et al., 2002). This vertical coordinate system allows for uniform thickness vertical layers near the surface and bottom over the slope with a smooth transition to the topography-following layers in the inner shelf and estuaries. That is critical to resolving the wind-driven surface mixed layer and sloping bottom boundary layer.

Furthermore, the present version of FVCOM contains several new modules, such as a semi-implicit solver, non-hydrostatic dynamics (Lai et al. in revision), advanced data Kalman Filter data assimilation packages developed by P. Malanotte-Rizzoli and her MIT colleagues, an unstructured-grid surface wave model (FVCOM-SWAVE) (Qi et al., 2008), and a sea ice model modified from the Los Alamos sea ice model (CICE; Hunke and Lipscomb 2008), a sediment model (FVCOM-SED) derived from the USGS community sediment model by G. Cowles, and a EPA-based water quality model (Zheng et al., 2004). An automatic nesting grid system is also implemented to FVCOM, which allows two different horizontal FVCOM runs through the nested boundary without need of interpolation from one to another.

Built with FVCOM as a core model, we have developed an integrated atmospheric-ocean model system called the "Northeast Coastal Ocean Forecast System (NECOFS)" for the northeast US coastal region with a computational domain stretching from the south of Long Island Sound to the northeastern part of the Scotian Shelf. This system includes 1) two regional meso-scale meteorological models (MM5 and WRF), and 2) GoM/GB FVCOM, and FVCOM-SWAVE. This system is in operation to provide 3-day forecast fields of water temperature, salinity, currents, surface elevation and other variables.

FVCOM has a Message-Passing-Interface parallelized model updated by the team effort of scientists at the University of Massachusetts-Dartmouth (UMASSD) and Woods Hole Oceanographic Institution (WHOI) (Chen et al., 2006a, b).

4.2 The computational domain, resolution and time step

In this report we used the first generation FVCOM[3] to provide a more fair comparison with MWRA's version of ECOM-si, but we have operational versions with higher resolution. The configuration of the first-generation GoM/GB FVCOM grid covered the entire GoM region with horizontal resolution of 1-2 km in Massachusetts Bay (**Figure 4.1**). A hybrid vertical coordinate was used in the vertical. There are total of 30 layers. In the region deeper than 60 m, the first five and last five layers were specified as spatially uniform layers with a thickness of 2 m. In the region shallower than 60 m, the sigma-coordinate was used, which has a smooth transition at the 60-m isobath with uniform vertical layer thickness of 2 m. The time step is 12 seconds for external mode and the ratio of the internal time step to the external time step was 10. This produces an internal time step of 120 seconds.

4.3 Forcing data

The forcing data (Table 4-1) are similar to those listed in Table 2-1, except that FVCOM does not require that the boundary elevation, temperature, and salinity be monthly-averaged. Instead, these come directly from the regional model without averaging. Otherwise, both models use the same meteorological forcing, freshwater discharges, tidal forcing, nudging, and initial conditions.

[3] http://fvcom.smast.umassd.edu

Table 4-1 Data used for external forcing of FVCOM and ECOM-si for 2005 Experiments D and E.

Parameters	Temporal averaging of forcing data for ECOM-si	Temporal averaging of forcing data for FVCOM	Source
Solar radiation	Hourly	Hourly	Primary: WHOI pyranometer. Secondary: MM5 with correction of satellite data
Air pressure Air temperature Winds	Hourly	Hourly	Primary: NOAA Buoy 44013 Secondary: Logan Airport
Spatially variable winds	Hourly	Hourly	MM5
Humidity	Hourly	Hourly	Logan Airport
River discharges	Daily	Daily	USGS
Outfall effluent flow	Daily	Daily	MWRA
Tidal forcing	12 minutes	12 minutes	Tidal prediction submodel
Boundary elevation, temperature, salinity	monthly	No averaging	Output from GoM/GB FVCOM
Nudging: GoMOOS Buoy B temperature, salinity, currents	Hourly	Hourly	University of Maine

4.4 Model – data comparisons for two models (Experiments D and E)

Comparisons are presented here for 1) temperature and salinity at the USGS buoy LT-A (Butman et al. 2009); 2) spatial distribution of surface water temperature and salinity during the May 2005 hydrographic survey period, and 3) Lagrangian particle trajectories. A detailed description of each case is given below.

USGS Buoy LT-A. FVCOM provides a more reasonable simulation of the water temperature and salinity at depths of 8 and 29 m (**Figure 4.2**). For example, ECOM-si failed to resolve the temperature drop in July, while this drop was captured by FVCOM. Also, the observations showed a rapid temperature rise in mid-August, which was resolved by FVCOM but not by ECOM-si. The biggest improvement in the RMS errors was for temperature at 29 m, where the error for FVCOM was 77% better than that for ECOM-si. Overall FVCOM was 54% better than ECOM-si ($p = 0.03$).

Table 4-2 RMS errors in temperature and salinity at USGS Buoy LT-A for two experiments.

		2005					
		temperature		salinity			
		8m	29m	8m	29m		
D	ECOM-si	1.62	0.52	0.39	0.27		
E	FVCOM	1.41	0.23	0.21	0.14	mean	p
	(D-E)/(D+E)/2)	0.14	0.77	0.60	0.63	0.54	0.03

Explanation of Table 4-2: same as Table 3.1.

T-S distributions in May 2005. In Section 3.4 we compared model to data by choosing a snapshot of the model results at a time equal to halfway through the survey. That was the simplest approach, and probably sufficient for a 2-3 day survey, but the red tide of 2005 prompted MWRA to conduct broad surveys throughout May 2005, so for that month we chose model results at a point and time coincident with the time of sampling that point.

FVCOM-computed temperature and salinity provided better agreement with observations than ECOM-si (**Figure 4.3**). Possibly due to open boundary issues, ECOM-si was too warm and too fresh outside of Massachusetts Bay.

Lagrangian drifter trajectories. James Manning of NOAA NEFSC released three near-surface drifters inside Massachusetts Bay in 2005 (Manning et al., 2009).

drifter ID	released (GMT)	retrieved (GMT)	duration tracked	depth
56202	6/28/2005 13:12h	7/10/2005 14:56h	12 days	drogued 4 m
57201	7/18/2005 14:52h	7/24/2005 20:24h	6 days	surface (1 m)
57202	7/18/2005 14:40h	7/23/2005 10:40h	5 days	surface (1 m)

Drifters #57201 and #57202 were released at different times on the same day, but their trajectories were substantially different, which suggests that the movement of drifters was very sensitive to the temporal and spatial variation of the currents. Both observed and model-predicted drifter trajectories were filtered by 40-hour low-passed filters and comparisons were made only for the low-frequency paths after filtering.

For drifter #56202, both FVCOM and ECOM-si predicted the correct direction of the drifter movement during the tracking period (**Figure 4.4**). The difference is that FVCOM showed the same clockwise rotation loop after the drifter was released, while ECOM-si did not. It seems that ECOM-si showed a more linear current pattern than FVCOM in this case, which caused the endpoint of the drifter track predicted by ECOM-si to be far away from the observed endpoint. For drifter #57201, the drifter moved eastward first and then turned northward. This trajectory path was captured by FVCOM but not by ECOM-si (**Figure 4.5**). The ECOM-si predicted drifter moved eastward first and then turned southward, in an opposite direction to the observation. Similar results were also shown for drifter #57202, which moved eastward first and then rotated clockwise in the off-coastal region (**Figure 4.6**). This feature was captured by FVCOM, but not by ECOM-si. The ECOM-si-predicted drifter moved in the same direction first

and then turned southward. The trajectories of drifters predicted by ECOM-si for drifters #57201 and #57202 were very similar, suggesting that ECOM-si did not resolve the spatial variation of the surface currents.

The poorer drifter prediction from ECOM-si (compared to FVCOM) may arise because it has much coarser horizontal resolution and the monthly averaged condition of water property and sea level at open boundary, plus its bottom bathymetry is heavily smoothed to match that coarse horizontal resolution.

5 Summary and conclusions

We provided several comparisons between model and data, between two models, and between two model's ability to fit the data.

	type	basis for comparison of model performance	nudging vs not nudging	spatial vs uniform winds	FVCOM vs ECOM-si
Fig 3.1 Tbl 3.1	time series	GoMOOS Buoy-A temperature and salinity	+27% (p=0.22)	+17% (p=0.06)	
Fig 3.2 Tbl 3.2	time series	GoMOOS Buoy-A currents	+ 2% (p=0.58)	+12% (p=0.07)	
Fig 3.3-3.6 Tbl 3.3-3.4	time series	Monitoring station temperature and salinity	+31% (p=0.02)	+ 4% (p=0.25)	
Fig 3.13-3.16, 3.19-3.22	map	Model-model difference in currents		suggested improvement	
Fig 3.17-3.18, 3.23-3.24	map	Model-model difference in temperature and salinity		suggested improvement	
Fig 3.25-3.31	map	Monitoring station temperature and salinity	Data compared to model without nudging and with uniform wind. Model captures general patterns only.		
Fig 3.32	time series	NOAA Buoy 44013 temperature	Data compared to model without nudging and with uniform wind. Model fails to capture noteworthy storm mixing.		
Fig 4.2, Tbl 4.2	time series	USGS Buoy LT-A temperature and salinity			+54% (p=0.03)
Fig 4.3	map	Monitoring station temperature and salinity			suggested improvement
Fig 4.4-4.6	map	Drifter tracks			suggested improvement

Overall, the model captured the seasonal variability and general patterns of water temperature and salinity, but was not able to resolve the short-term variability in temperature and salinity, particularly for cooling events observed at the NOAA Buoy 44013. In addition, predicted currents often disagreed with measurements.

The 2006-2007 ECOM-si experiments of Section 3 show that temporal and spatial variability of currents, temperature, and salinity in Massachusetts Bay were influenced substantially by hydrographic conditions and inflow at the open boundary, and by the spatial variation of the wind field. Including these helped improve the model simulation.

Further improvements in the temporal and spatial fit were gained by using FVCOM, largely because the available version has a higher resolution, and in part because its triangular grid more readily fits an irregular coastline.

6 Recommendations

1) We recommend that MWRA shift the hydrodynamics model from ECOM-si to FVCOM. In general, FVCOM is at least as good as ECOM-si, and the present version of FVCOM is clearly superior.

FVCOM is the core hydrodynamics model in the Northeast Coastal Ocean Forecast System (NECOFS), which is now in operational model producing 3-day surface weather and ocean forecasts every day. The NECOFS regional GoM/GB FVCOM grid includes a higher resolution sub-domain Massachusetts Bay grid that can be used directly for the Bay Modeling Service work. This approach eliminates the need (and effort) to construct the open boundary conditions (required to run the much-lower resolution ECOM-si model) using methods which involve tuning and other approaches with weak scientific support. Shifting to FVCOM at this time also takes advantage of ongoing NECOFS development and applications and existing scientific studies on the physical and ecosystem processes in Massachusetts Bay and the Gulf of Maine that are using FVCOM.

2) We recommend that MWRA hydrodynamic modeling incorporate the spatial wind field. This appears to offer improvements, and is not difficult to do. It is already incorporated into recent versions of FVCOM.

3) We recommend that future reports for MWRA focus more on process studies and less on validation. Previous reports have sufficiently covered validation. Rather, we should focus on understanding the key processes that are controlling the occurrence of unusual ecosystem events that directly affects the water quality in Massachusetts Bay. We had a discussion meeting with Dr. Rocky Geyer (Woods Hole Oceanographic Institution) on future directions, who suggested that we should focus the Bay Modeling Service on case studies of the coupled physical-biological processes that cause the spring and fall blooms, low DO, and harmful algae blooms, and other processes that directly relate to the MWRA mission. Based on our experiences in modeling 2006 and 2007 for MWRA, we think this is a good direction to go.

Furthermore, many processes related to the temporal and spatial variability of DO in Massachusetts Bay are still unknown. Focusing on case studies in future modeling efforts will improve understanding the dynamics relevant to ecosystem variation in this region, which is pivotal for guiding better coastal environmental assessment and prediction in Massachusetts Bay.

7 References

Blumberg, A. F, 1994. A primer for ECOM-si. Technical Report, HydroQual, Inc. Mahwah, New Jersey, 101 pp.

Burchard, H., 2002. Applied turbulence modeling in marine waters. Springer:Berlin- Heidelberg-New York-Barcelona-Hong Kong-London-Milan Paris-Tokyo, 215 pp.

Butman, B. C. R. Sherwood, P. S. Dalyander, 2008. Northeast storms ranked by wind stress and wave-generated bottom stress observed in Massachusetts Bay, 1990-2006. Continental Shelf Research, 28, 1231-1245.

Butman, Bradford, Dalyander, P.S., Bothner, M.H., Borden, Jonathan, Casso, M.A., Gutierrez, B.T., Hastings, M.E., Lightsom, F.L., Martini, M.A., Montgomery, E.T, Rendigs, R.R., and Strahle, W.S., 2009, Long-term oceanographic observations in Massachusetts Bay, 1989-2006: U.S. Geological Survey Data Series 74, v. 3.0, DVD-ROM. Also available online at http://pubs.usgs.gov/ds/74/. Also see http://stellwagen.er.usgs.gov/mbay_lt.html

Chen, C. and R. Beardsley, 1995. A numerical study of stratified tidal rectification over finite-amplitude banks, part I: symmetric banks. Journal of Physical Oceanography, 25, 2090-2110.

Chen, C., R. Beardsley, and R. Limeburner, 1995. A numerical study of stratified tidal rectification over finite- amplitude banks, part II: Georges Bank. Journal of Physical Oceanography, 25, 2111-2128.

Chen, C., R. C. Beardsley, and P. J. S. Franks, 2001. A 3-D prognostic model study of the ecosystem over Georges Bank and adjacent coastal regions. Part I: physical model. Deep Sea Research, 48, 419-456.

Chen, C., H. Liu, and R. Beardsley, 2003. An unstructured grid, finite-volume, three dimensional, primitive equations ocean model: Application to coastal ocean and estuaries. Journal of Atmospheric and Ocean Technology, 20 (1), 159–186.

Chen, C., Z. Wu, R. C. Beardsley, S. Shu, and C. Xu, 2005. Using MM5 to hindcast the ocean surface forcing fields over the Gulf of Maine and Georges Bank region. Journal of Atmospheric and Oceanic Technology, 22(2): 131-145.

Chen, C, R. C. Beardsley and G. Cowles, 2006a. An unstructured grid, finite-volume coastal ocean model (FVCOM) system. Special Issue entitled “Advance in Computational Oceanography”, Oceanography, 19(1), 78-89.

Chen, C., R.C. Beardsley, and G. Cowles, 2006b. An unstructured grid, finite-volume coastal ocean model-FVCOM user manual, School for Marine Science and Technology, University of Massachusetts Dartmouth, New Bedford, Second Edition. SMAST/UMASSD Technical Report-06-0602, 318 pp.

Dudhia, J., D. Gill, K. Manning, W. Wang, C. Bruyere, J. Wilson and S. Kelly, 2003. PSU/NCAR mesoscale modeling system tutorial class notes and user’s guide, MM5 modeling system version 3, Mesoscale and Microscale Meteorology Division, National Center for Atmospheric Research.

Foreman, M.G.G. 1978. Manual for tidal currents analysis and prediction. Pacific Marine Science Report. 78-6. Institute of Ocean Sciences, Patricia Bay, British Columbia. 57 pp.

Franks, P. J.S. and C. Chen, 1996. Plankton production in tidal fronts: a model of Georges Bank in summer. Journal of Marine Research, 54, 631-651.

Franks, P. J. S. and C. Chen, 2001. A 3-D prognostic model study of the ecosystem over Georges Bank and adjacent coastal regions. Part II: coupled biological and physical model. Deep Sea Research, 48, 457-482.

Hunke, E. C. and W. H. Lipscomb (2008). CICE: the Los Alamos Sea Ice Model, Documentation and Software, Version 4.0. Los Alamos National Laboratory Tech. Rep. LA-CC-06-012. http://oceans11.lanl.gov/trac/CICE/wiki/RefPublications

HydroQual, Inc. and R.P. Signell, 2001. Calibration of the Massachusetts and Cape Cod Bays Hydrodynamic Model: 1998-1999. Boston, Massachusetts Water Resources Authority. ENQUAD 2001-12, 170pp.

Ji. R., C. Chen, P. J. S. Franks, D. W. Townsend, E. G. Durbin, R. C. Beardsley, R. G. Lough and R. W. Houghton, 2006. Spring phytoplankton bloom and associated lower trophic level food web dynamics on Georges Bank: 1-D and 2-D model studies. Deep Sea Research II: GLOBEC special issue, 53, 2656-2683.

Jiang, M. S. and M. Zhou, 2008. The Massachusetts Bay hydrodynamics model: 2005 simulation. Massachusetts Water Resources Authority, Environmental Quality Department Report ENQUAD 2008-12., 118pp.

Lai, Z., C. Chen, G. Cowles and R. C. Beardsley, A non-hydrostatic version of FVCOM-validation experiment I: surface standing and solitary waves. Journal of Geophysical Research, to be submitted.

Lai, Z., C. Chen, G. Cowles and R. C. Beardsley, A non-hydrostatic version of FVCOM-validation experiment II: Lock-exchange flow and internal solitary waves. Journal of Geophysical Research, to be submitted.

Libby PS, Borkman DG, Geyer WR, Keller AA, Turner JT, Mickelson MJ, Oviatt CA. 2009. Water column monitoring in Massachusetts Bay 1992-2007: focus on 2007 results. Boston: Massachusetts Water Resources Authority. Report 2009-04. 162 p.

Mellor, G. L., and T. Yamada, 1982. Development of a turbulence closure model for geophysical fluid problems. Rev. Geophys. Space Phys., 20, 851-875.

Pawlowicz, R., B. Beardsley, and S. Lentz, "Classical tidal harmonic analysis including error estimates in MATLAB using T_TIDE", Computers and Geosciences 28 (2002), 929-937.

Pettigrew N.R., 2009. University of Maine, GoMOOS Moored Buoy Program. http://gyre.umeoce.maine.edu/GoMoos/gommrg.phtml

Pieterzak, J. J. B. Jakobson, H. Burchard, H. J. Vested, and O. Petersen, 2002. A three dimensional hydrostatic model for coastal and ocean modeling using a generalized topography following co-ordinate system. Ocean Modeling, 4: 173-205.

Qi, J. C. Chen, R. C. Beardsley, W Perrier, G. Cowles and Z. Lai, 2008. An unstructured-grid finite-volume wave model (FVCOM-SWAVE): implementation, validations and applications. Ocean Modeling, in revision.

Signell, R.P., H. L. Jenter, and A. F. Blumberg, 1996. Circulation and effluent dilution modeling in Massachusetts Bay: model implementation, verification and results. USGS Open File Report 96-015, U.S. Geological Survey, Woods Hole.

Smagorinsky, J., 1963. General circulation experiments with the primitive equations, I. The basic experiment. Monthly Weather Review, 91, 99–164.

Tian R, Chen C, Xu Q, Xue P, Cowles GW, Beardsley RC, Rothschild BJ. 2009. The Massachusetts Bay water quality model: 2006-2007 simulation. Boston: Massachusetts Water Resources Authority. Report 2009-10. 123 p.

Zheng, L. C. Chen and F. Y. Zhang, 2004. Development of water quality model in the Satilla River Estuary, Georgia. Ecological Modeling, 178, 457-482.

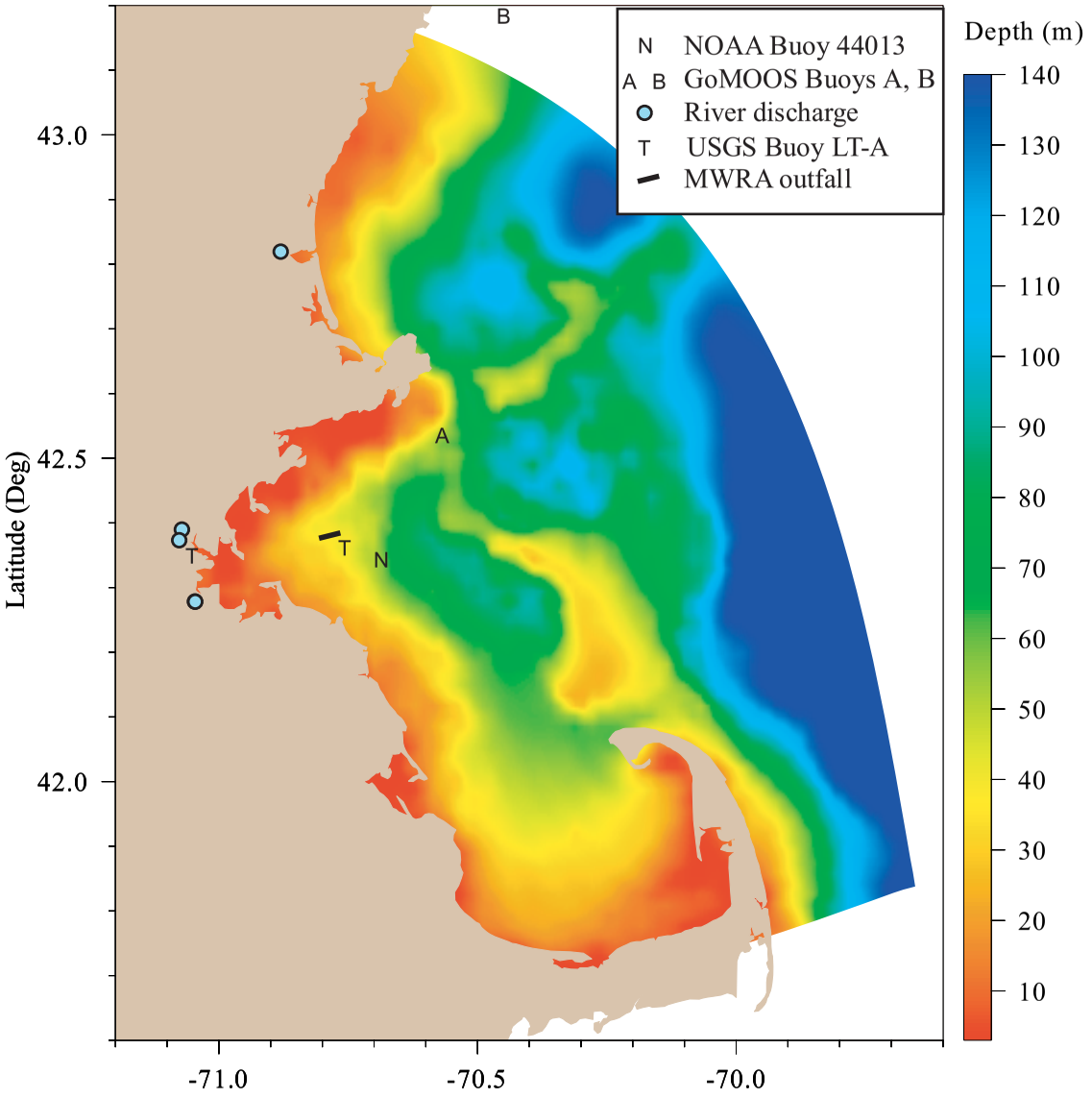

Fig. 1.1 Bathymetry and buoy locations in Massachusetts Bay.
N NOAA Buoy 44013
A B GoMOOS Buoys A and B
River discharge
T USGS Buoy LT-A
MWRA outfall

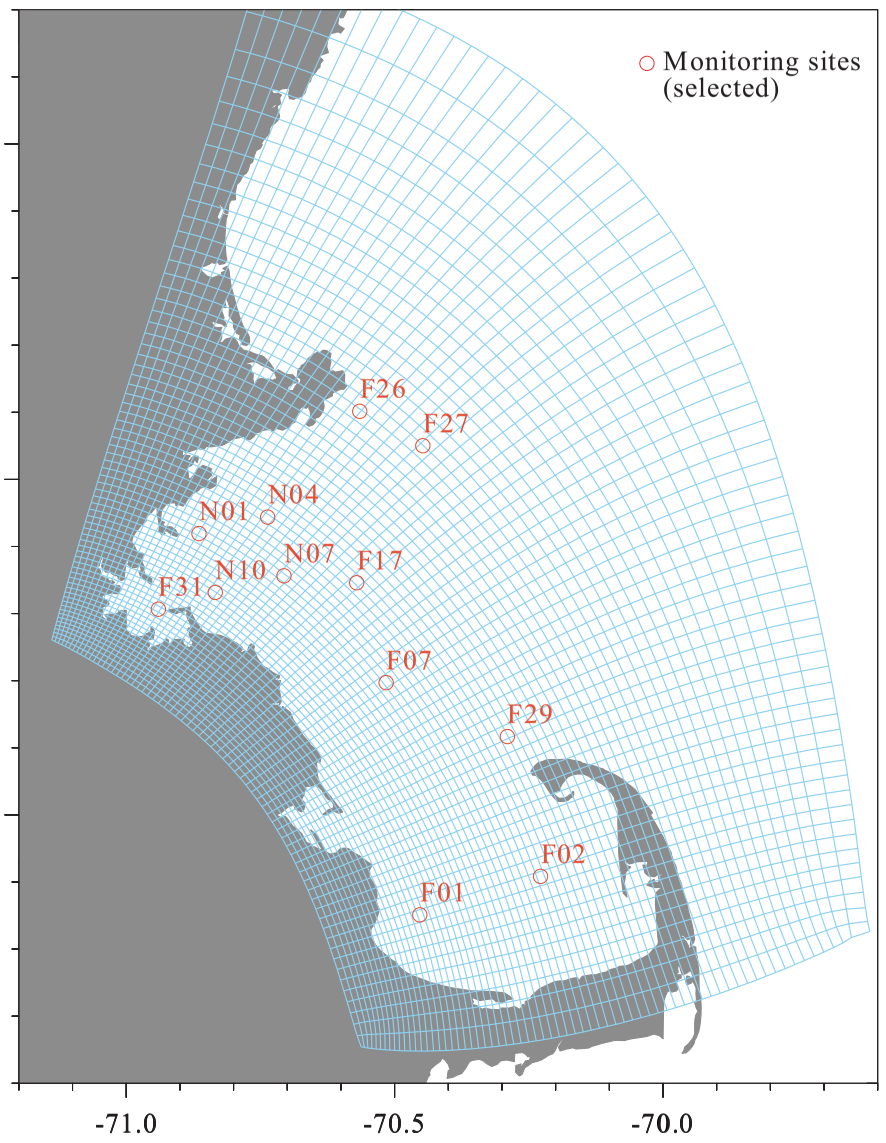

Fig 2.1 ECOM-si computational domain and curvilinear grids. Total grid points: 76×76.
Hydrographic monitoring sites selected for model/data comparisons.

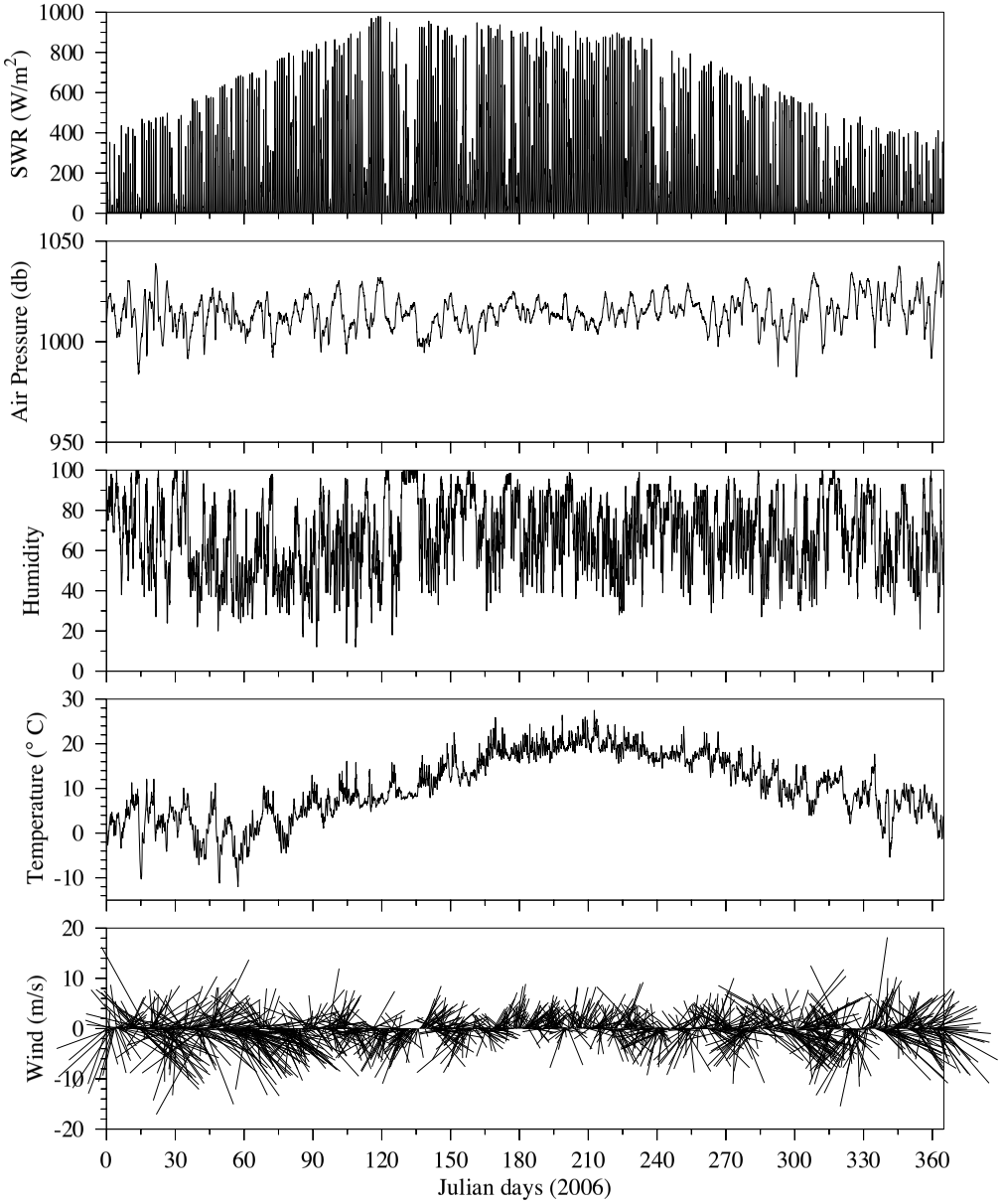

Figure 2.2 Shortwave radiation, air pressure, humidity, air temperature and wind velocity vectors recorded on NOAA Buoy 44013 from 00:00 AM January 1 2006 to 00:00 AM January 1 2007. All data were sampled over hourly intervals.

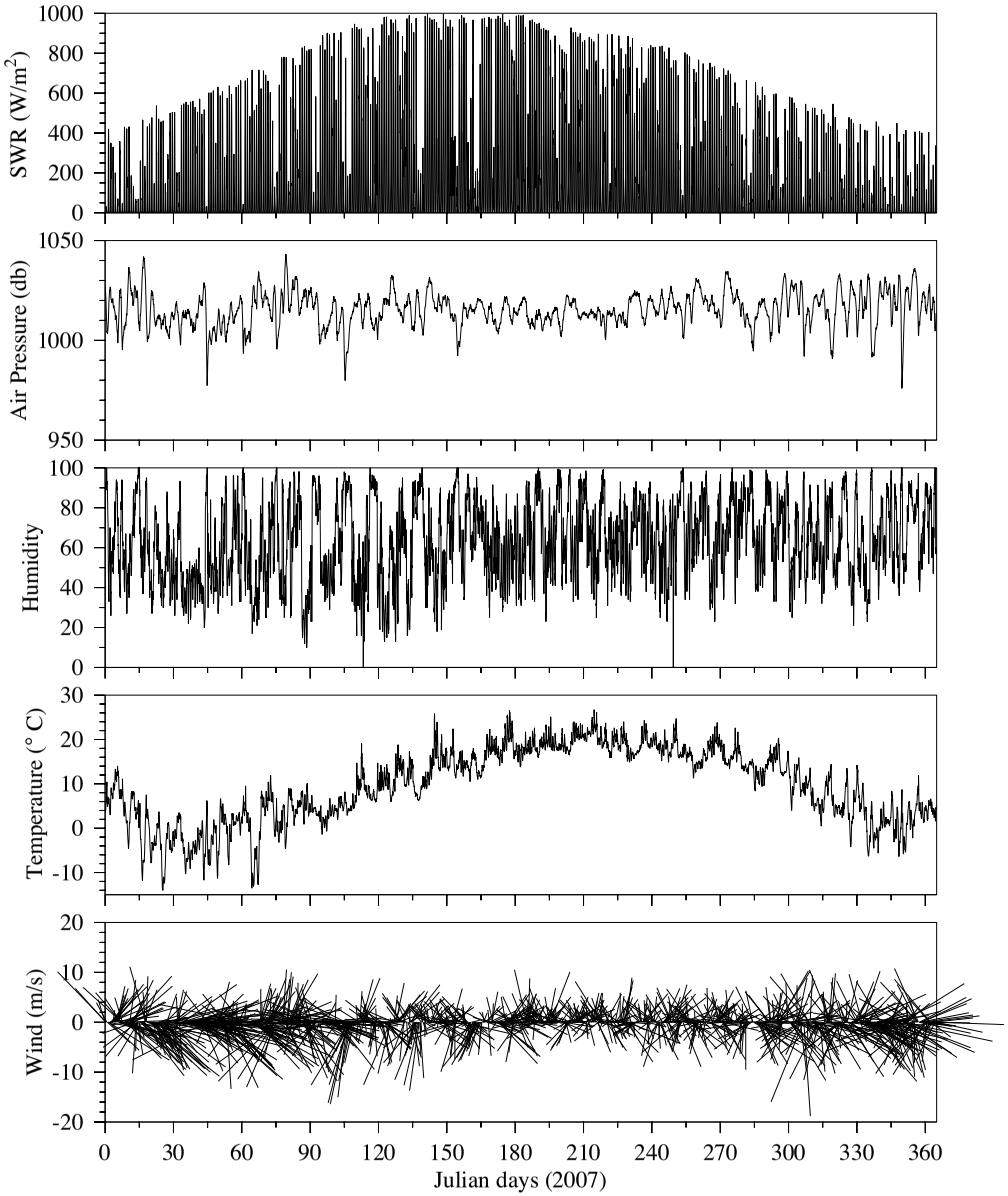

Figure 2.3 Shortwave radiation, air pressure, humidity, air temperature and wind velocity vectors recorded on NOAA Buoy 44013 from 00:00 AM January 1 2007 to 00:00 AM January 1 2008. All data were sampled over hourly intervals.

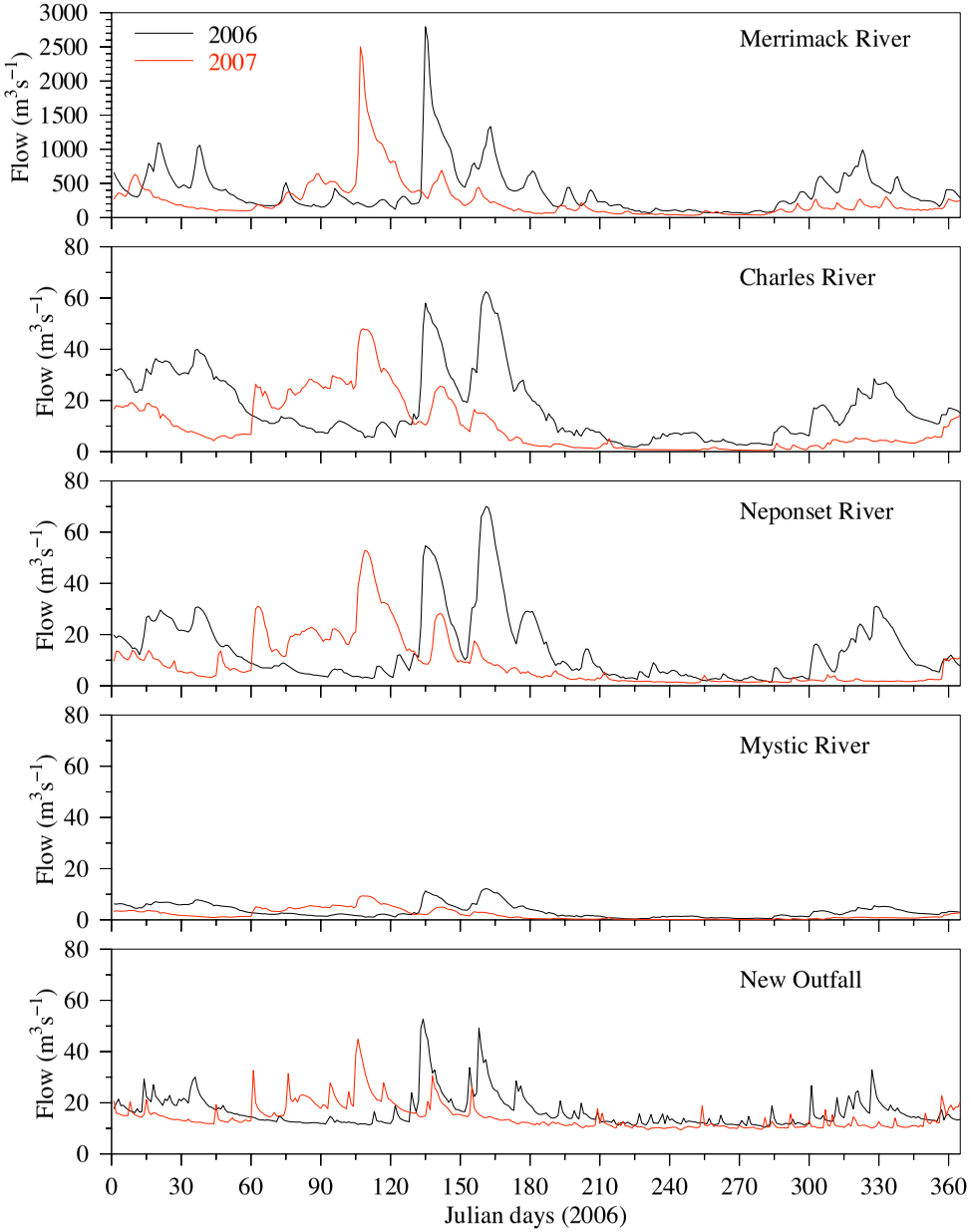

Figure 2.4 Daily discharges from the Merrimack River, the Charles River, the Neponset River, the Mystic River, MWRA outfall for 2006 (black line) and 2007 (red line).

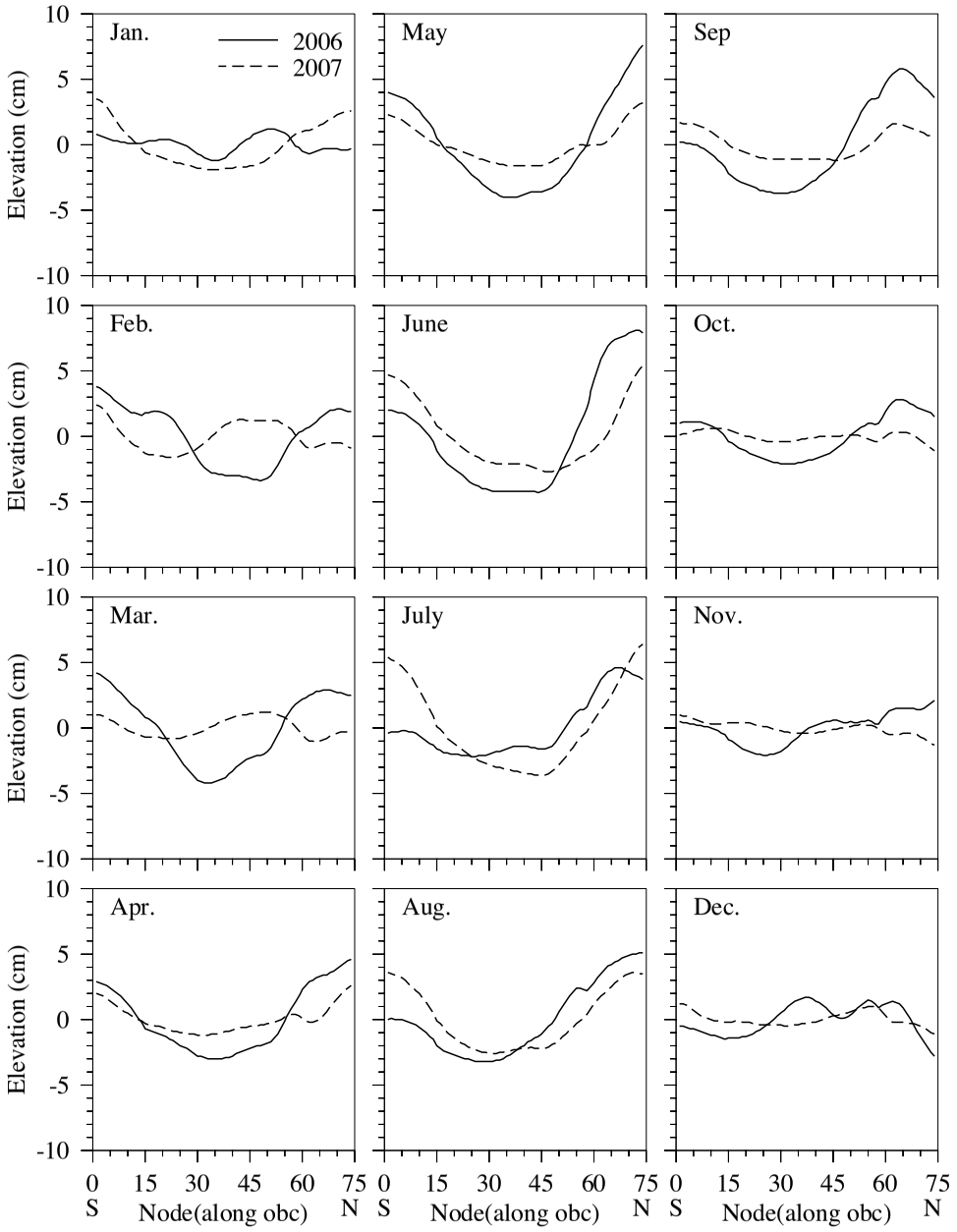

Figire 2.5 Monthly averaged 40-hour low-passed filtered surface elevations along the open boundary for 2006 (solid line) and 2007 (dashed line). The data are from the hindcast simulation results of FVCOM.

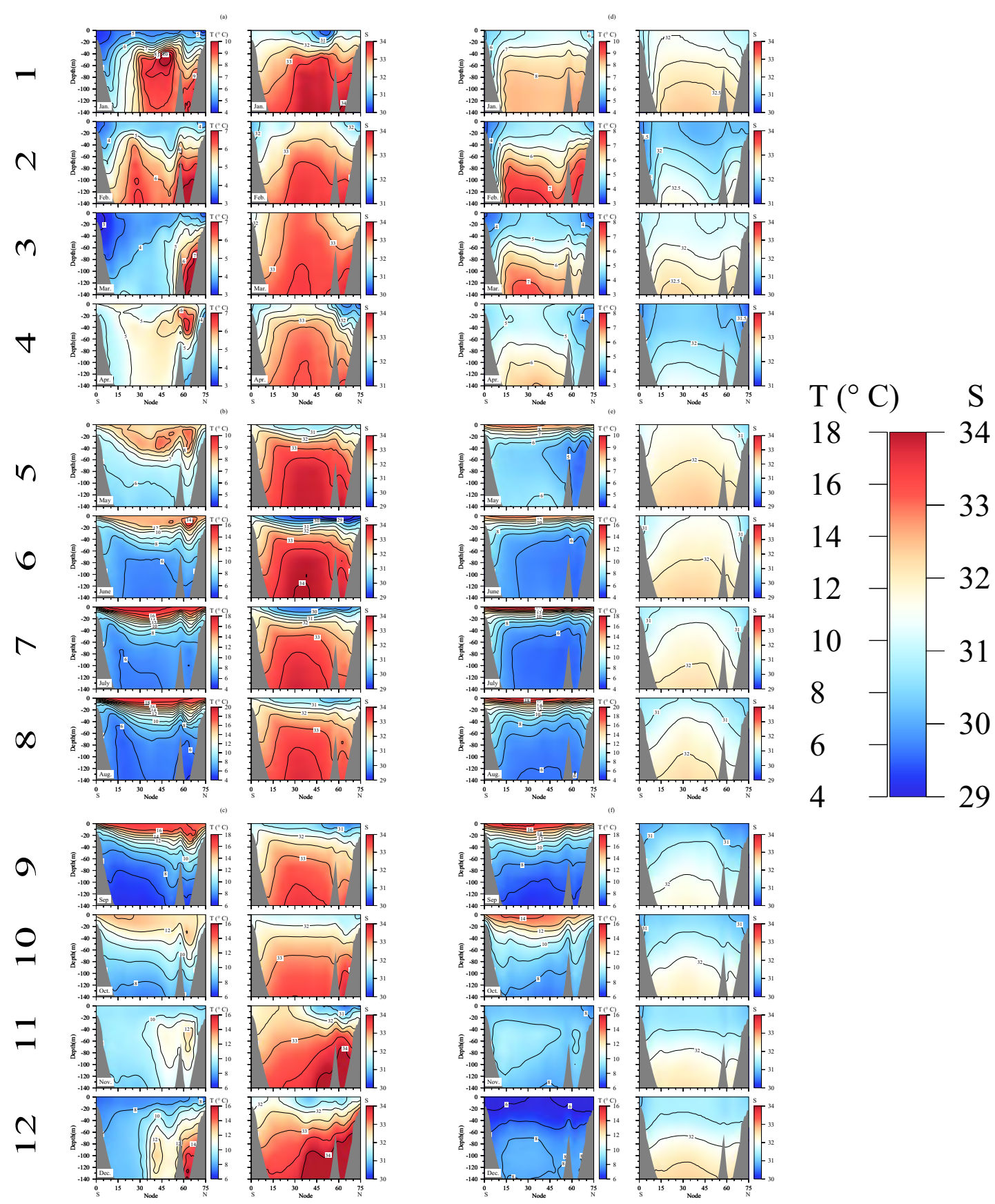

Fig. 2.6. Monthly boundary values of temperature and salinity specified for ECOMsi for 2006 and 2007. Obtained from a larger nested model (GOM-FVCOM).

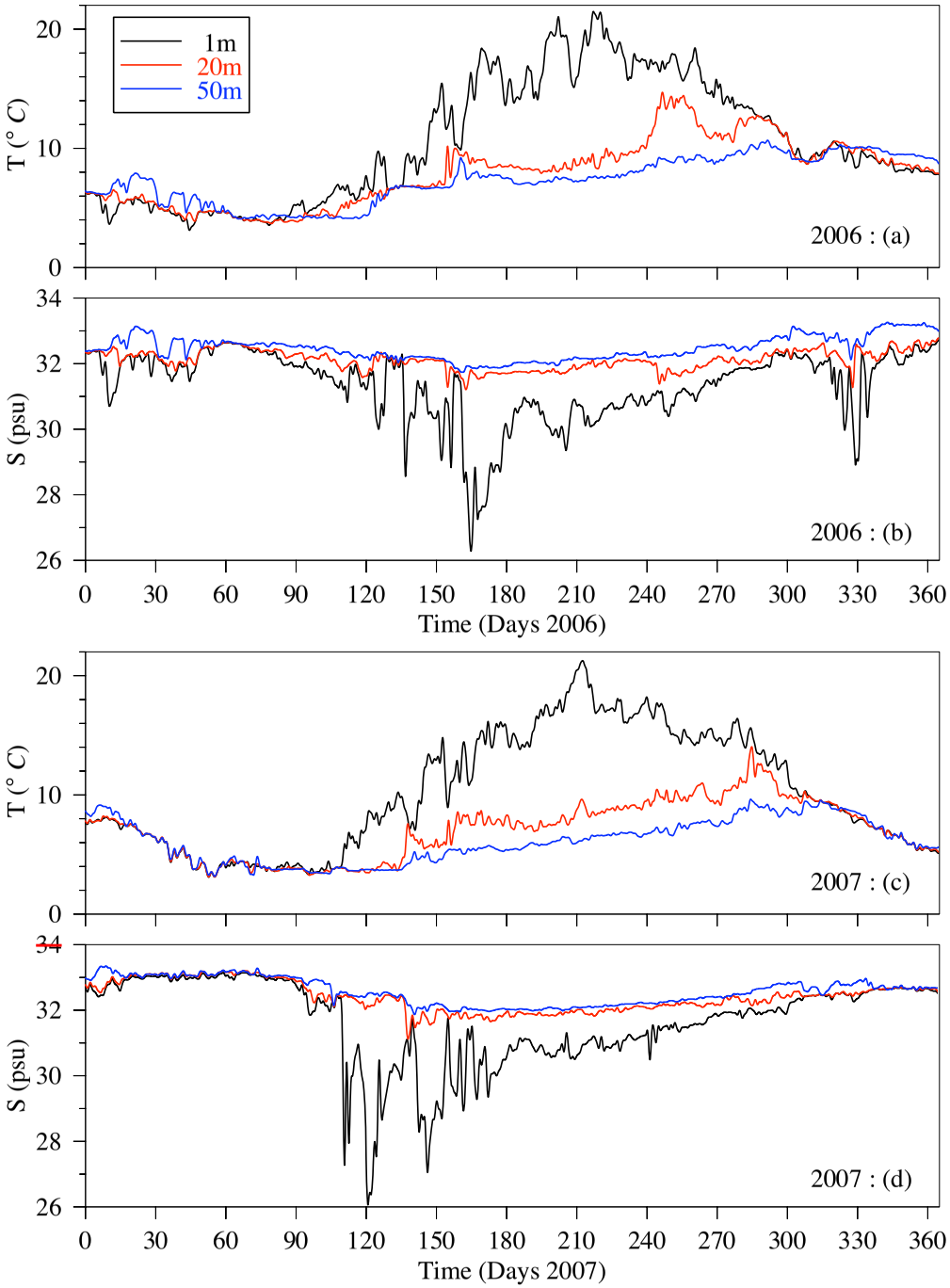

Figue 2.7 Times series of water temperature and salinity recorded at 1, 20 and 50 m on GoMOOS Buoy B in 2006 (upper two panels) and 2007 (lower two panels). T: temperature and S: salinity.

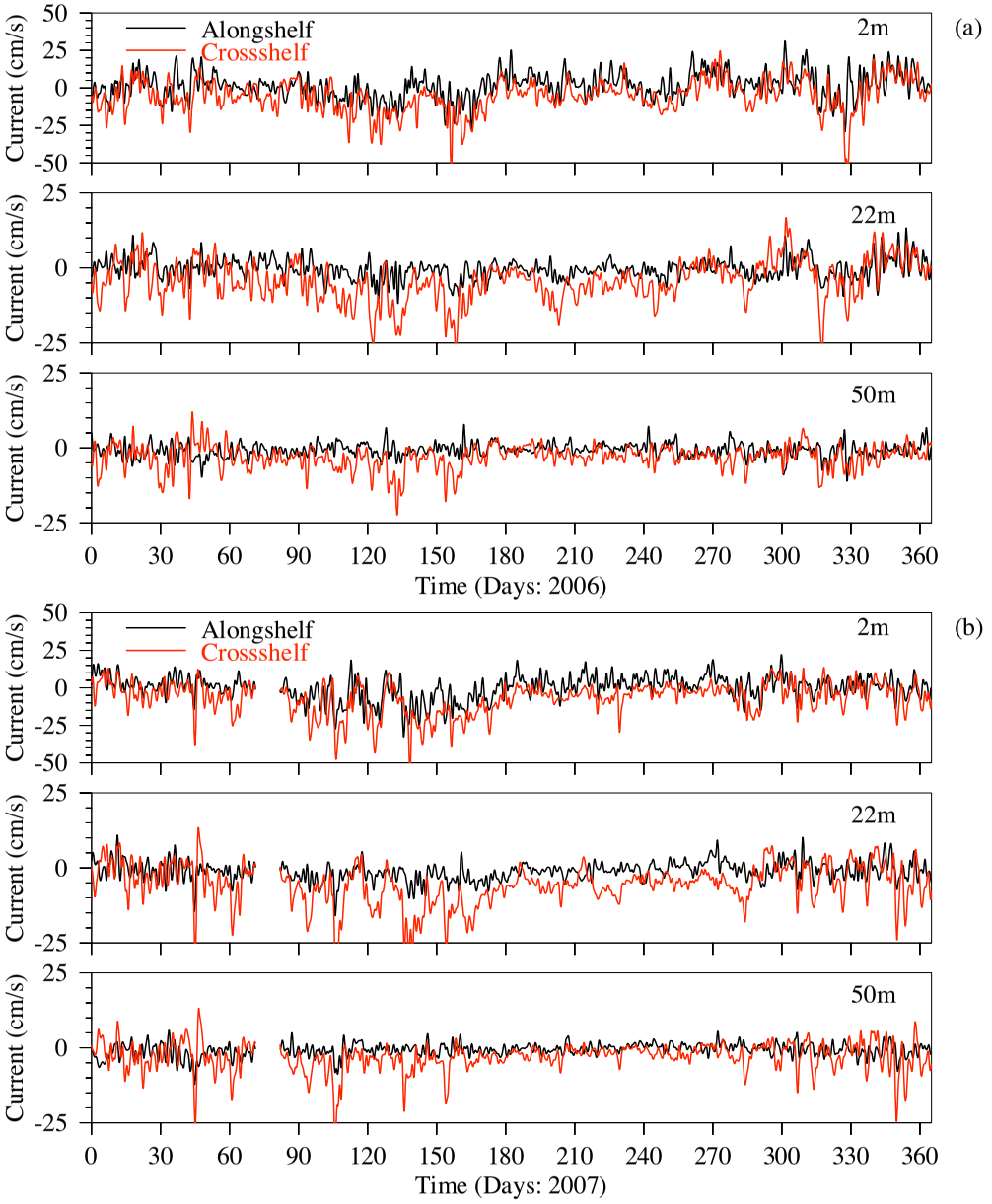

Figure 2.8 Time series of along-shelf (black line) and cross-shelf (red line) currents recorded hourly at 2, 22 and 50 m on GoMOOS Buoy B in 2006 (upper two panels) and 2007 (lower two panels).

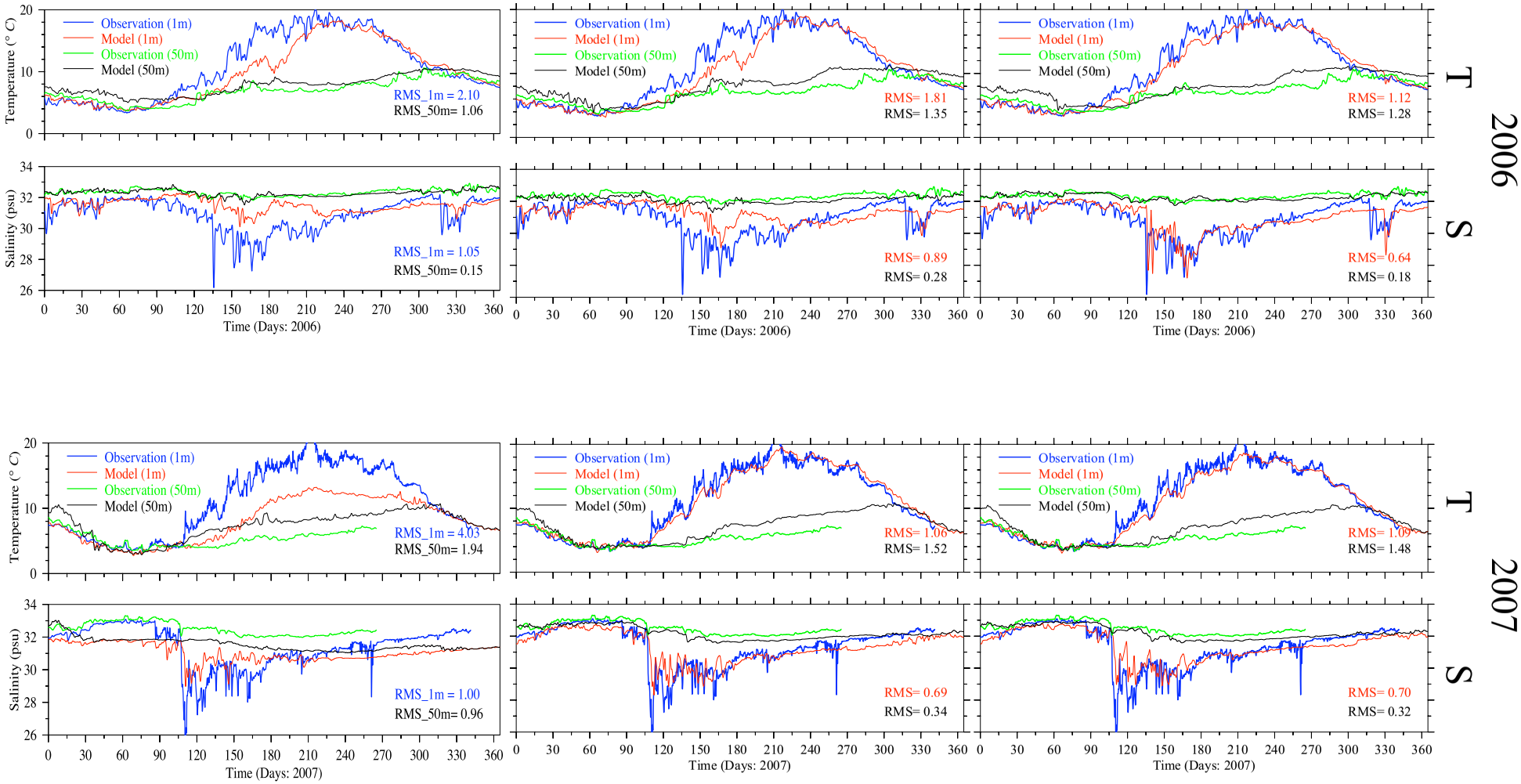

Fig. 3.1 Comparison of 3 model experiments to observations from GoMOOS Buoy A. Year 2006 and 2007 temperature and salinity at 1m and 50m depth.

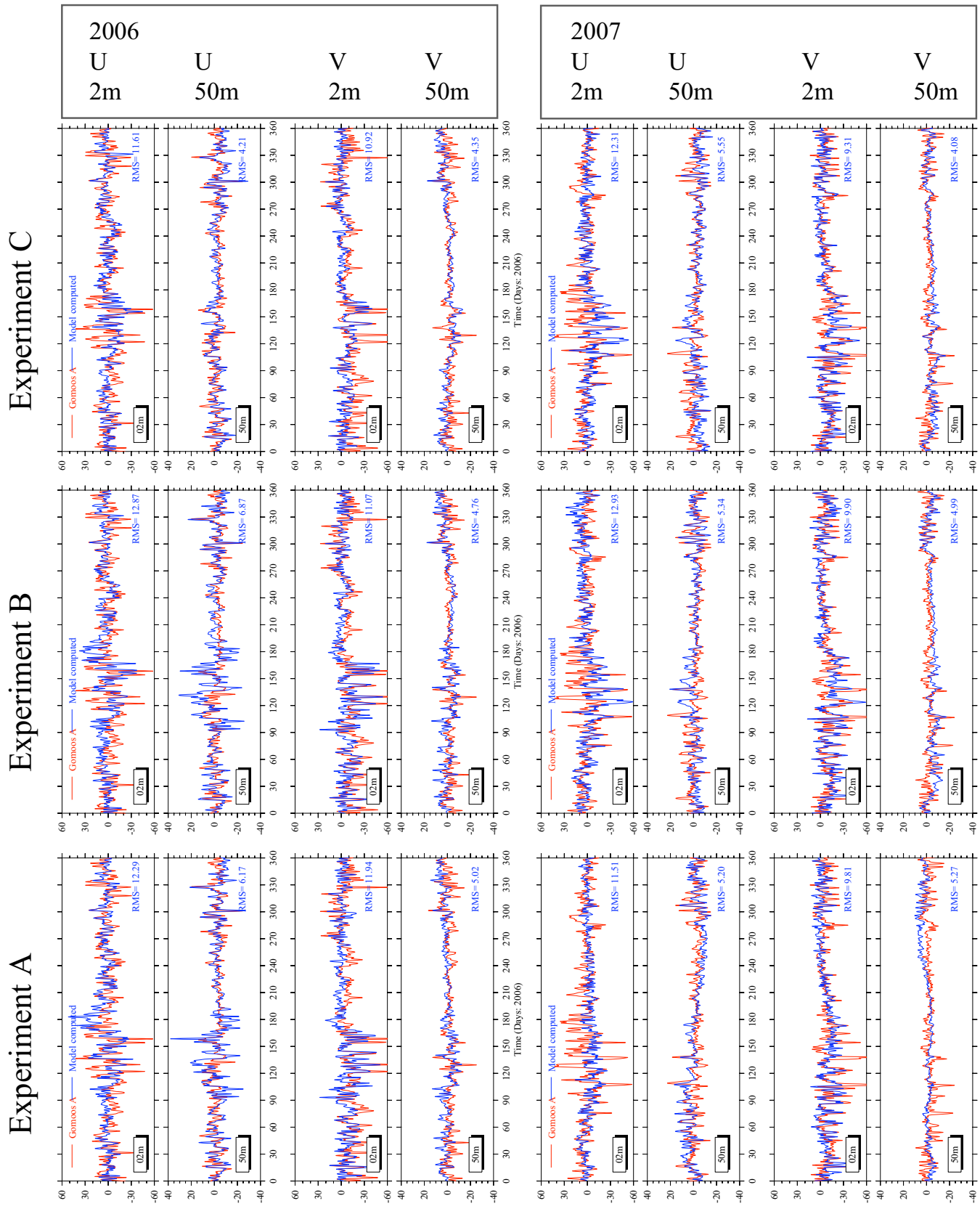

Fig. 3.2 Comparison of 3 model experiments to observations from GoMOOS Buoy A. Year 2006 and 2007 current velocity. U= eastward, V= northward (cm/s). At 2m and 50m depth.

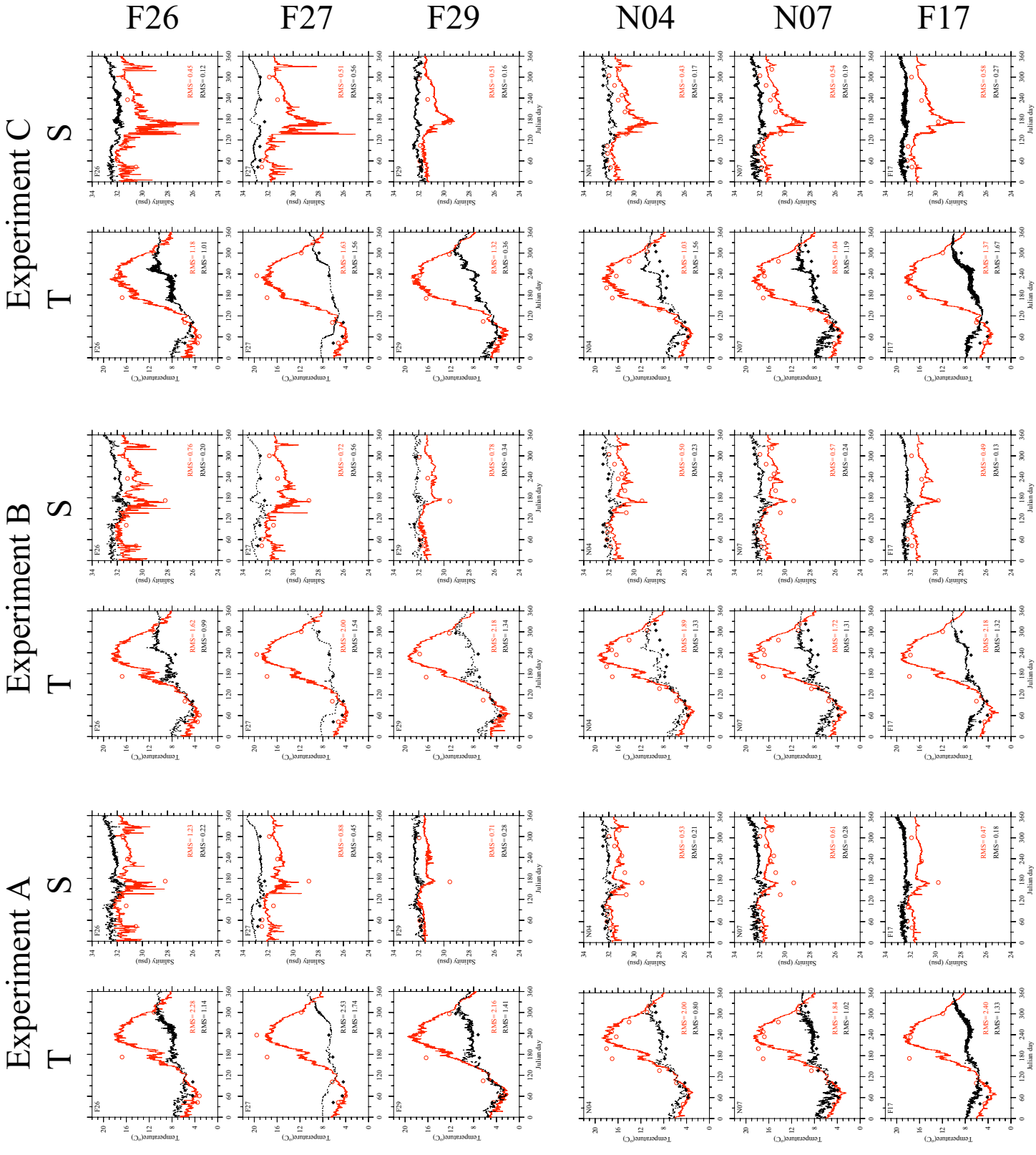

Fig. 3.3 Year 2006. Comparison of 3 model experiments to observations from monitoring sites. Temperature and salinity near the surface and bottom. Three sites from offshore region close to the open boundary, plus three sites from interior of the Bay near 50m isobath.

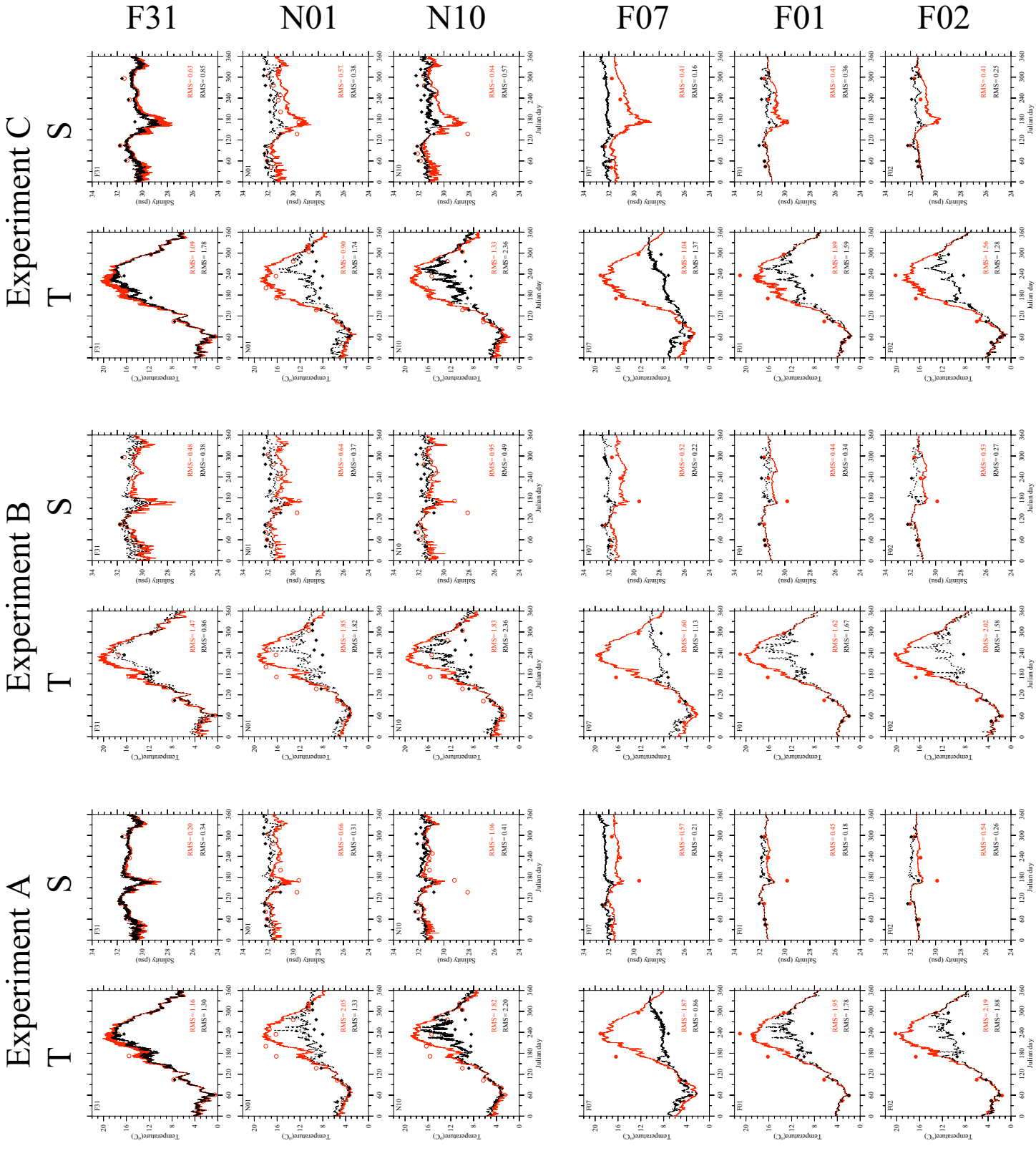

Fig. 3.4 Year 2006. Comparison of 3 model experiments to observations from monitoring sites. Temperature and salinity near the surface and bottom. Three sites from northwestern coastal area or shallower than 30m near Boston Harbor, plus three sites from middle and southern area of the bay.

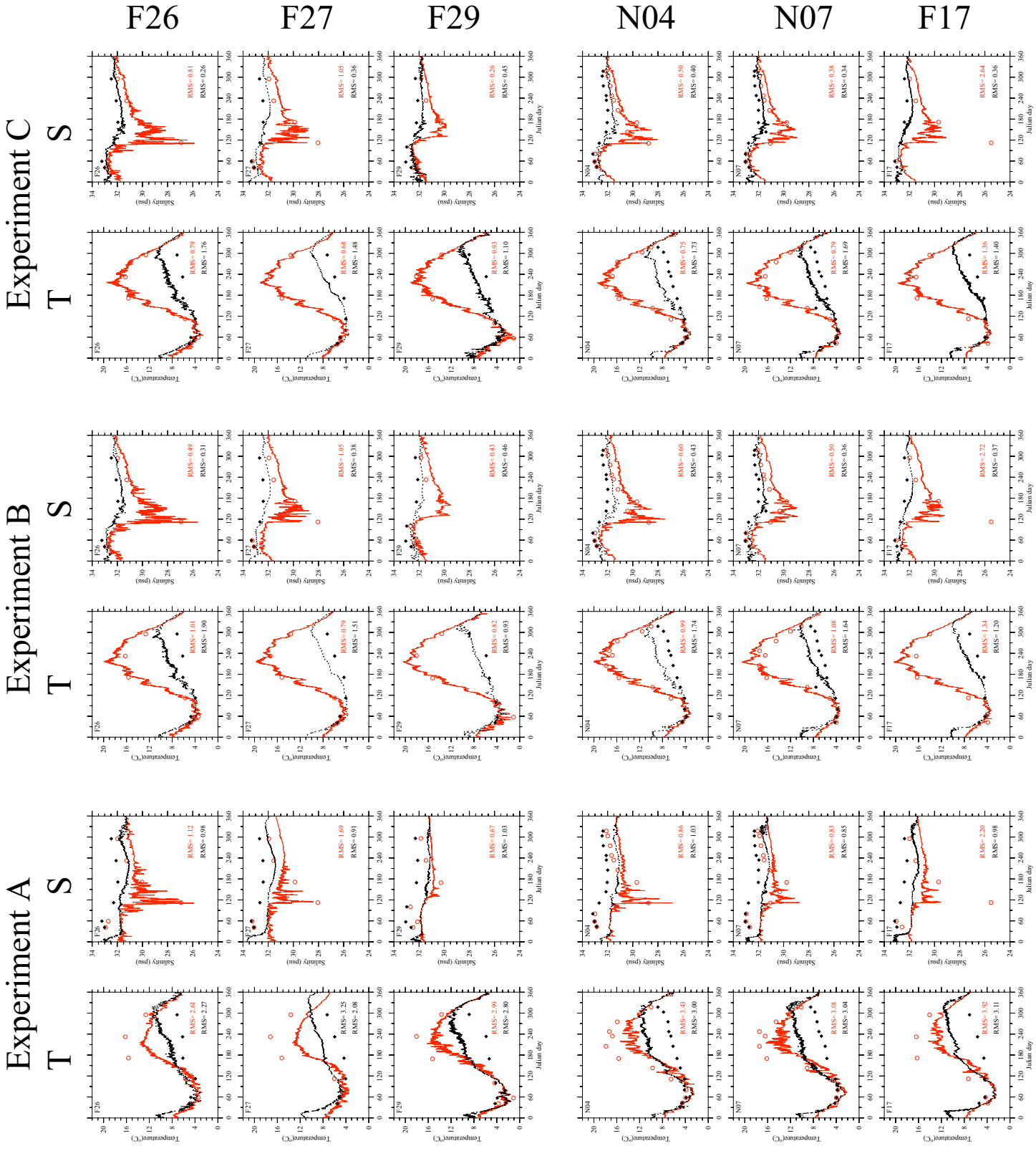

Fig. 3.5 Year 2007. Comparison of 3 model experiments to observations from monitoring sites. Temperature and salinity near the surface and bottom. Three sites from offshore region close to the open boundary, plus three sites from interior of the Bay near 50m isobath.

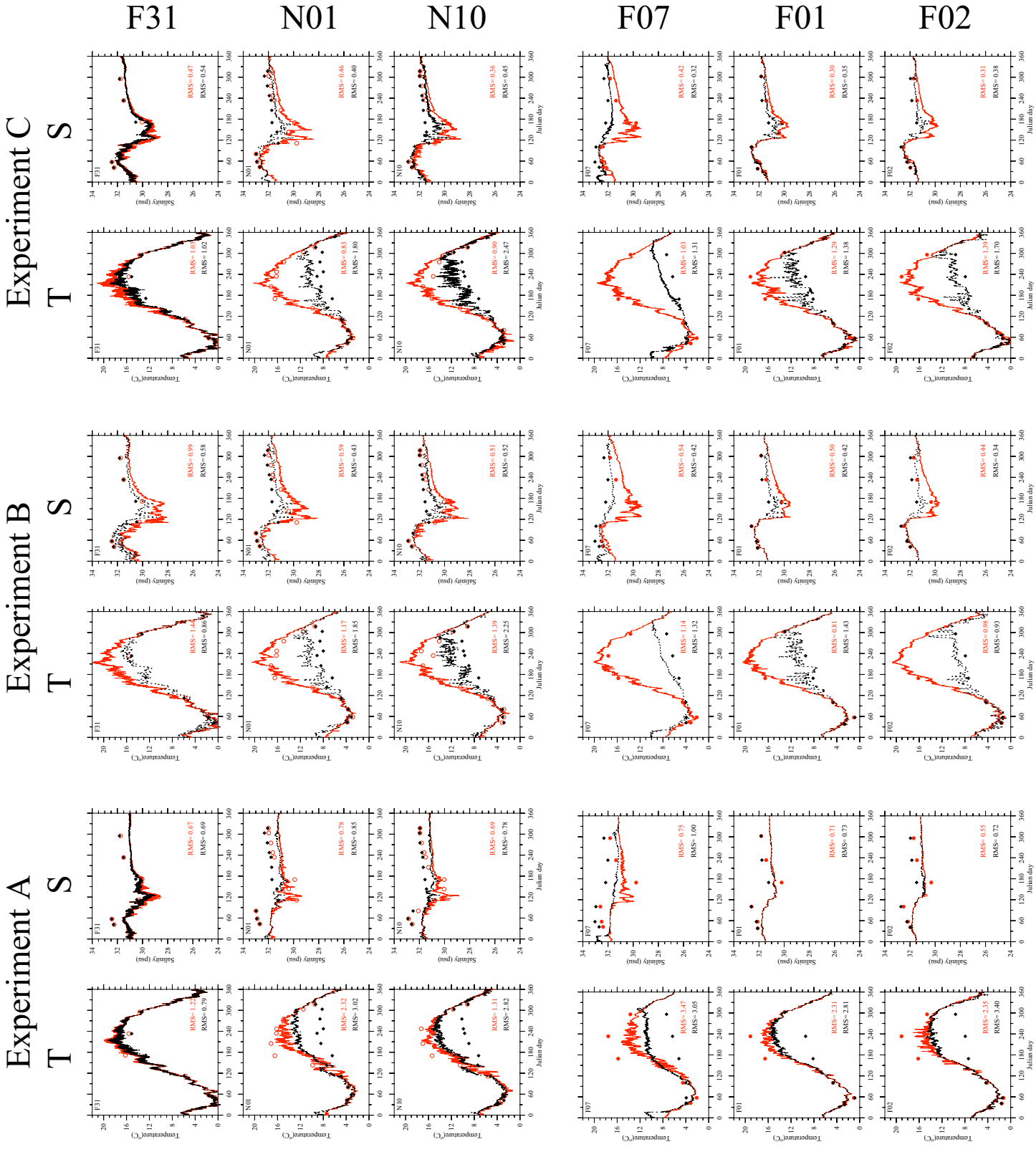

Fig. 3.6 Year 2007. Comparison of 3 model experiments to observations from monitoring sites. Temperature and salinity near the surface and bottom. Three sites from northwestern coastal area or shallower than 30m near Boston Harbor, plus three sites from middle and southern area of the bay.

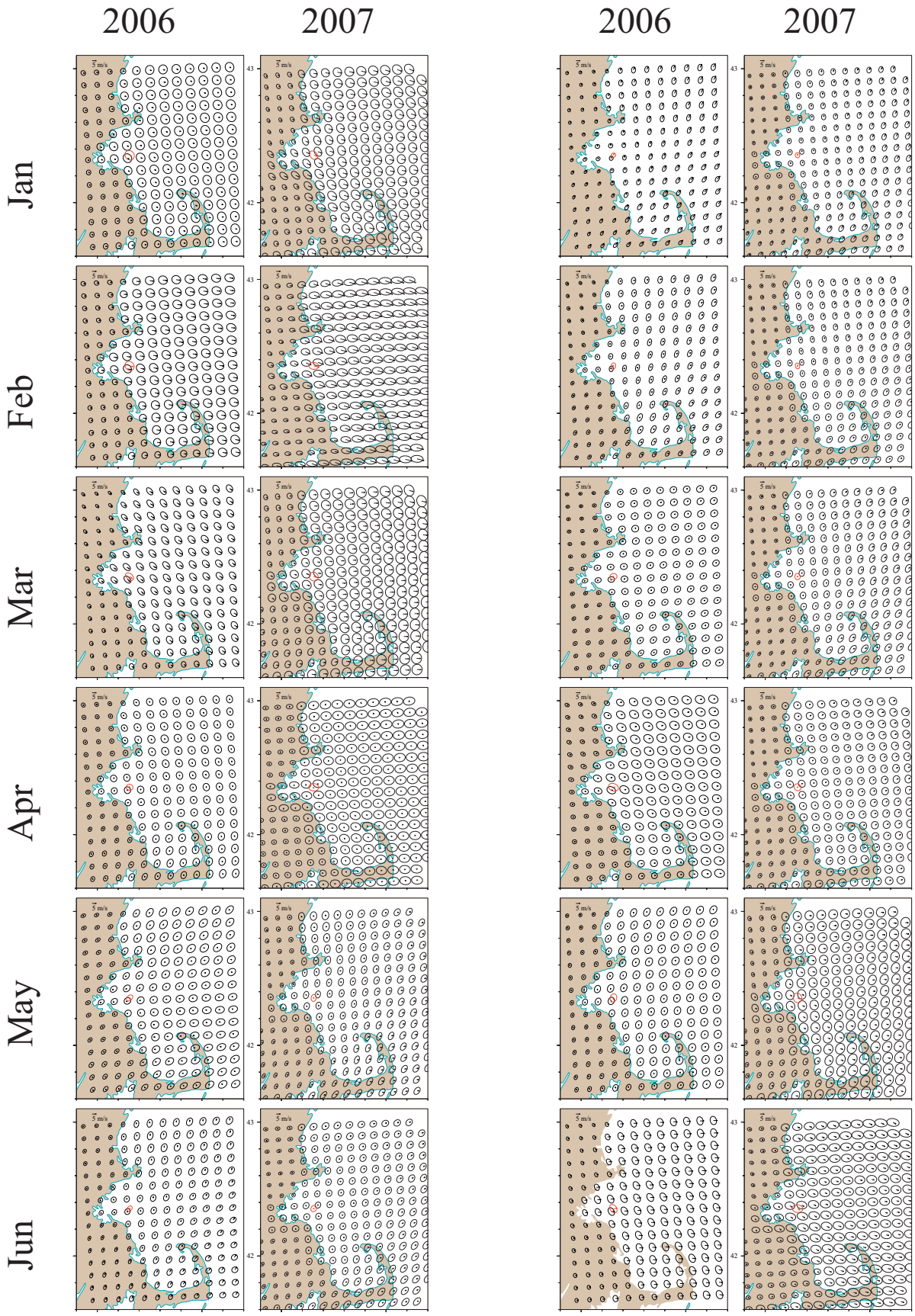

Figure 3.7 Monthly-averaged wind velocity at the 10-m plus variance ellipse over the horizontal resolution of 9 km. The red vector and ellipse were calculated based on the NOAA Buoy 44013.

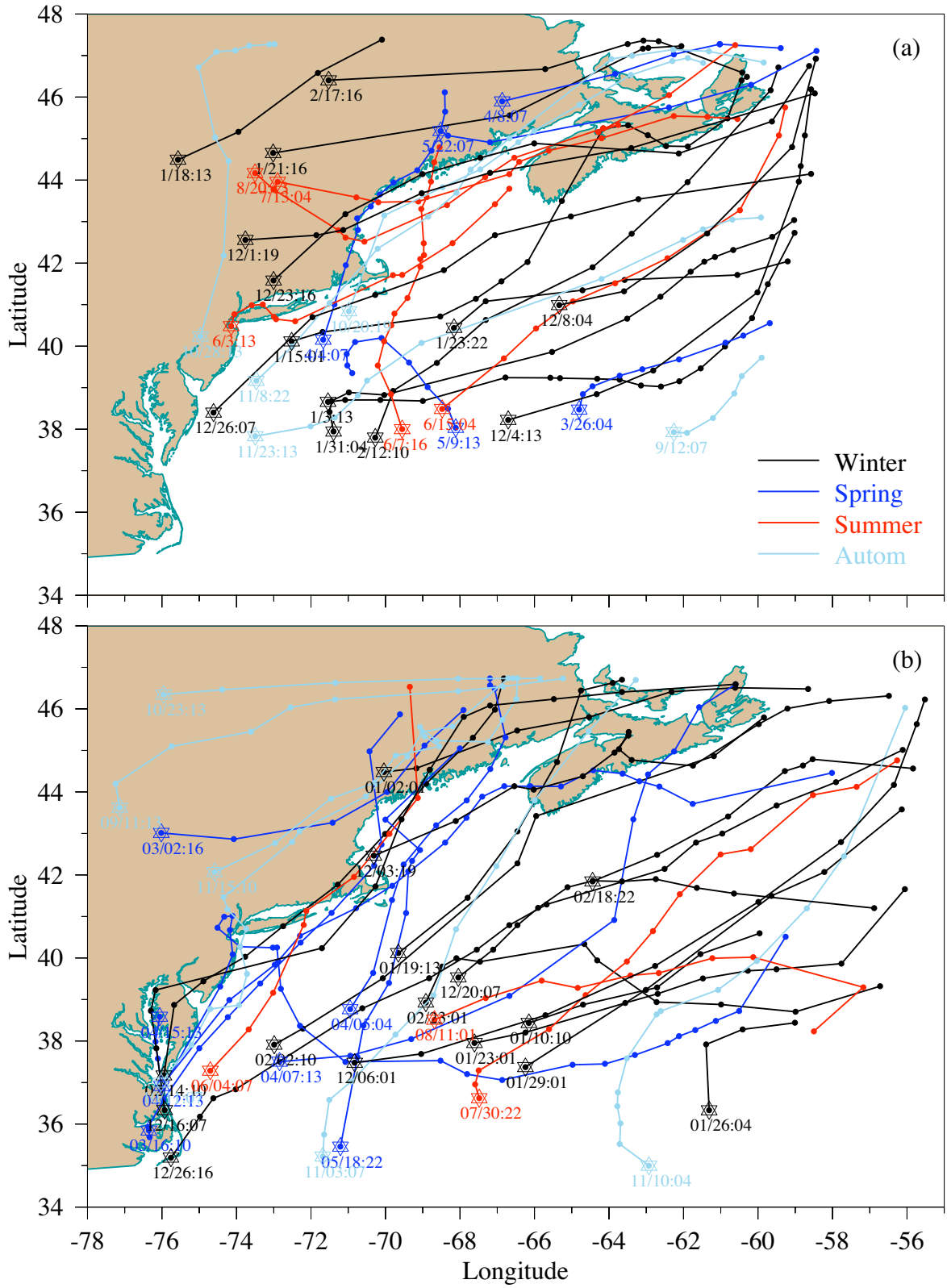

Figure 3.8 Paths of storms or center of the cold air fronts over and around the Gulf of Maine in 2006 (upper panel) and 2007 (lower panel). The number listed on each line was the started time: mm/dd: hh. Flled dots: locations every 3 hours.

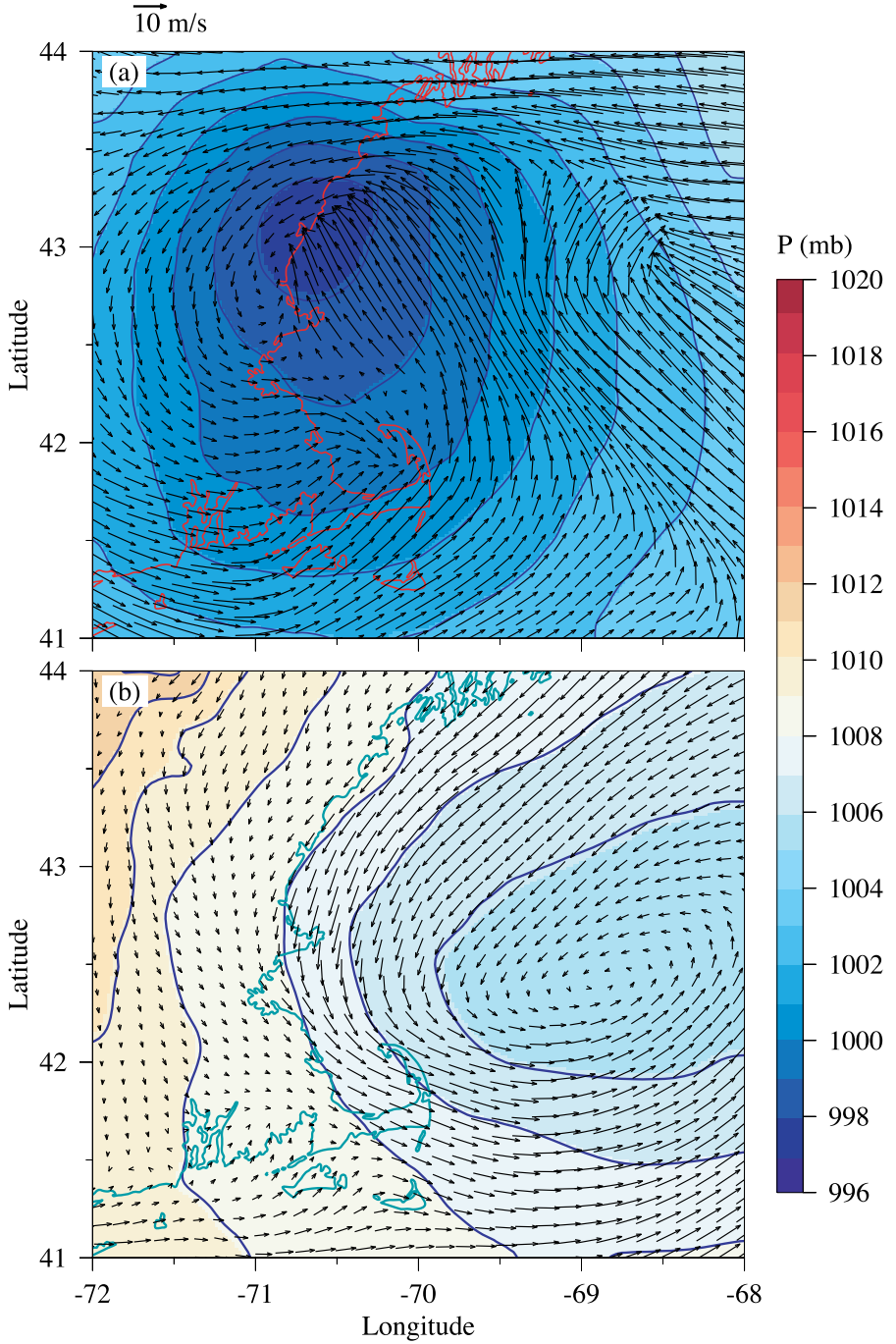

Figure 3.9 Distributions of near-surface wind velocity vectors (m/s) and air pressure (mb) in the western Gulf of Maine region at 11:00 EST April 4 (upper) and 17:00 EST June 8 (lower) 2006.

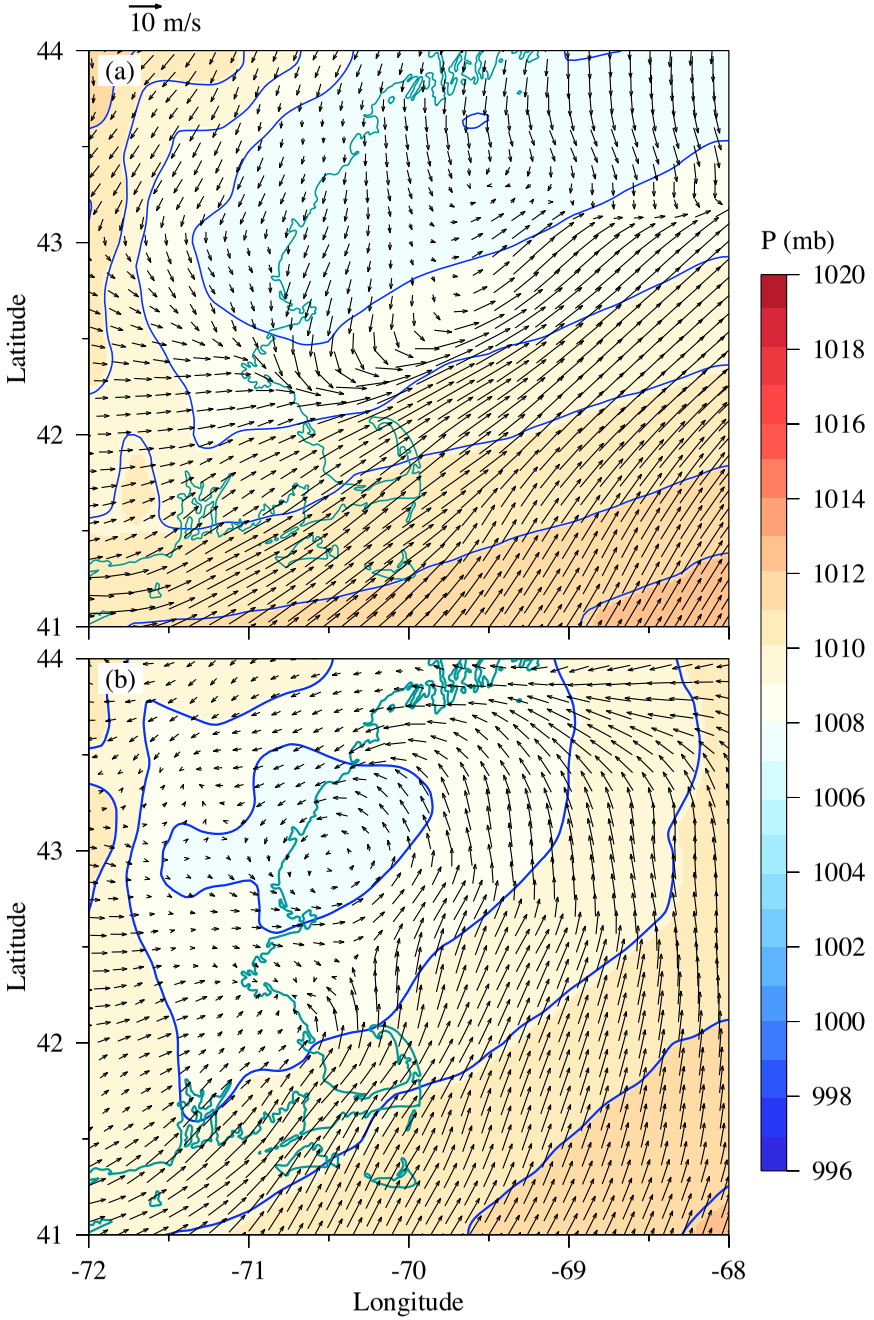

Figure 3.10 Distributions of near-surface wind velocity vectors (m/s) and air pressure (mb) in the western Gulf of Maine region at 08:00 EST July 13 (upper) and 14:00 EST August 20 (lower) 2006.

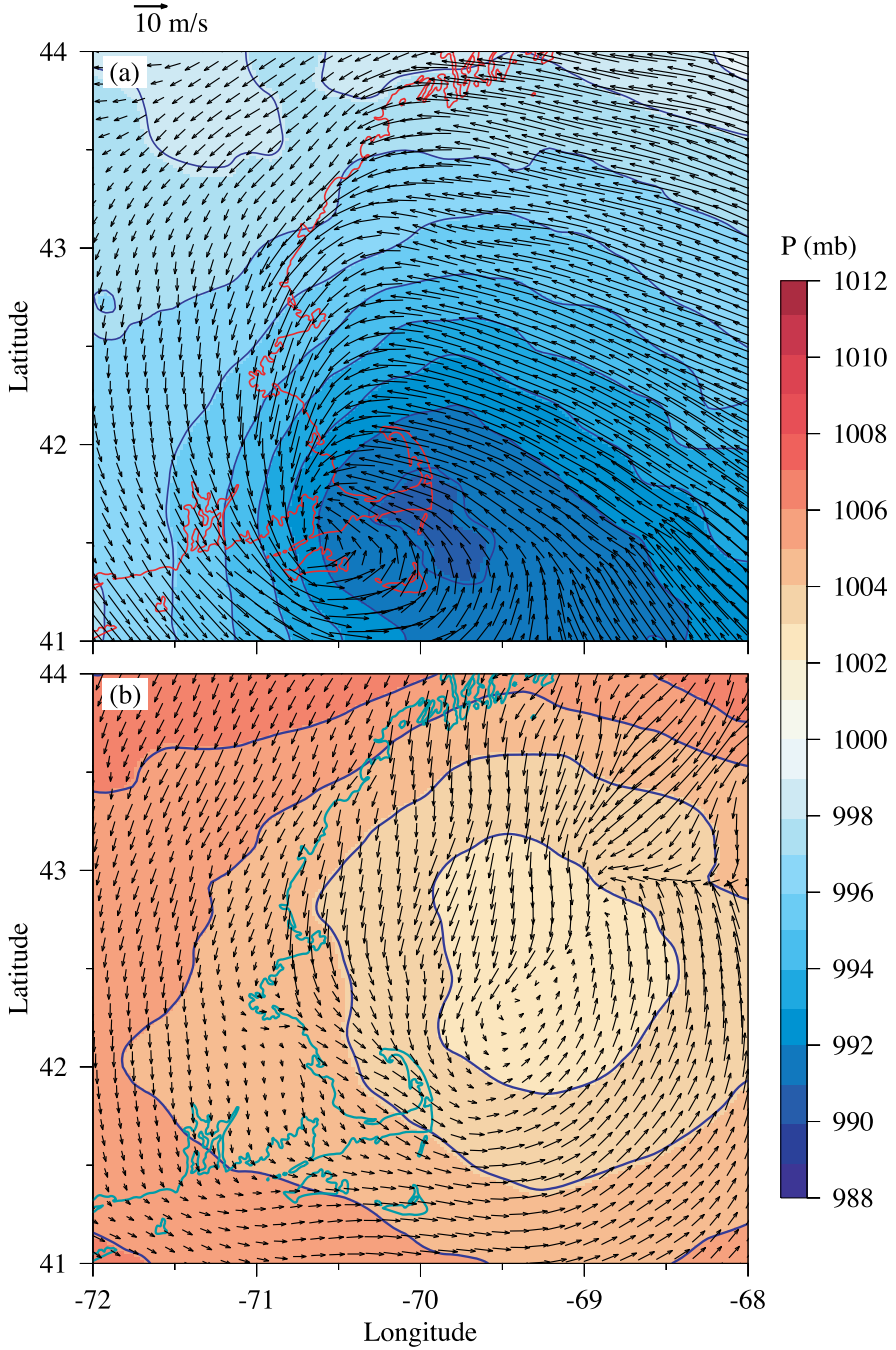

Figure 3.11 Distributions of near-surface wind velocity vectors (m/s) and air pressure (mb) in the western Gulf of Maine region at 05:00 EST April 5 (upper) and 11:00 EST May 19 (lower) 2007.

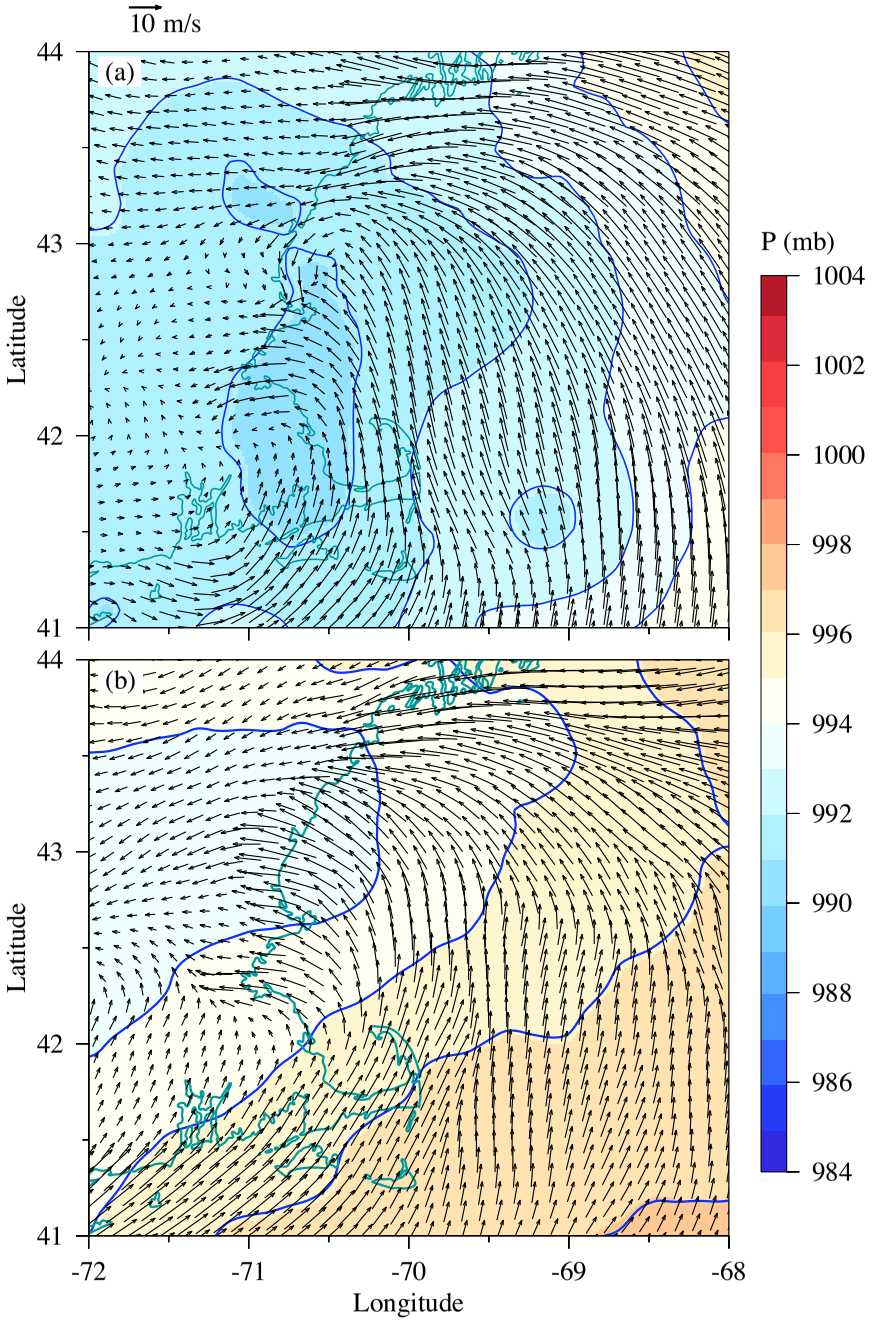

Figure 3.12 Distributions of near-surface wind velocity vectors (m/s) and air pressure (mb) in the western Gulf of Maine region at 08:00 EST June 4 (upper) and 14:00 EST October 12 (lower) 2007.

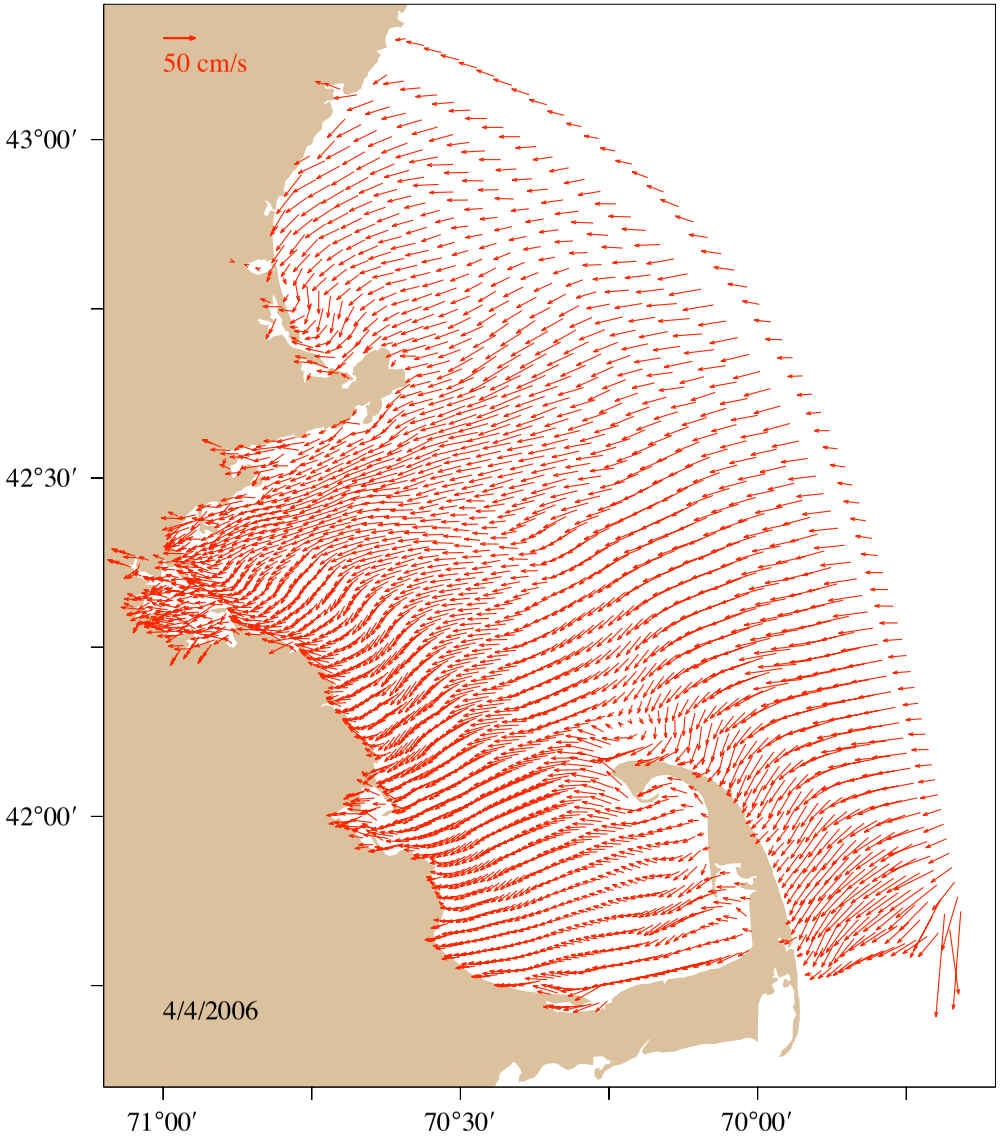

Figure 3.13 Difference of model-computed M2 tidally averaged near-surface currents for the cases with spatially non-uniform and single buoy winds on April 4 2006.

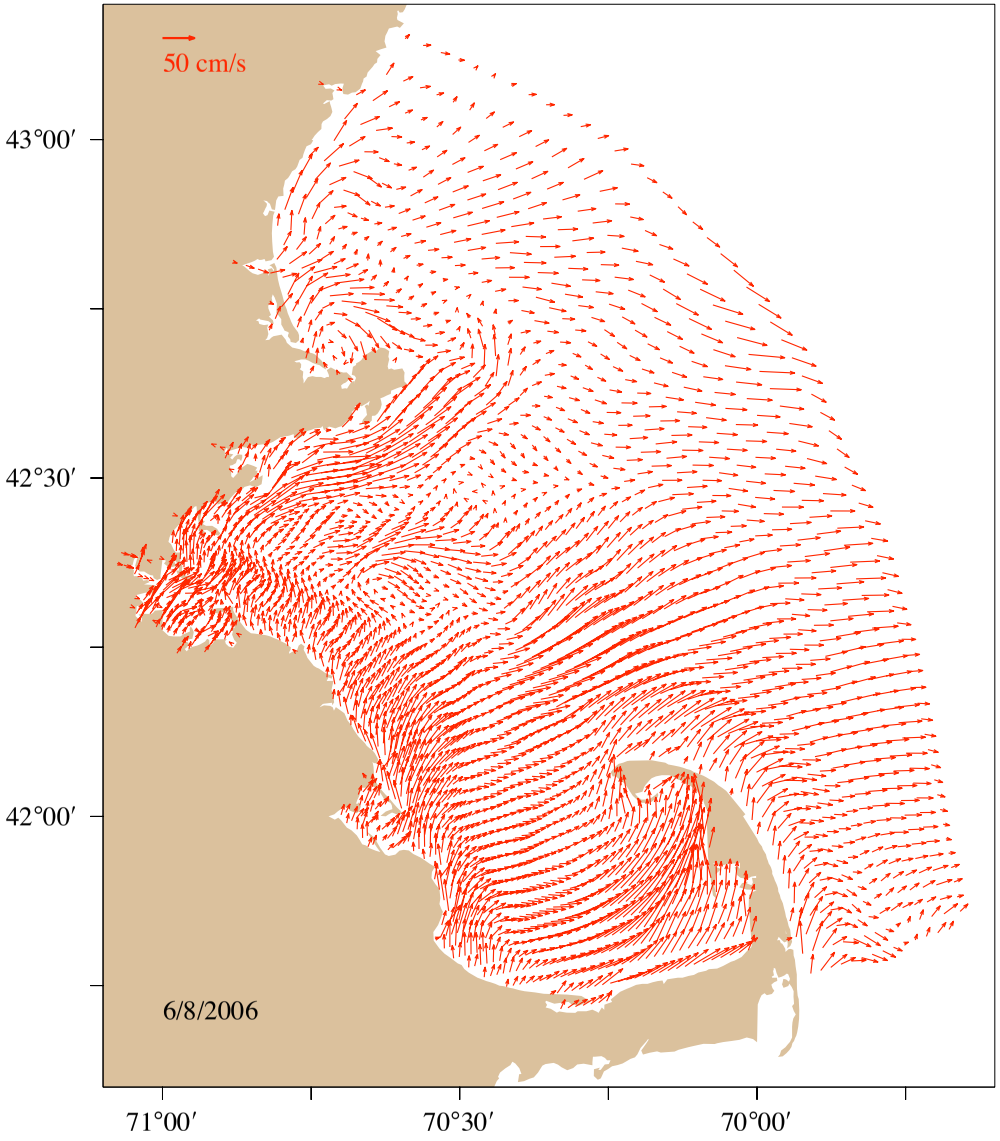

Figure 3.14 Difference of model-computed M2 tidally averaged near-surface currents for the cases with spatially non-uniform and single buoy winds on June 8 2006.

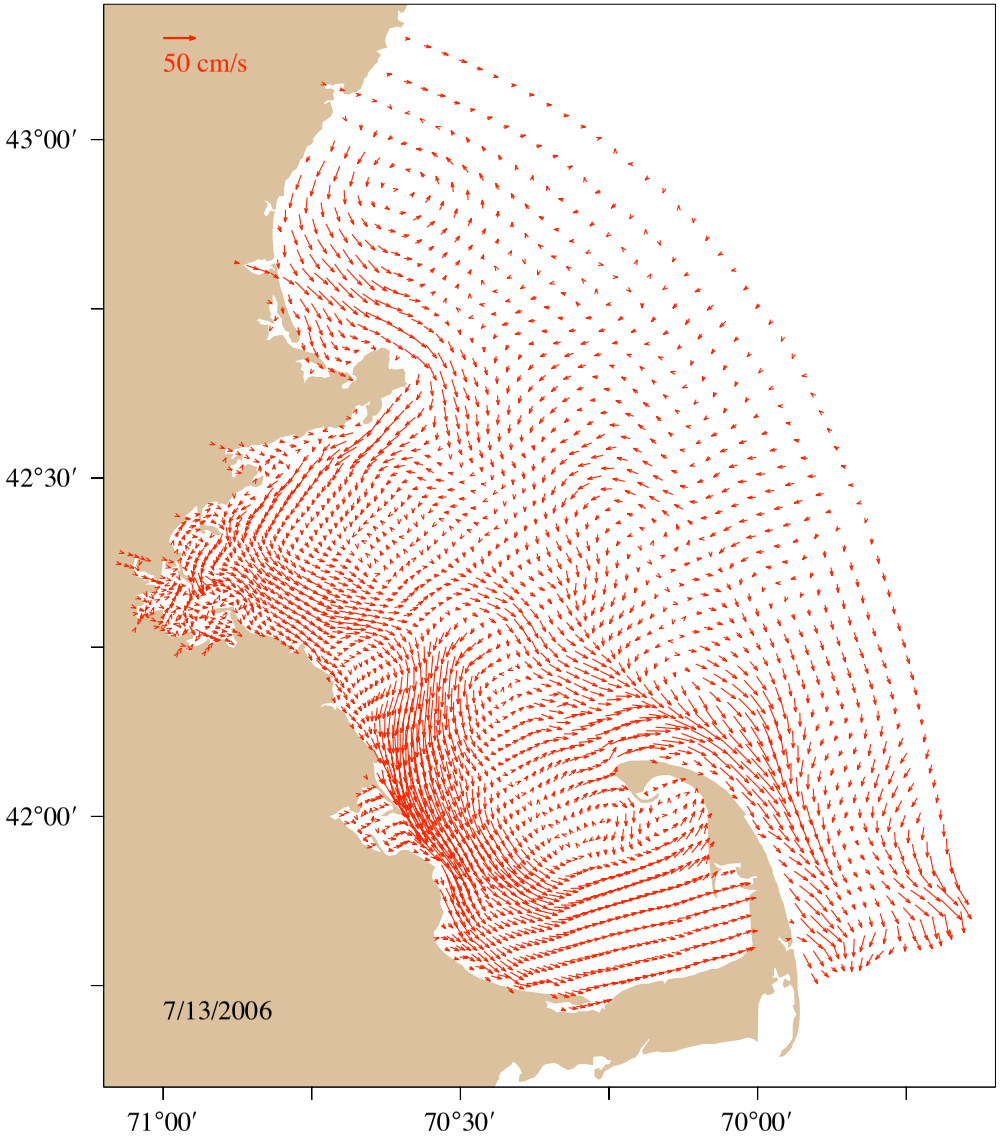

Figure 3.15 Difference of model-computed M2 tidally averaged near-surface currents for the cases with spatially non-uniform and single buoy winds on July 13 2006.

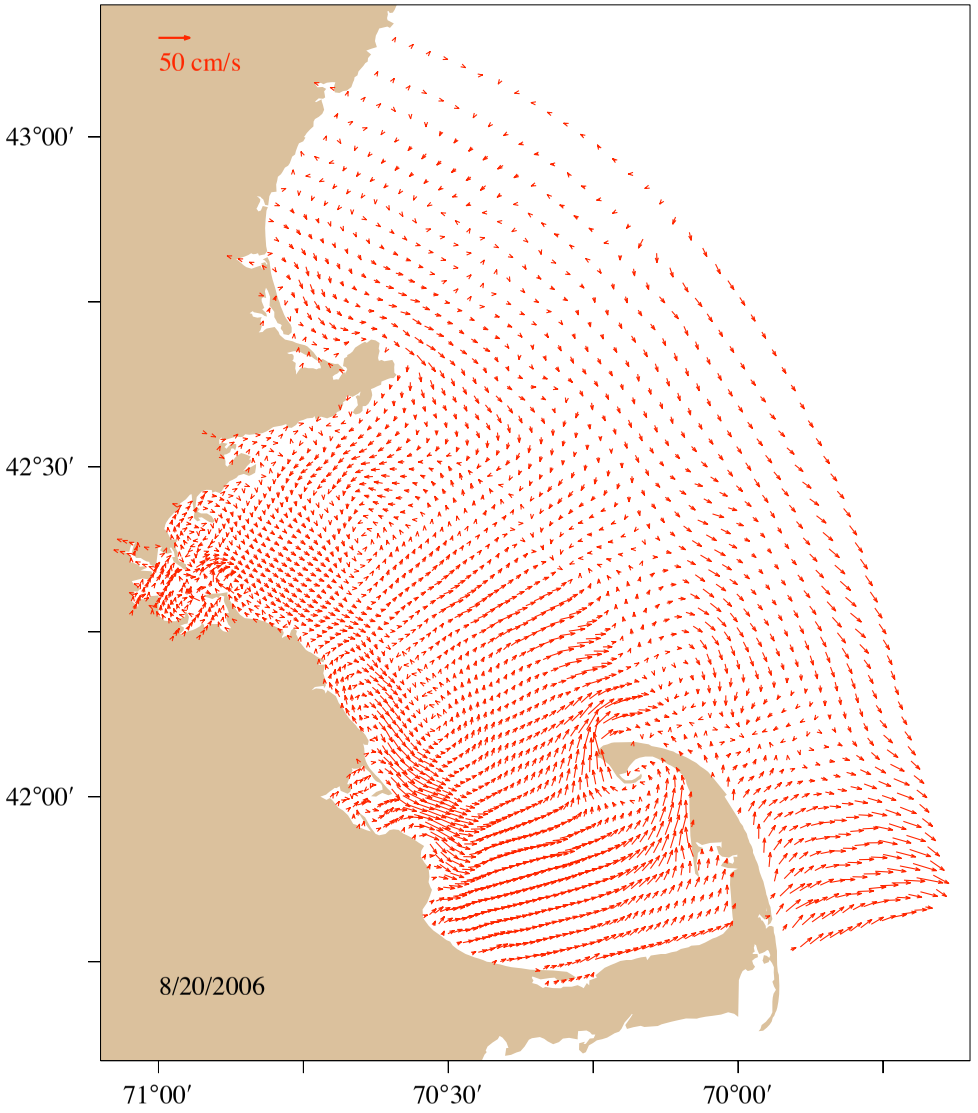

Figure 3.16 Difference of model-computed M2 tidally averaged near-surface currents for the cases with spatially non-uniform and single buoy winds on August 20 2006.

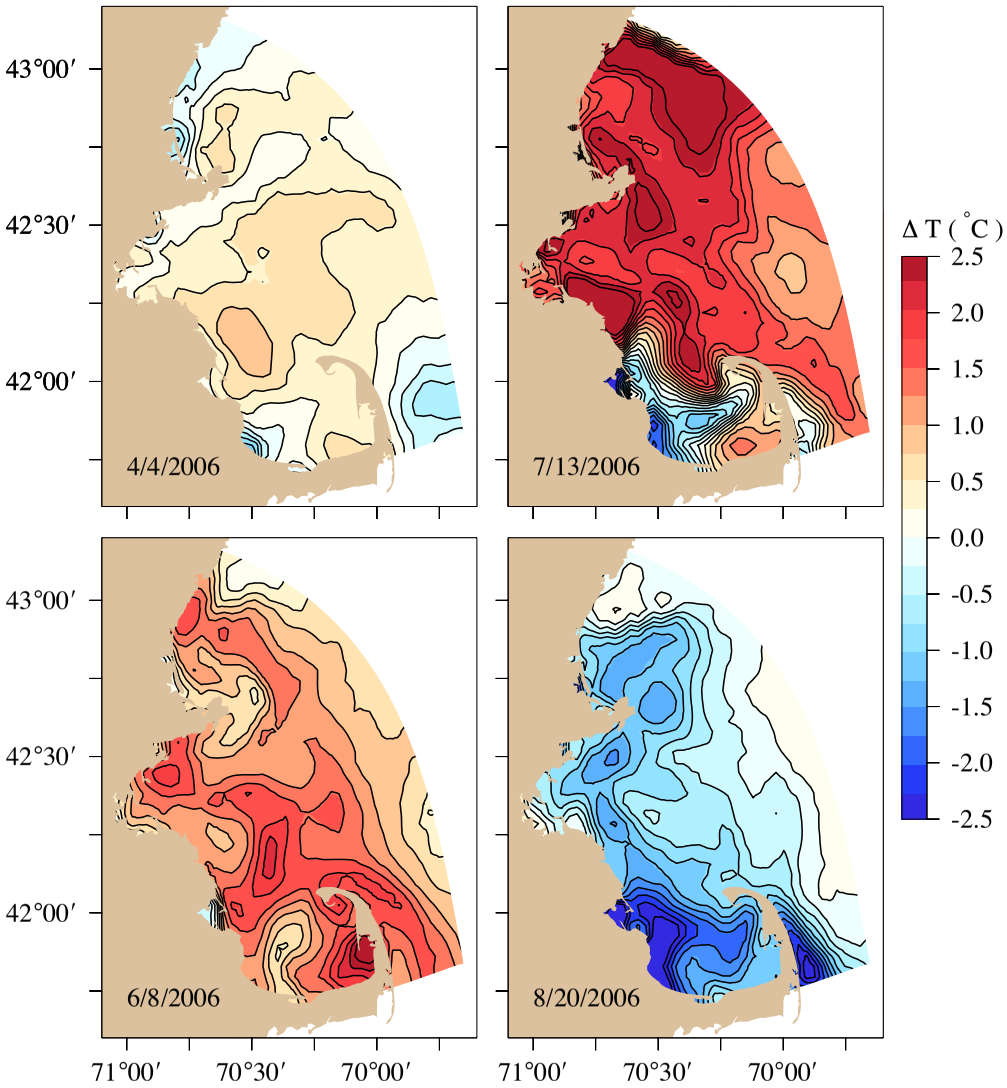

Figure 3.17 Difference of the M2 tidally averaged temperatures at the middle of the first sigma layer for the cases with spatially non-uniform and single buoy winds on April 4, June 8, July 13 and August 20 2006.

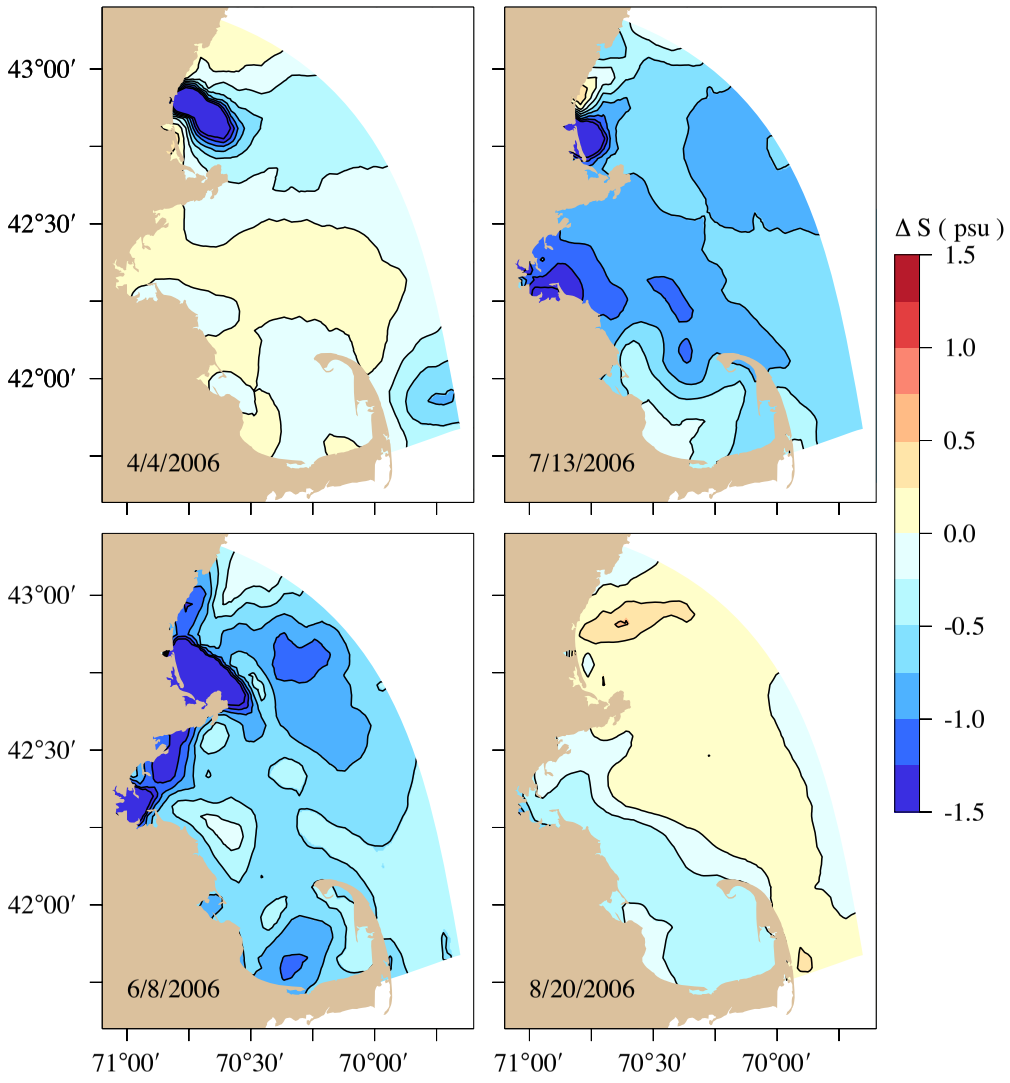

Figure 3.18 Difference of the M2 tidally averaged salinities at the middle of the first sigma layer for the cases with spatially non-uniform and single buoy winds on April 4, June 8, July 13 and August 20 2006.

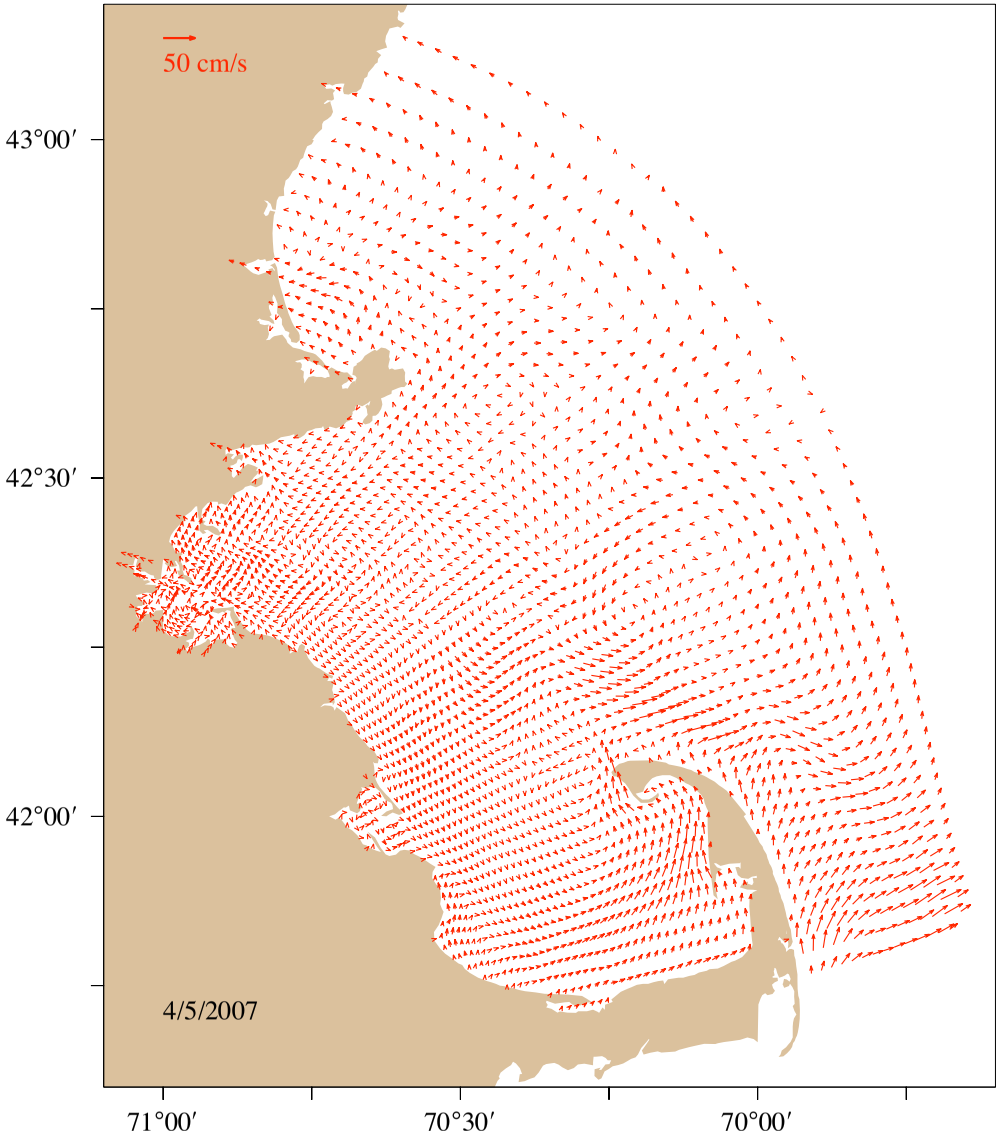

Figure 3.19 Difference of model-computed M2 tidally averaged near-surface currents for the cases with spatially non-uniform and single buoy winds on April 5 2007.

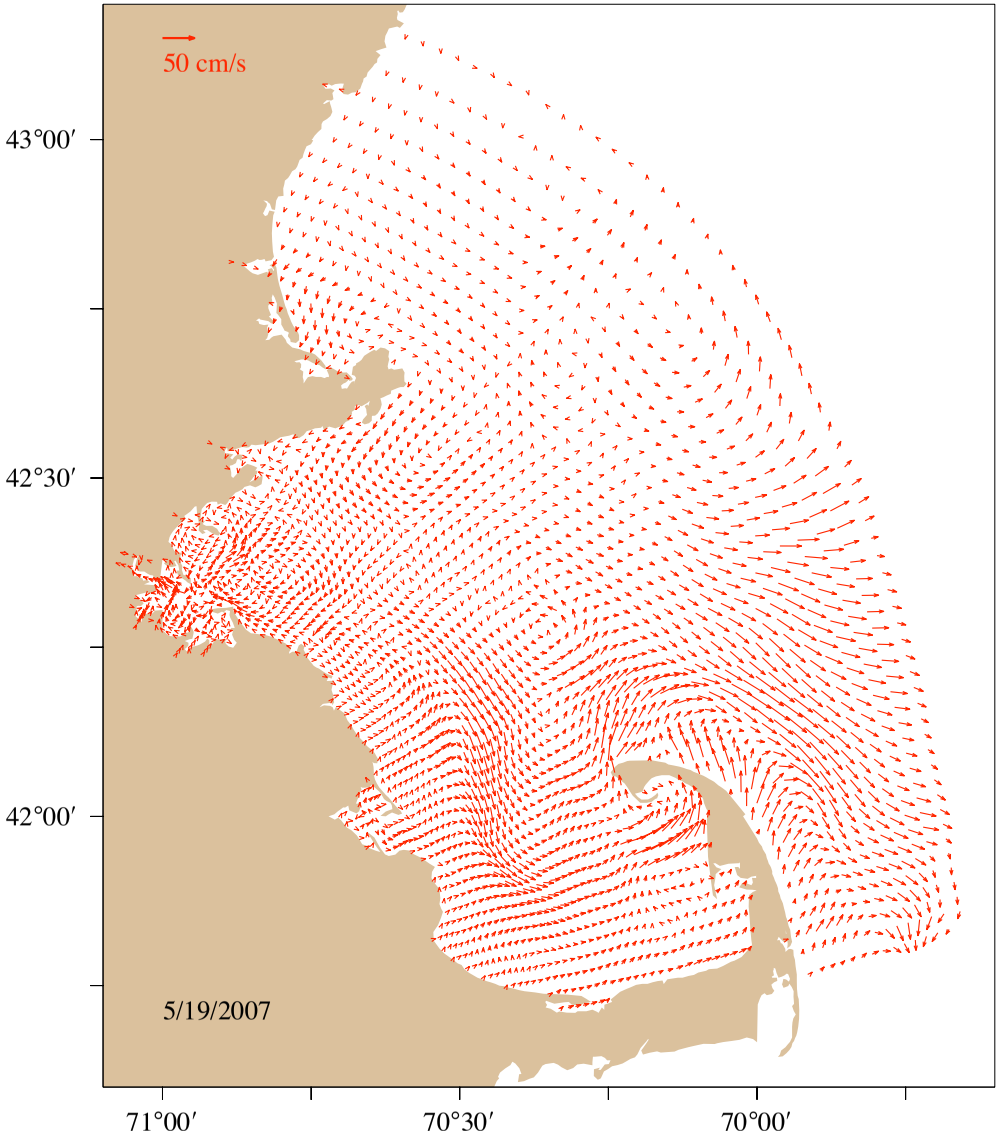

Figure 3.20 Difference of model-computed M2 tidally averaged near-surface currents for the cases with spatially non-uniform and single buoy winds on May 19 2007.

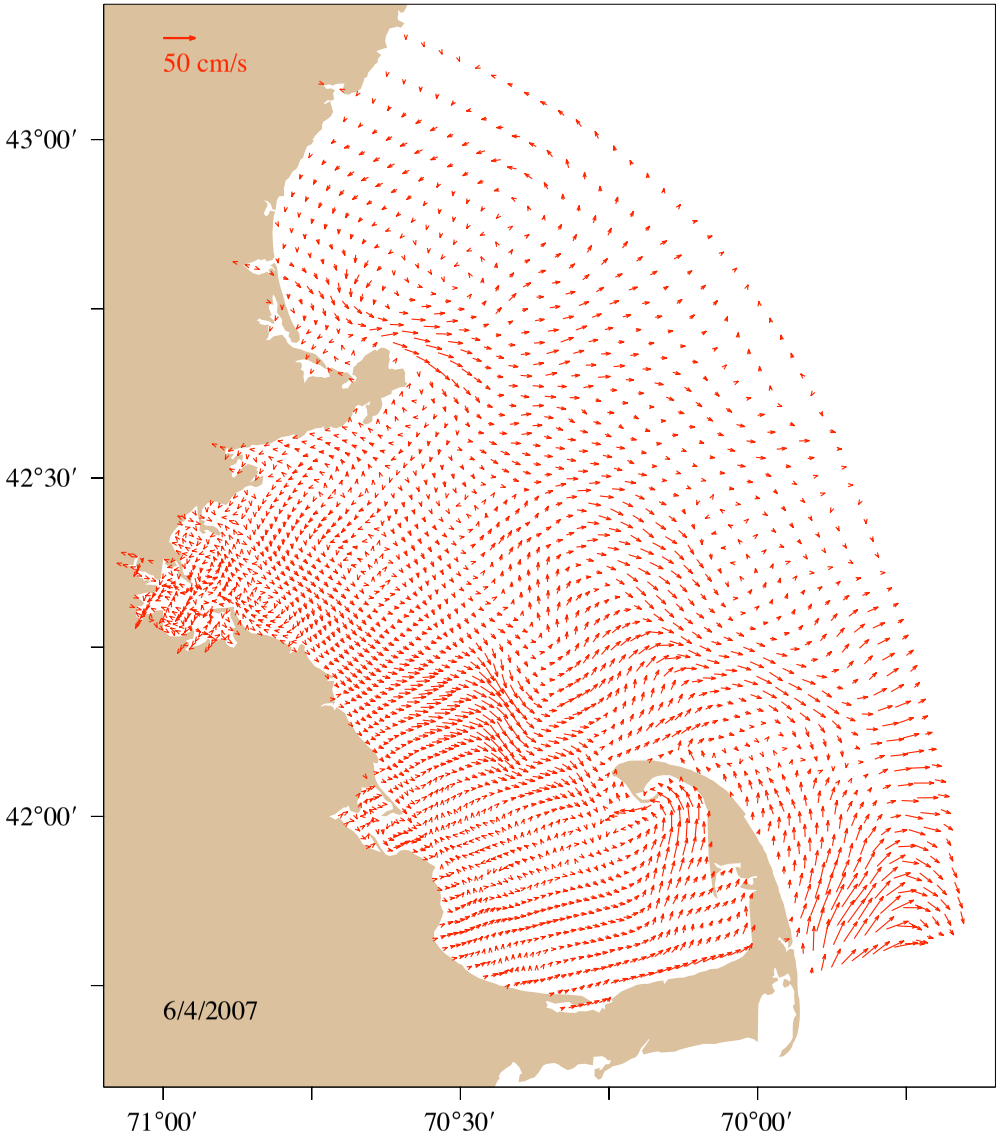

Figure 3.21 Difference of model-computed M2 tidally averaged near-surface currents for the cases with spatially non-uniform and single buoy winds on June 4 2007.

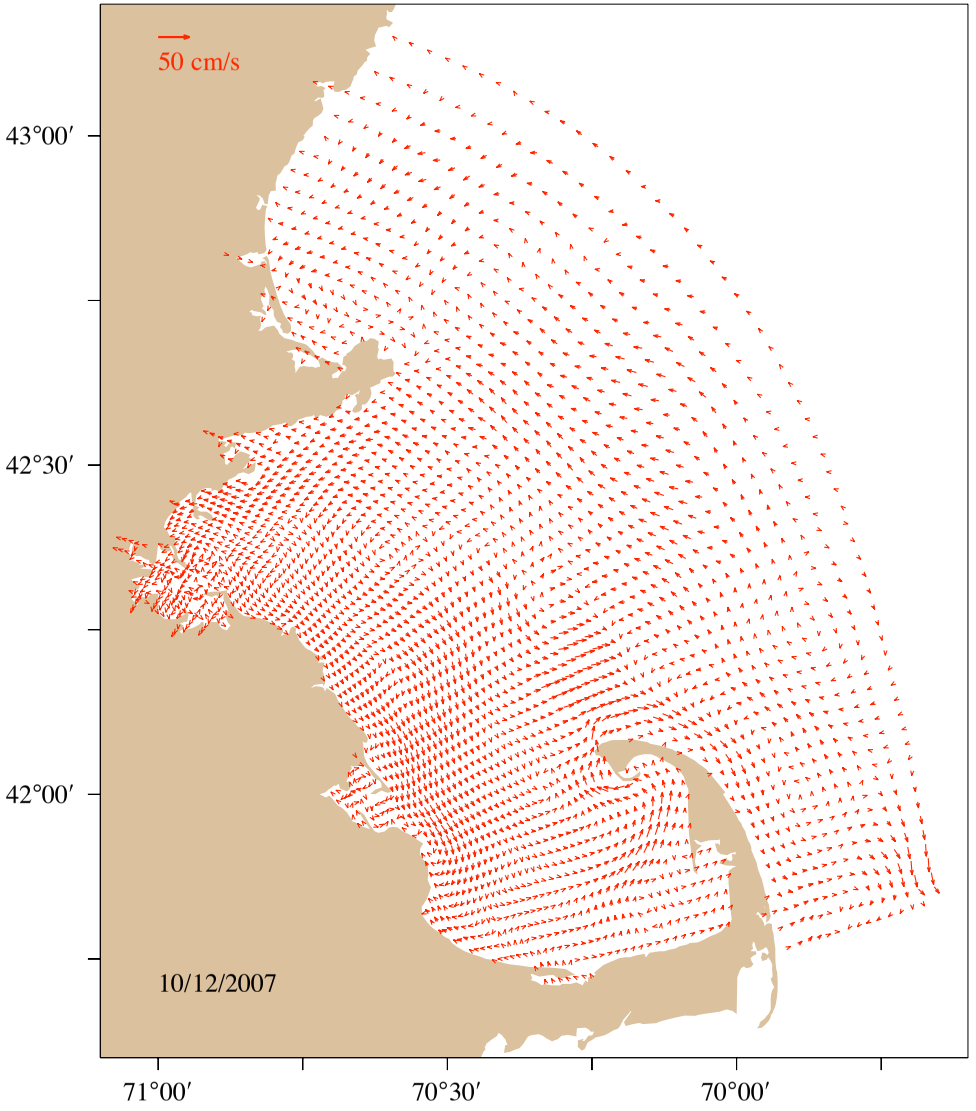

Figure 3.22 Difference of model-computed M2 tidally averaged near-surface currents for the cases with spatially non-uniform and single buoy winds on October 12 2007.

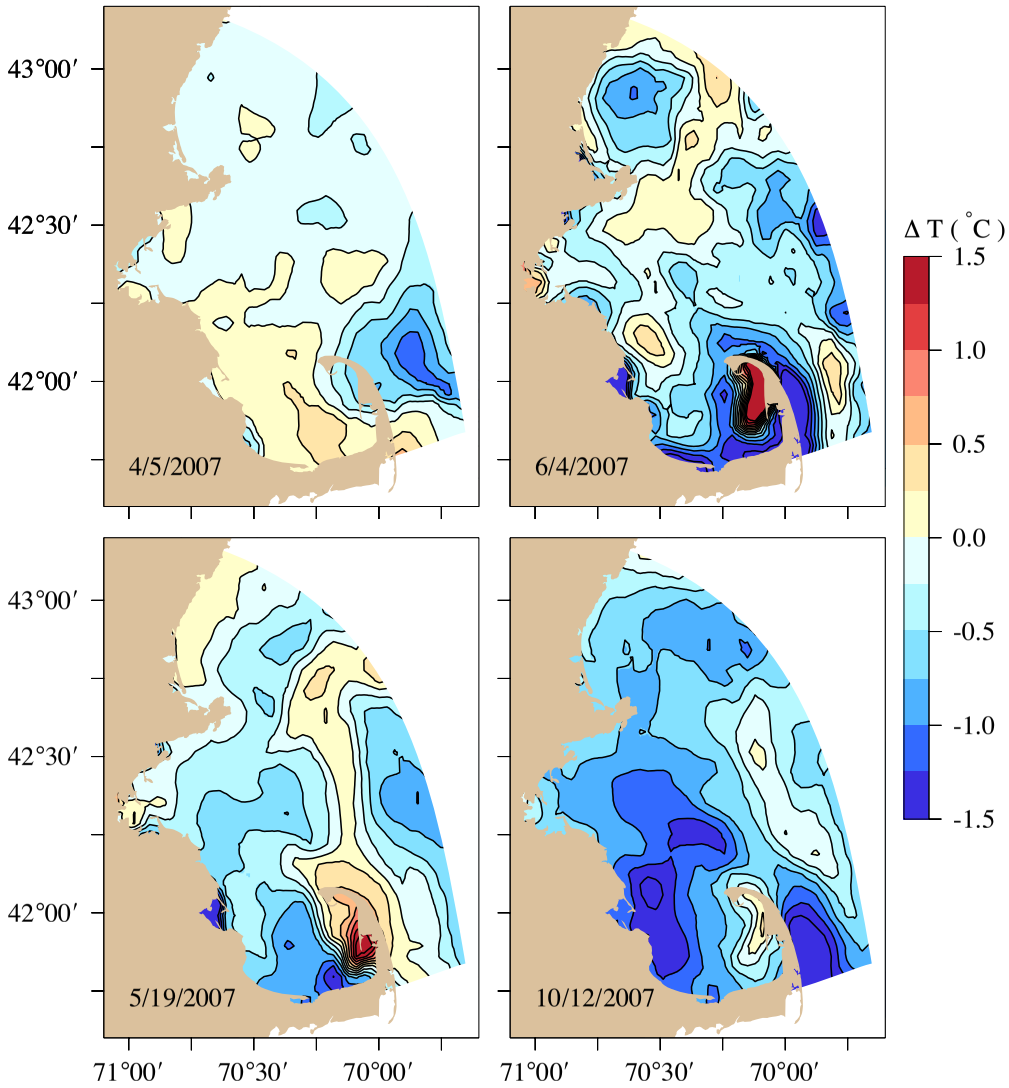

Figure 3.23 Difference of the M2 tidally averaged temperatures at the middle of the first sigma layer for the cases with spatially non-uniform and single buoy winds on April 5, May 19, June 4 and October 12 2007.

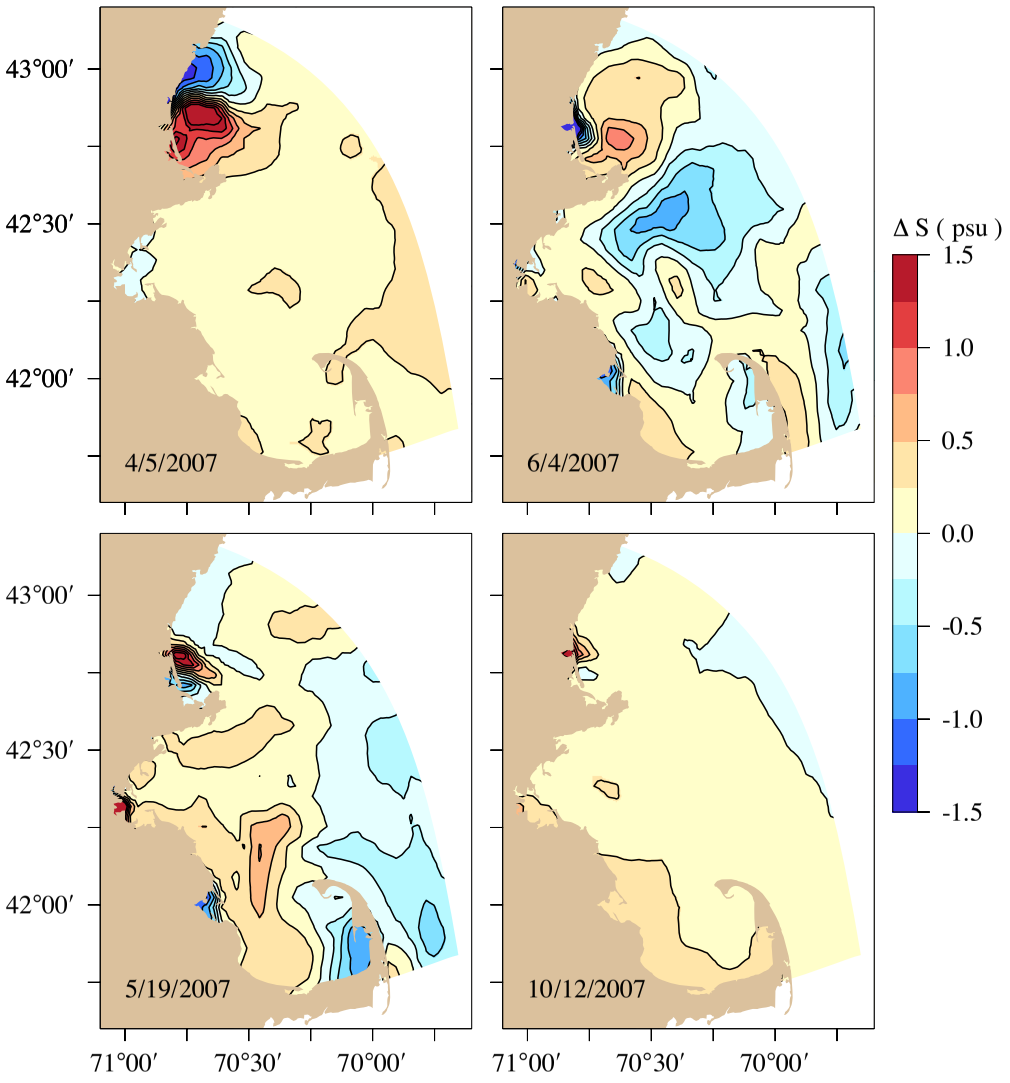

Figure 3.24 Difference of the M2 tidally averaged salinities at the middle of the first sigma layer for the cases with spatially non-uniform and single buoy winds on April 5, May 9, June 4 and October 12 2007.

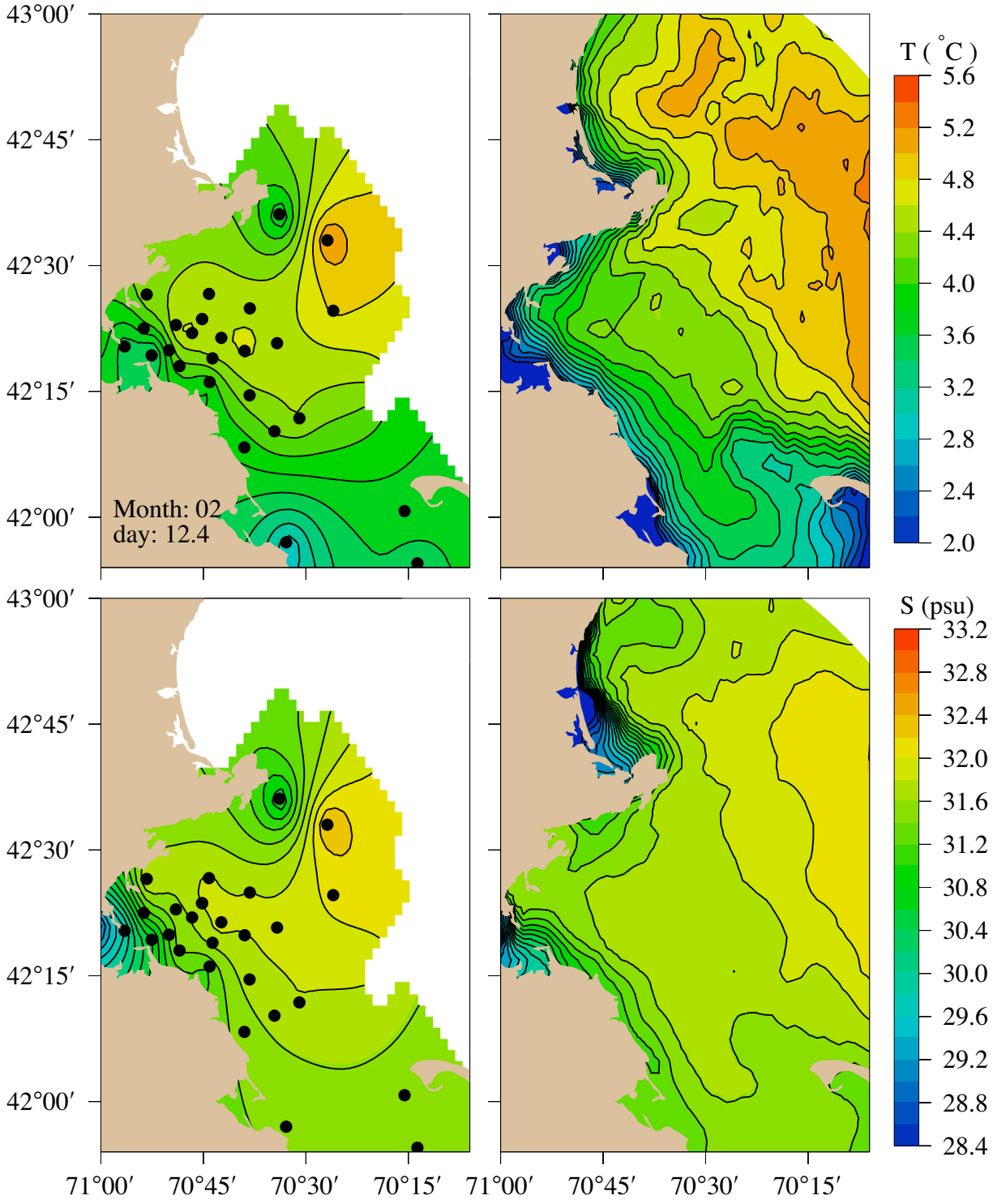

Figure 3.25 Comparison between observed (left) and model-computed (right) near-surface temperatures (upper panels) and salinities (lower panels) on day 12.4, February 2006.

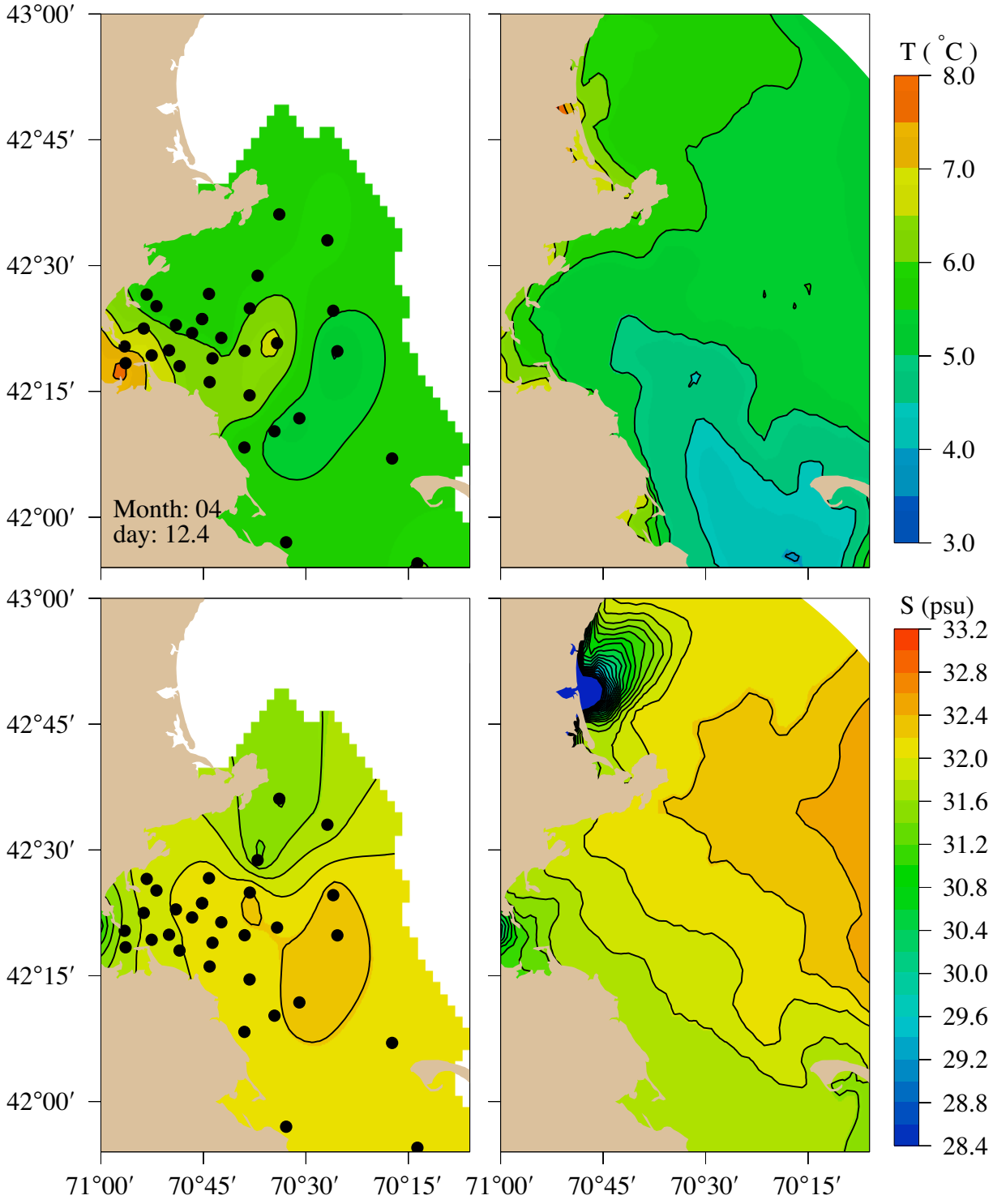

Figure 3.26 Comparison between observed (left) and model-computed (right) near-surface temperatures (upper panels) and salinities (lower panels) on day 12.4, April 2006.

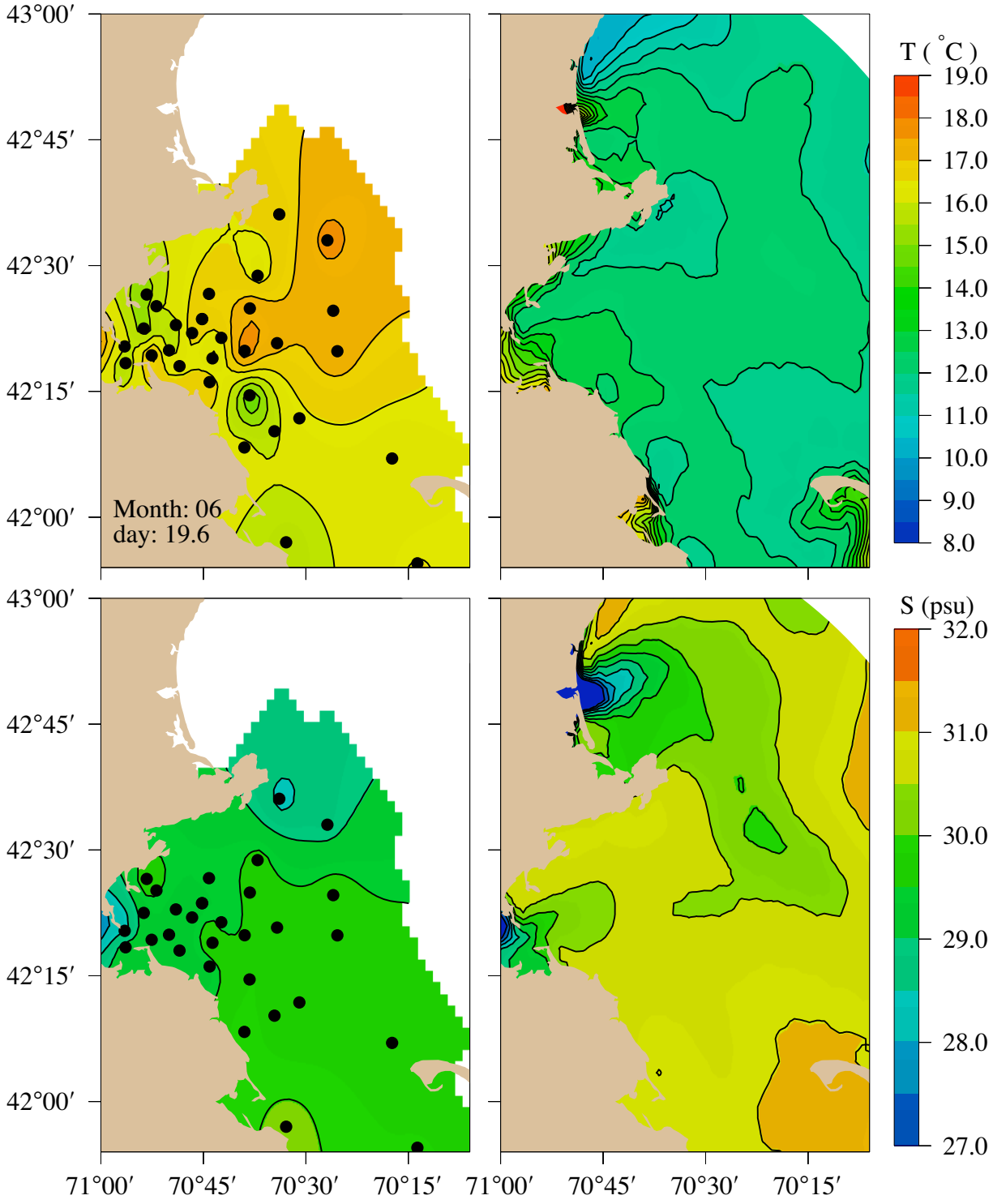

Figure 3.27 Comparison between observed (left) and model-computed (right) near-surface temperatures (upper panels) and salinities (lower panels) on day 19.6, June 2006.

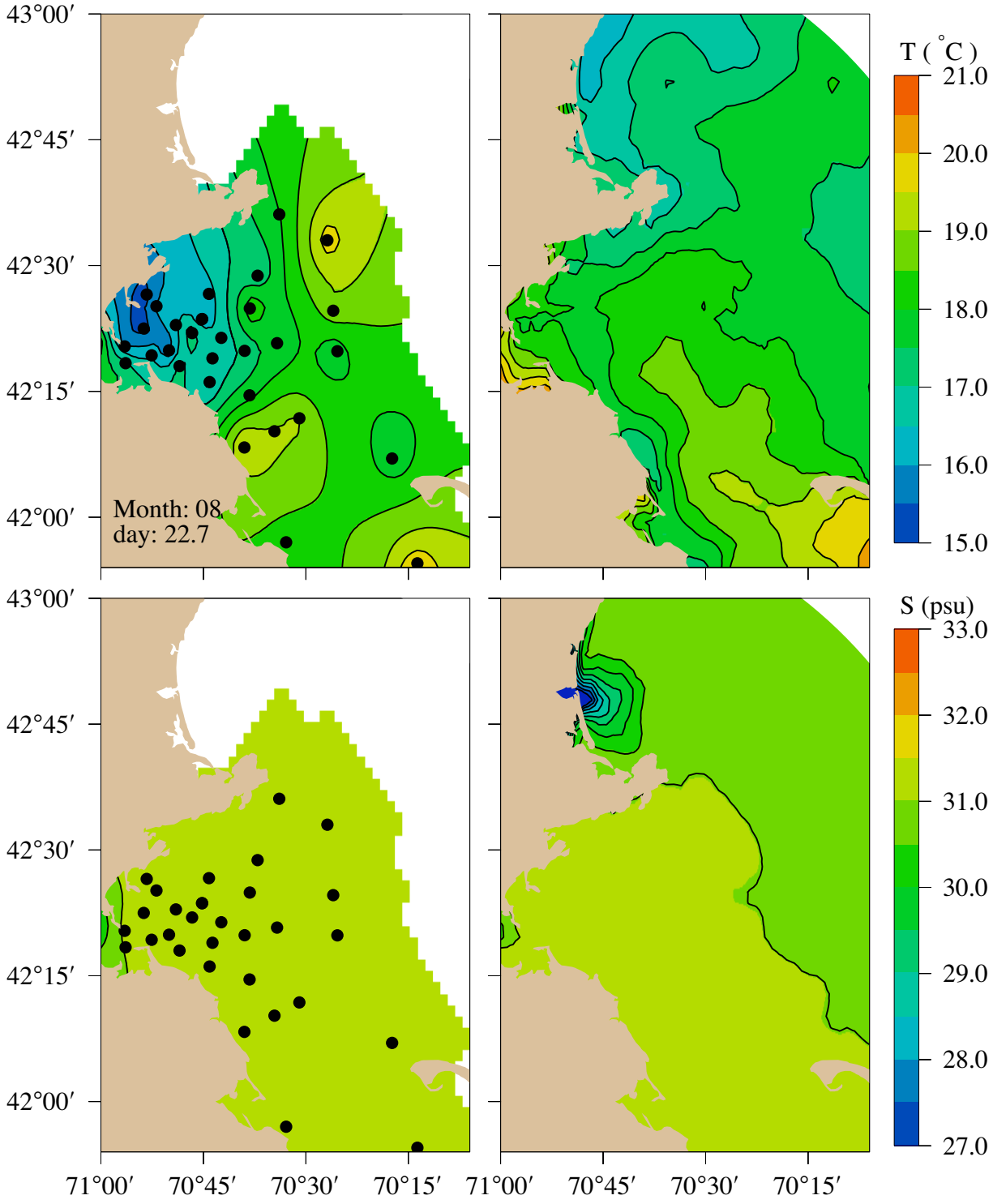

Figure 3.28 Comparison between observed (left) and model-computed (right) near-surface temperatures (upper panels) and salinities (lower panels) on day 22.7, August 2006.

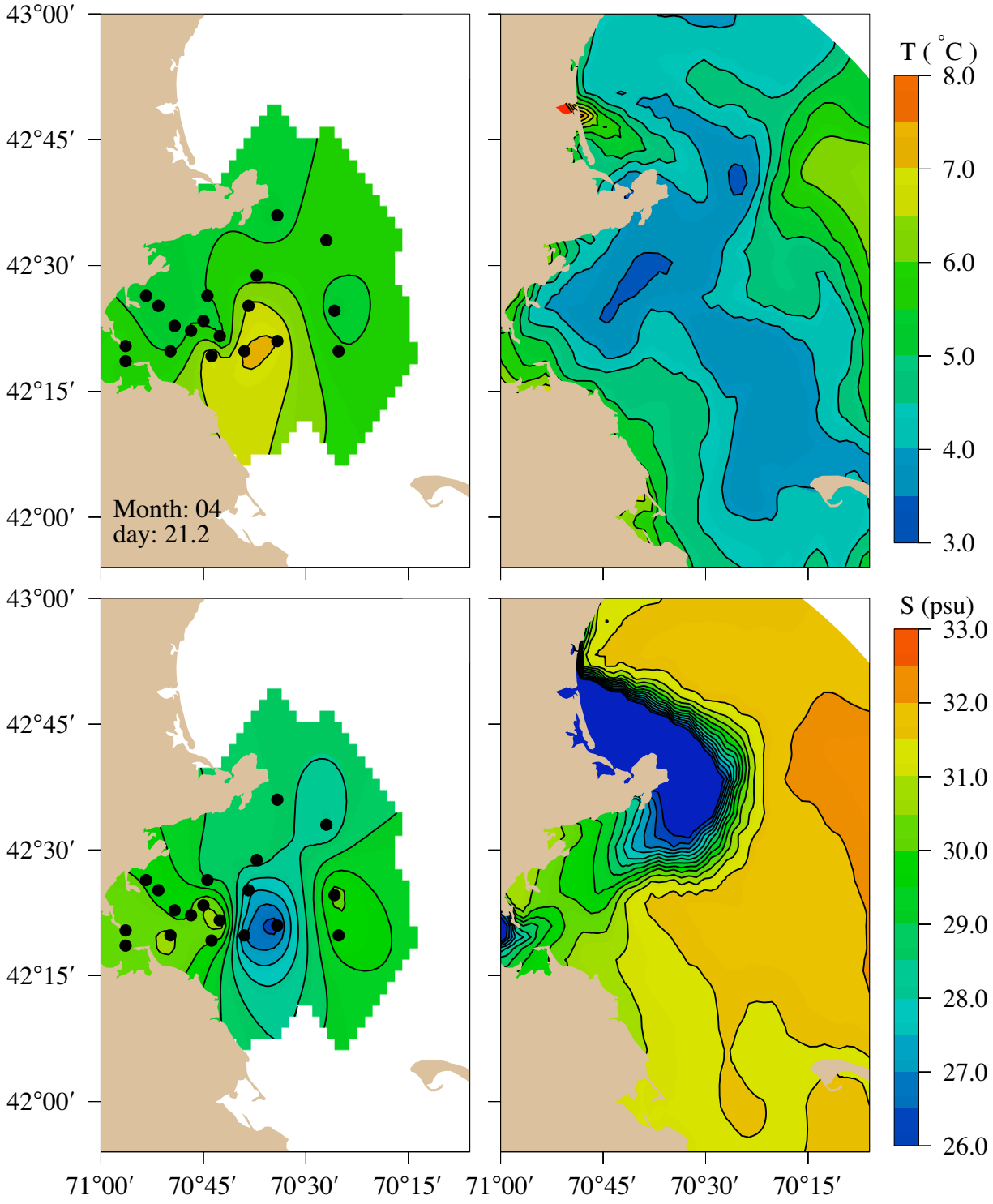

Figure 3.29 Comparison between observed (left) and model-computed (right) near-surface temperatures (upper panels) and salinities (lower panels) on day 21.2, April 2007.

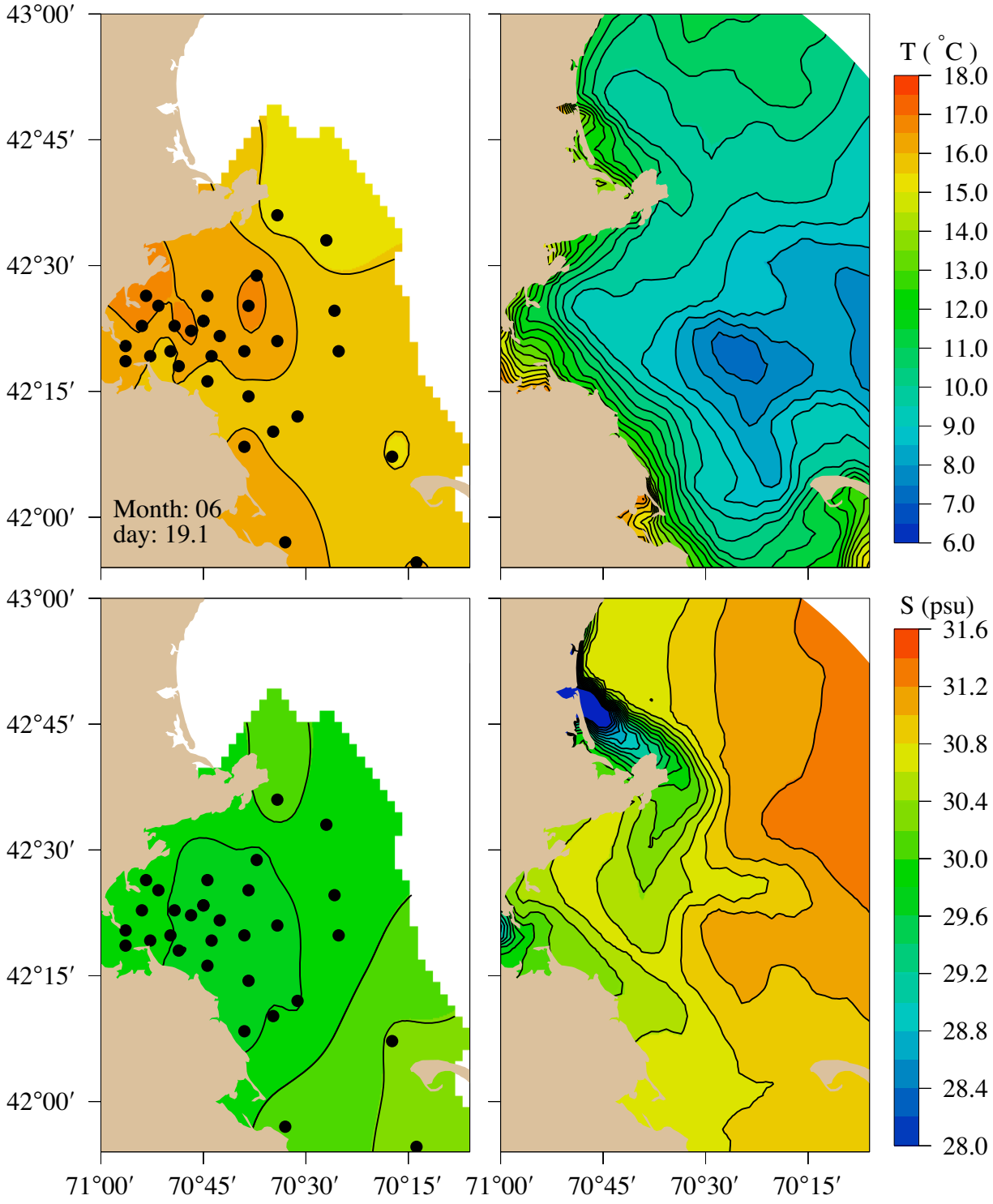

Figure 3.30 Comparison between observed (left) and model-computed (right) near-surface temperatures (upper panels) and salinities (lower panels) on day 19.1 June 2007.

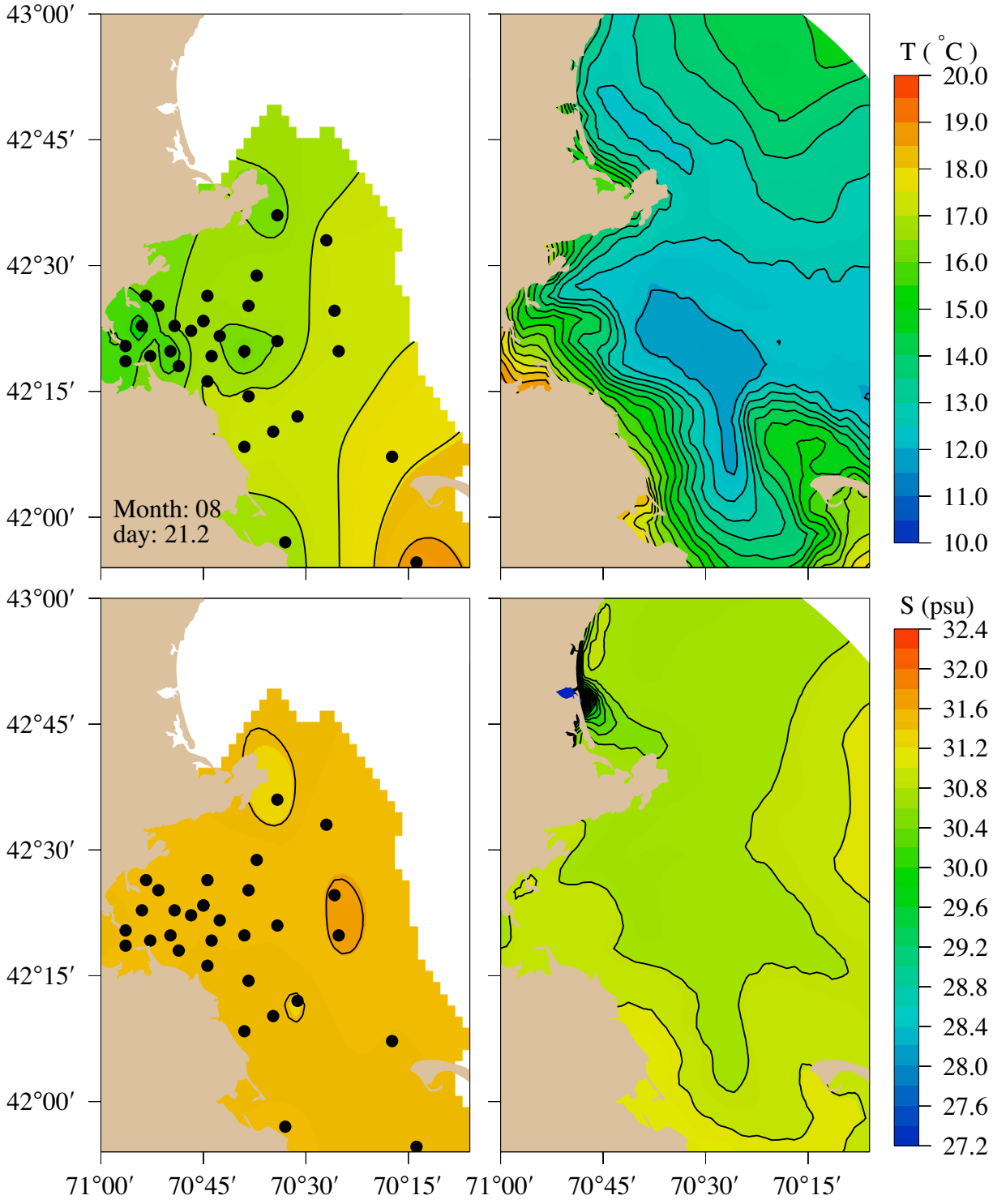

Figure 3.31 Comparison between observed (left) and model-computed (right) near-surface temperatures (upper panels) and salinities (lower panels) on day 21.2, August 2007.

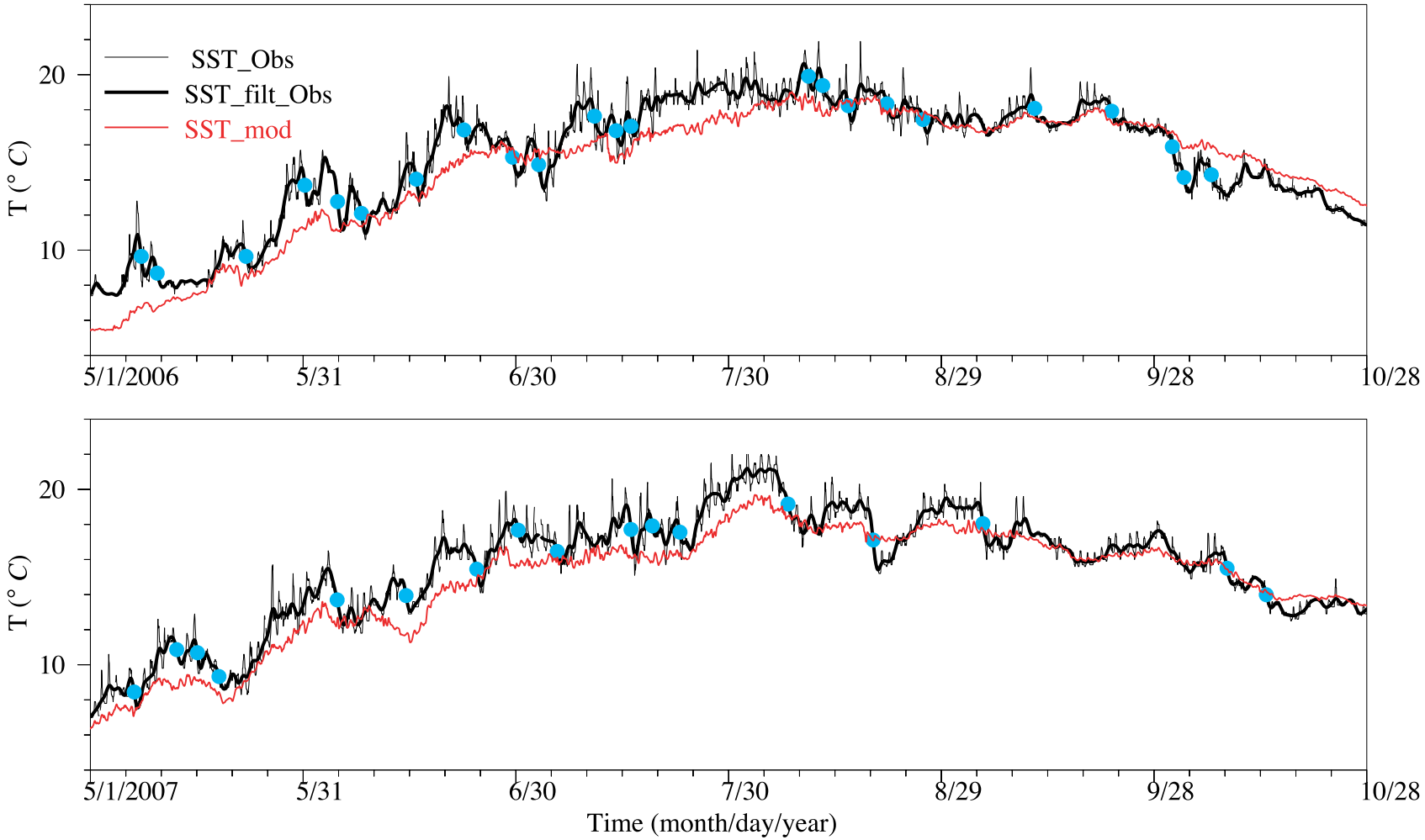

Figure 3.32 Comparison of observed and ECOM-si-detected cooling events on NOAA Buoy 44013 in Mass Bay for 2006 (upper) and 2007 (lower). Thin black solid line: the observed hourly sea surface temperature; thick black solid line: the low-passed filtered sea surface temperature; and red line: the ECOM-si computed hourly sea surface temperature. ● Blue dots identify noteworthy cooling events.

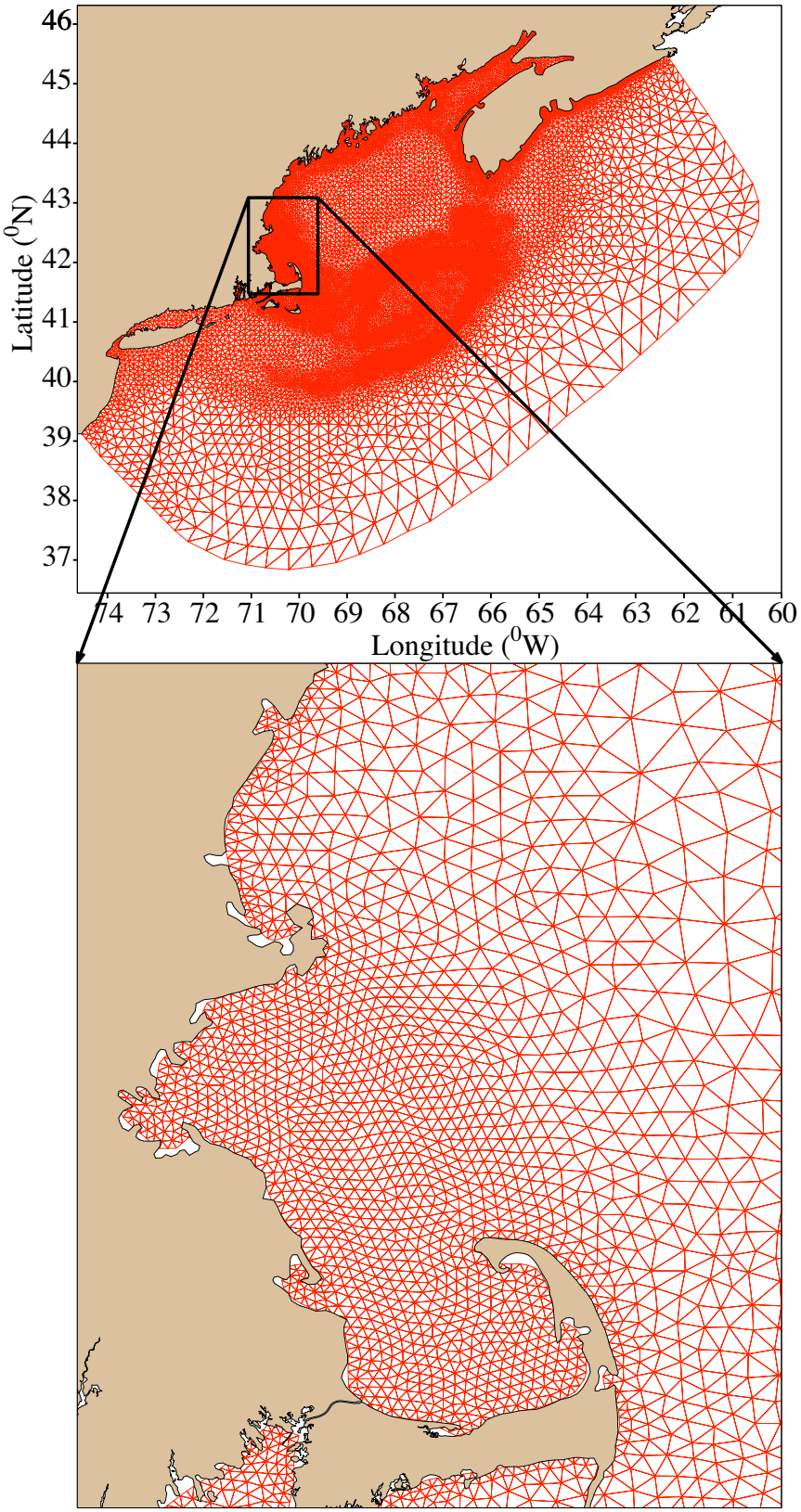

Figure 4.1 Unstructured grid of the first generation Gulf of Maine FVCOM.

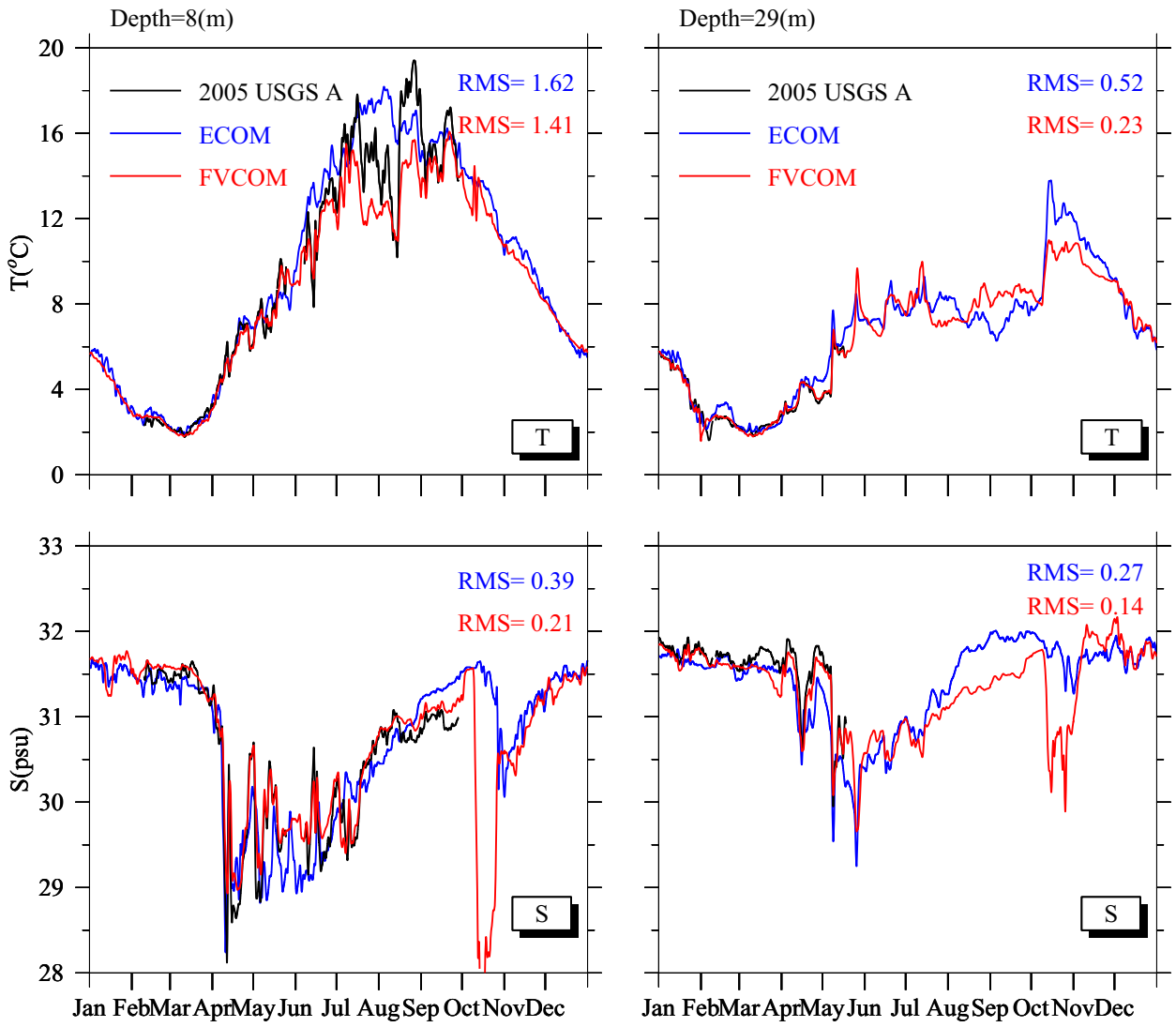

Figure 4.2 Comparison of observed, ECOM-si- and FVCOM-computed temperatures (upper) and salinities (lower) at 8 m (left) and 29 (m) on USGS Buoy A for 2005. Black: observed; blue: ECOM-si; Red: FVCOM.

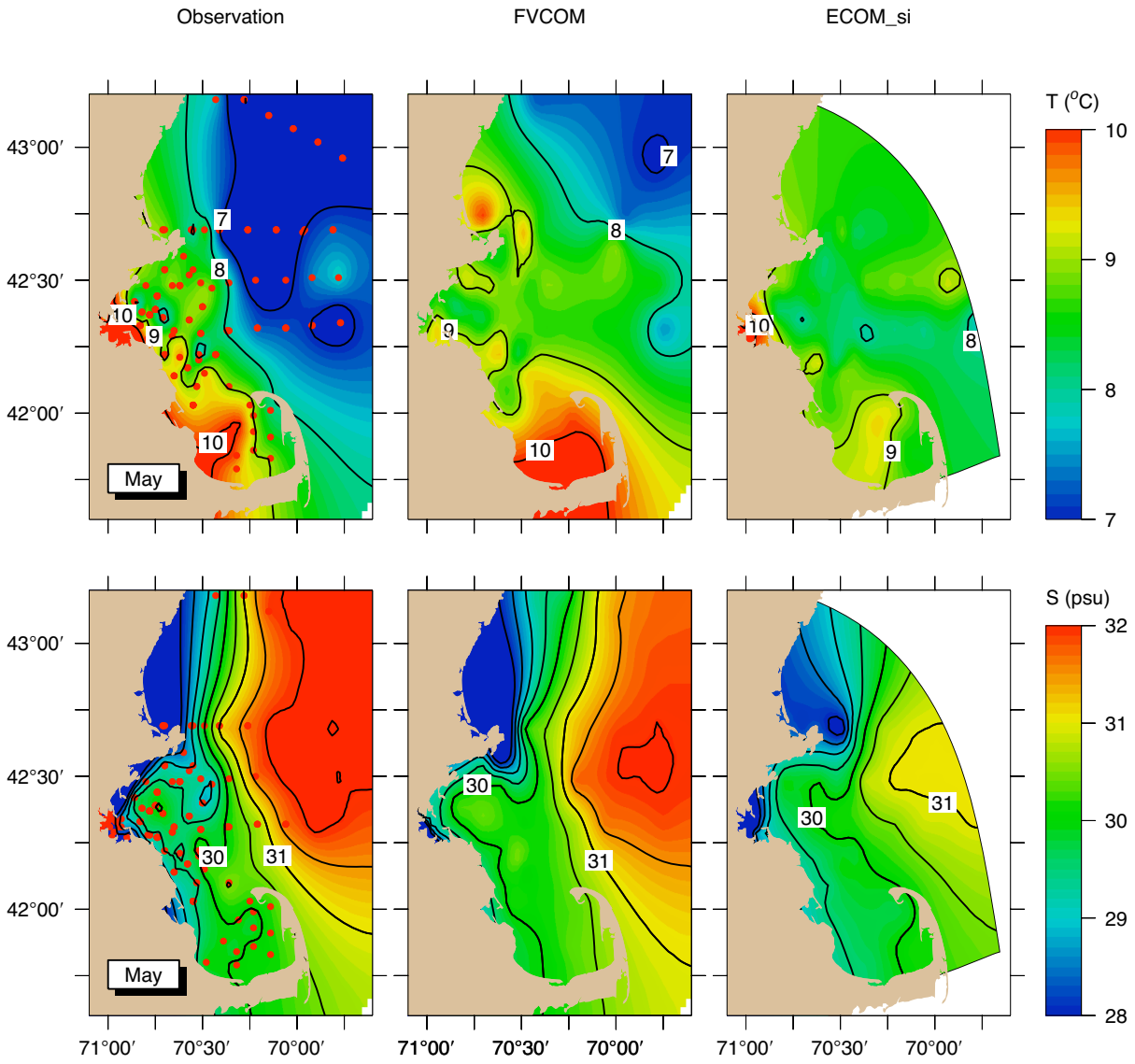

Figure 4.3 Comparison of distributions of observed, FVCOM- and ECOM-si-computed near-surface temperatures (upper) and salinities (lower) during May 2005 hydrographic survey. The model results were output at the same time when the measurements were made at individual sites.

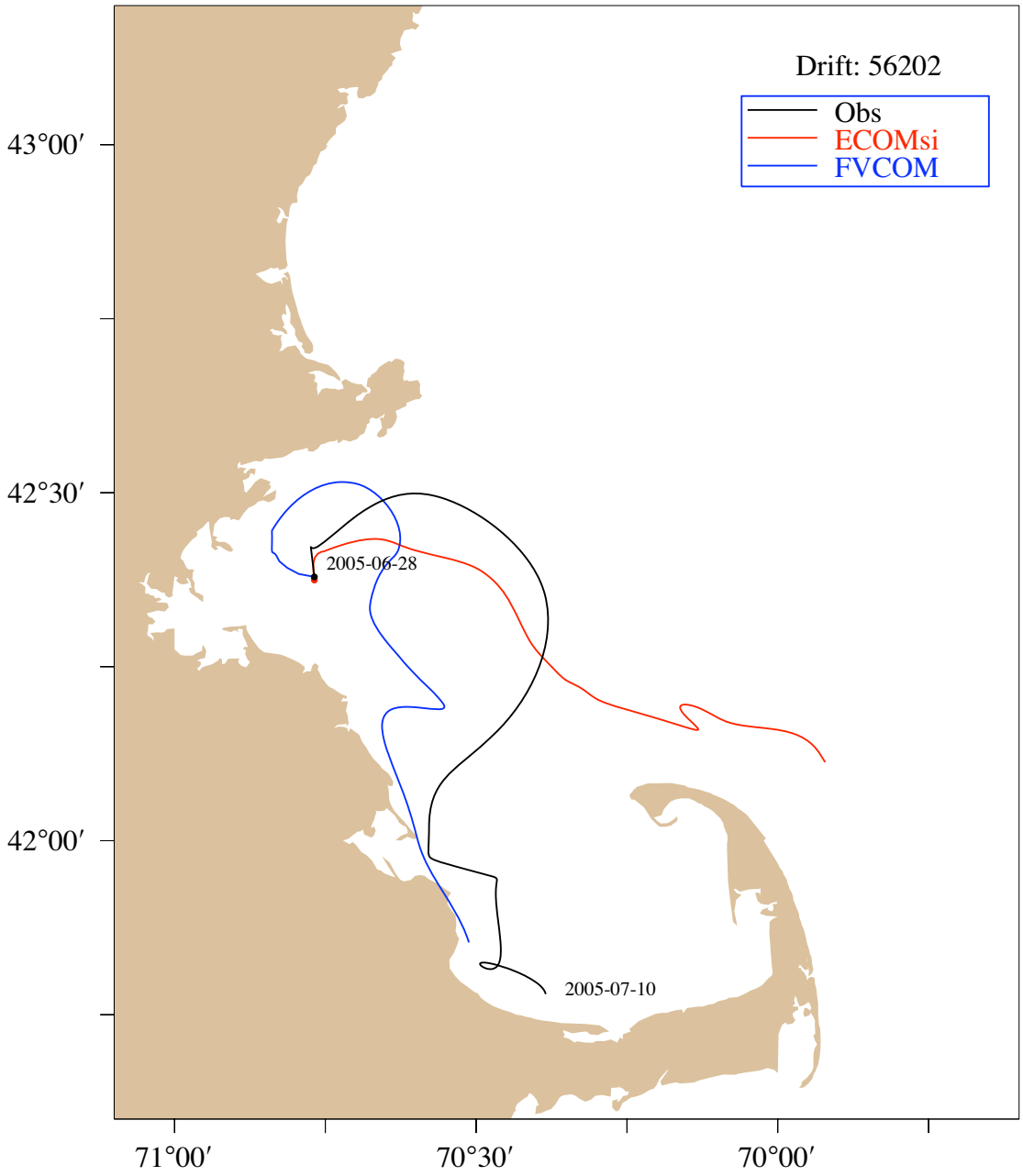

Figure 4.4 Comparison of distributions of observed, ECOM-si-and FV COM-computed 40-h low passed filtered trajectories of the subsurface drifter#56202. The drifter was released at June 28 2005 and tracked until July 10 2005. The red dot was the location of the release.

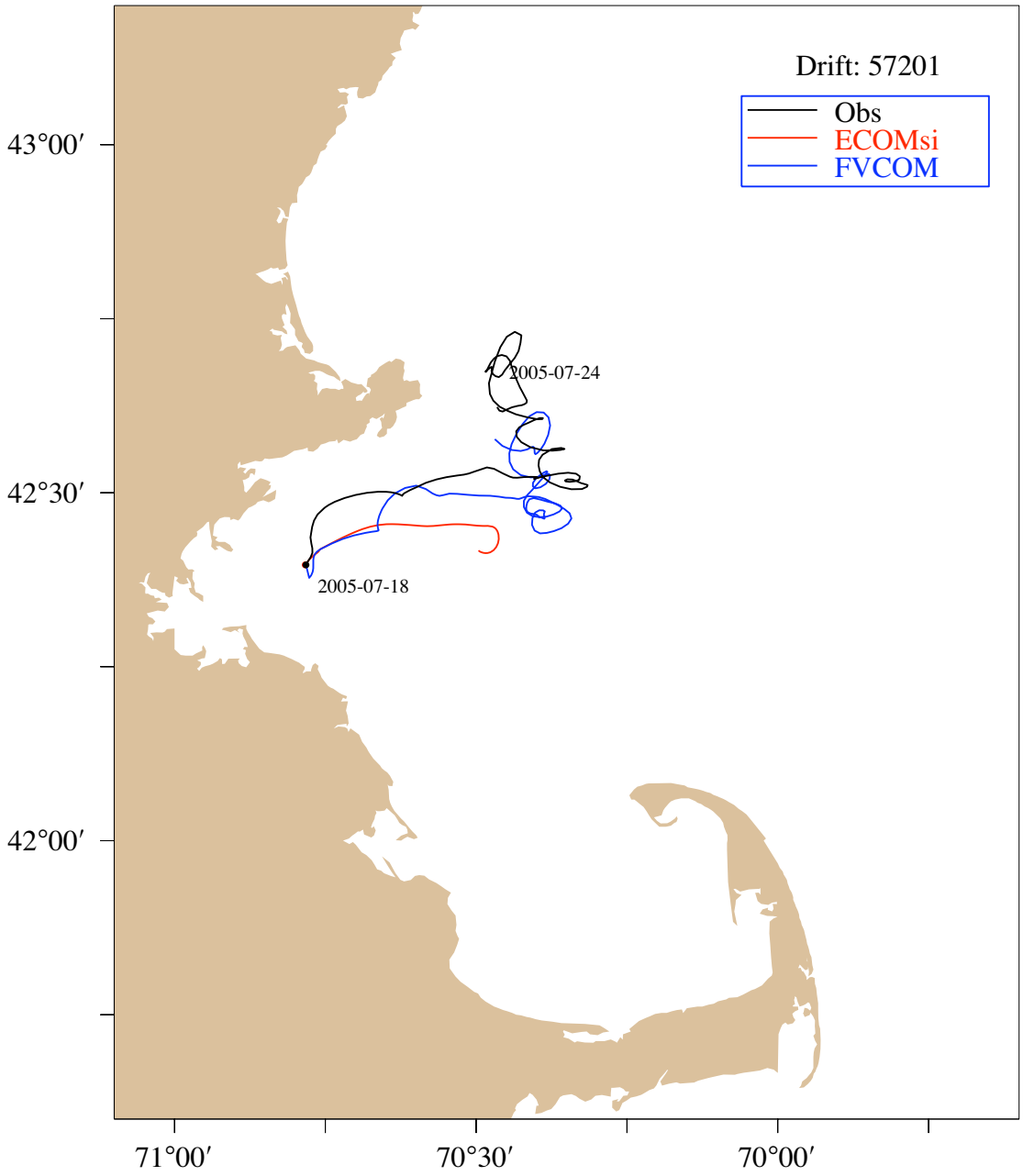

Figure 4.5: Comparison of distributions of observed, ECOM-si-and FV COM-computed 40-h low passed filtered trajectories of the surface drifter#57201. The drifter was released at July 18 2005 and tracked until July 24 2005. The red dot was the location of the release.

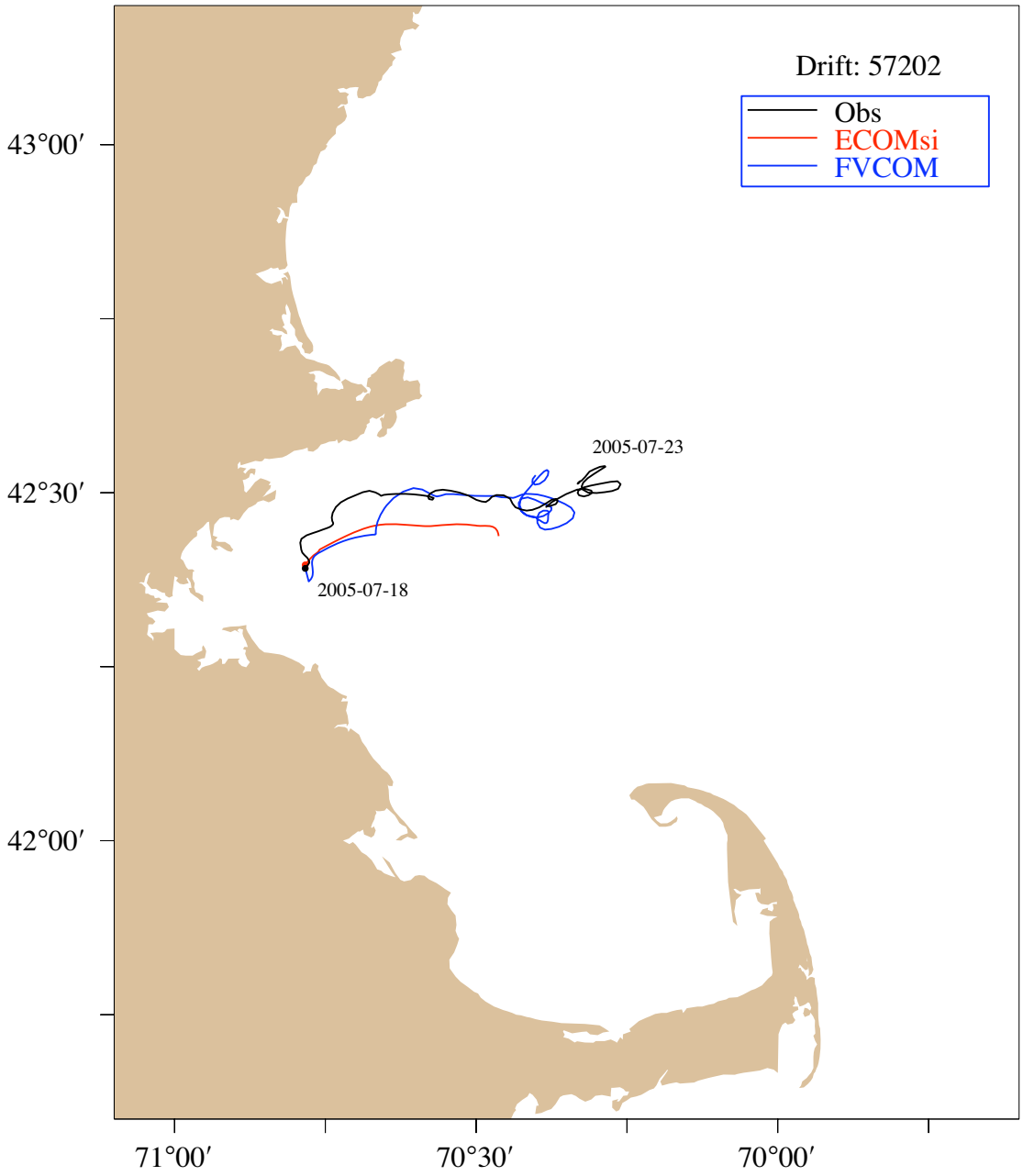

Figure 4.6: Comparison of distributions of observed, ECOM-si-and FV COM-computed 40-h low passed filtered trajectories of the surface drifter#57202. The drifter was released at July 18 2005 and tracked until July 23 2005. The red dot was the location of the release.

Massachusetts Water Resources Authority
Charlestown Navy Yard
100 First Avenue
Boston, MA 02129
(617) 242-6000
http://www.mwra.state.ma.us